Prospects of sprayed CZTS thin film solar cells from the perspective of material characterization and device performance

Thesis submitted to

Cochin University of Science and Technology

in partial fulfilment of the requirements

for the award of the degree of

Doctor of Philosophy

Rajeshmon. V. G.

Thin Film Photovoltaic Division

Department of Physics

Cochin University of Science and Technology

Cochin – 682 022, Kerala, India

November 2013

Prospects of sprayed CZTS thin film solar cells from the perspective of material characterization and device performance

Ph.D Thesis in the field of Thin Film Photovoltaics

Author

Rajeshmon. V. G.
Thin Film Photovoltaic Division
Department of Physics
Cochin University of Science and Technology
Cochin – 682 022, Kerala, India
email: rajeshvgopinath@gmail.com

Supervising Guide

Dr. K. P. Vijayakumar
Professor, Department of Physics
Cochin University of Science and Technology
Cochin – 682 022, India
email: kpv@cusat.ac.in

November 2013

Thin Film Photovoltaic Division, Department of Physics, Cochin University of Science and Technology, Cochin – 682 022, Kerala, India.

Department of Physics
Cochin University of Science and Technology
Cochin – 682 022

Dr. K. P. Vijayakumar
Professor

Certificate

Certified that the thesis entitled ***"Prospects of sprayed CZTS thin film solar cells from the perspective of material characterization and device performance"*** submitted by **Mr. Rajeshmon. V. G.** is an authentic record of research work carried out by him under my supervision at the Department of Physics in partial fulfilment of the requirements for the award of degree of Doctor of Philosophy of Cochin University of Science and Technology and the work embodied in this thesis has not been included in any other thesis submitted previously for the award of any other degree.

Cochin – 22
Date: 04/11/2013

Prof. K. P. Vijayakumar
Supervising Guide

Phone: +91 4842577404. **Fax:**. +91 484 2577595. **Email:** kpv@cusat.ac.in

Declaration

I hereby declare that the thesis entitled *"**Prospects of sprayed CZTS thin film solar cells from the perspective of material characterization and device performance**"* submitted for the award of degree of Doctor of Philosophy of Cochin University of Science and Technology is based on the original work done by me under the guidance of **Dr. K. P. Vijayakumar**, Professor, Department of Physics, Cochin University of Science and Technology, Cochin - 682 022 and this work has not been included in any other thesis submitted previously for the award of any other degree.

Cochin – 22
Date: 04/11/2013

Rajeshmon. V. G.

Dedicated to

My beloved mother & sister

Acknowledgement

Words can never be enough in expressing how thankful I am to those incredible people in my life who made this thesis possible. I would like to thank them for making my time during my research in the Institute, a period I will treasure.

I am deeply indebted to my guide, Prof. K.P. Vijayakumar, for his invaluable guidance throughout my stay here as a PhD student. He has been a great source of inspiration and support for me, and has helped me grow up as a qualified PhD from a postgraduate student. He has been very broadminded in allowing me to select my own research problems and do the research I really liked, while guiding me along to avoid the pitfalls. His affection for me is fondly remembered. From him I have learned to think critically, to select problems, to solve them and to present their solutions. Each meeting with him added invaluable aspects to my work and broadened my perspective. Many thanks for your ongoing leadership and friendship.

I am intensely indebted to Prof. C. Sudha Kartha for her very useful assistance and counseling in overcoming various bottlenecks during the works and for her comments during my work presentations and drafting of my thesis. It is only because of her that I got an opportunity to pursue a research career immediately after M.Sc. I deeply appreciate her incessant encouragement.

I am also grateful to the Head, Dept. of Physics, Prof. B. Pradeep and all the former Heads of the Department– Prof. M.R. Anantharaman, Prof. Godfrey Louis & Prof. T. Ramesh Babu for permitting me to use the research facilities in the department. I am thankful to all the faculty members of the Dept. of Physics for their kind support and motivation from my post graduate level itself. I express my sincere thanks to all the office and library staff during my period for their cooperation and help.

I also thank Dr. Y. Kashiwaba and Ms. T. Abe of Department of Electrical and Electronics Engineering, Iwate University, Japan, for their great help in the XPS analysis of my samples. I extend my thanks to Dr. K.B. Jinesh, IIST, Trivandrum, Dr. T. Shripathi, ESCA Lab and Molecular Spectroscopy Lab, UGC-DAE Consortium for Scientific Research, Indore Centre, Dr. M.K. Jayaraj, Department of Physics, CUSAT, Cochin and Dr. K. Rajeev Kumar, Department of Instrumentation, CUSAT, Cochin for their timely help.

I am fortunate to have a friend like Poornima. N, who has opened her problems to me and in turn motivating me many times in the last 8 years. She helped me through the totally alien landscape of writing documents properly. She has supported me not only by providing a research assistantship over almost six years, but also academically and emotionally through the rough road to finish this thesis.

I owe special thanks to Dr. Rajesh Menon M.R & Dr. Tina Sebastian who guided me with their invaluable suggestions, lightened up the way in my darkest times and encouraged me a lot in the research life. I can see the good shape of my thesis because of the help and suggestions of especially Deepu and also from Vipin and Gisa in formatting the entire thesis.

I would like to express my special thanks to Subin Thomas not only for being a great soul but also for being there to listen when I needed an ear. He has been an amazing friend and support for both my academic and personal life. It's my fortune to gratefully acknowledge the support of some special individuals like Sajeesh, Sreeroop, Sanal, Priyesh, Nijo, Tharanath and Arun Aravind, Hasna for their valuable company and motivation throughout my research and personal life.

I am indebted to my lab colleagues for providing a stimulating and fun filled environment. Again, without following any specific order, I express my sincere thanks to my lab mates Santhosh, Sreejith, Titu, Rajesh C.S, Anshad, Geethu, Gincy, Aswathy, Jisha, Jubimol, Jaffer, Anas, Jalaja, Nithya, Aneesh

George, Saneesh and Subramanian for their affection and invaluable help extended towards me.

I remember with great appreciation my seniors Dr. R. Jayakrishnan, Dr. R Sreekumar, Dr. Deepa K.G, Dr. Meril Mathew, Dr. Anitha R Warrier, Dr. Pramitha V, Dr. V.C Kishore, Dr. T.V Vimal Kumar, Dr. Angel Susan Cherian, Dr. Senoy Thomas, for their valuable suggestions during the initial stages of my work. I express my sincere thanks to all my friends in the Physics Department, other Departments and hostels in CUSAT for their loving support throughout my life at CUSAT.

I am deeply indebted to my mother for her love, encouragement and support. I express my heartiest gratitude to Kunjettan, Abhilash and Lijo for being with me always, in overcoming my personal hurdles, without any hesitation. I express my eternal gratitude to my sister and brother in law for their affection and love.

Rajeshmon. V. G

Preface

The escalating cost of the traditional sources of energy- fossil fuels such as coal, petroleum and natural gas- reminds that petroleum resources will be exhausted in a relatively short period of time. This energy crisis forced developing countries to reduce or postpone important development programs, so as to have enough fund to purchase petroleum to keep their economies operating. In the case of nuclear power plants- another source of conventional energy- there are problems related to fuel processing and dumping of used fuel. To overcome such perennial issues associated with conventional sources of energy, most countries, including India, have shifted their focus to develop non-conventional renewable sources of energy.

A more feasible alternative to petroleum, coal, and nuclear reactors in developing countries is the direct and indirect use of solar energy, which is renewable, abundant, decentralized and non-polluting. Solar cells constitute a decisive technology for overcoming global environmental and energy problems. Current trends suggest solar energy will play an important role in future energy needs. Solar energy alone has the capacity to meet all the energy needs of the Earth for the foreseeable future. Despite all these benefits of solar cells and nearly 55 years after their invention, Photovoltaic solar cells are generating only 0.04 % of the world's on-grid electricity due to the high cost of solar cells, making it beyond the reach of the common consumer. For widely used 'Si' solar cell, wafer costs account for over 50 % of the total module cost.

One way of eliminating this major cost component is by replacing Si-wafers by thin films of semiconductors deposited onto a supporting substrate. Thin film solar cells based on direct band gap materials such as copper indium (gallium) diselenide (CIGS) and cadmium telluride (CdTe) have reached the commercialization stage with highest reported conversion efficiency of 15 % in

module. Unfortunately there are drawbacks to both of these technologies. Cadmium as well as Tellurium is toxic and there are issues around the potential scarcity, and consequent volatility in cost, of both Indium and Tellurium. So we should find alternative to these materials, while considering a long term production.

This thesis is devoted to the development of a relatively new, rapidly developing quaternary semiconducting material (viz., Cu_2ZnSnS_4) used for photovoltaic applications. This semiconductor, commonly known as CZTS, is closely related to a family of materials that have been used for solar cell applications. It is a compound semiconductor made of copper, zinc, tin and sulfur, which are sufficiently abundant elements; none of them is harmful to the environment even at large scale usage. Aim of this study is to fabricate CZTS solar cells through chemical spray pyrolysis (CSP) technique. At first the influence of various spray parameters like substrate temperature, spray rate, precursor ratio etc. on the opto-electronic properties of CZTS films will be studied in detail. Then the fabrication of CZTS/In_2S_3 hetero junctions and various ways to improve the performance parameters will be tried.

Chapter 1 of the thesis outlines the problems of energy economy and the need of solar energy with detailed description of thin film solar cells. This chapter also tries to give the picture of various possible materials for photovoltaic device applications including 'Si' and various compound semiconductors. A detailed discussion about the material CZTS is presented including the structural, optical and electrical properties. An elaborate review of CZTS films deposited using various vacuum as well as non-vacuum techniques are presented. Starting from the report of first CZTS based device, the path towards the current efficiency level is also explained in detail.

Chapter 2 focuses on the basics of theory of solar cells. Starting from p-n junction, formation of space charge region, bending of conduction and valence bands are explained. J-V characteristics of junction under dark and illuminated condition are also explained in detail. Detailed description of different

performance parameters of the device like open circuit voltage, short circuit current etc. is also presented in this chapter.

Chapter 3 deals with preparation and characterization of CZTS thin films through systematic variation of various spray parameters. Effect of variation of four different parameters were studied namely, choice of precursor, substrate temperature, precursor ratio and spray rate. Two different precursors for tin (viz. stannous chloride & stannic chloride) and two different precursors for zinc (viz. Zinc acetate and zinc chloride) were tried. From the structural, electrical, morphological, optical and junction studies, zinc acetate and stannic chloride were adjudged as the precursor for zinc and tin respectively. By varying substrate temperature from 300 to 400 ^{o}C, CZTS films were prepared and through various characterizations, 350 ^{o}C was fixed as the optimum substrate temperature. In order to get stoichiometric CZTS film 'Cu' concentration in the precursor solution is varied from 0.01 M to 0.03 M by fixing the molarities of 'Zn', 'Sn' and 'S' at 0.01, 0.01 and 0.12 M respectively. Single phase stoichiometric CZTS film was obtained for 'Cu' concentration of 0.015 M. To study the effect of spray rate on the optoelectronic properties of sprayed CZTS thin films, we varied the spray rate from 2 ml/min to 10 ml/min. From structural and optical analysis 6 ml/min was adjudged as the optimum spray rate.

Chapter 4 is on the fabrication of heterojunction using CZTS as the absorber layer and In_2S_3 as the buffer layer. Efficiency of the device, prepared using CZTS as absorber layer and pristine In_2S_3 as buffer layer, was only 0.3 %. Low short circuit current and fill factor due to the high series resistance of the device were identified as the reasons for poor performance. Since the major reason for series resistance is the high resistance of the In_2S_3 buffer layer, "Ex-situ" diffusion of 'In' was done in order to reduce the resistivity. Different thickness of 'In' were deposited over the In_2S_3 buffer layer through vacuum evaporation and annealed at 100 ^{o}C for 1 hour in order to diffuse it in to the layer. Analysis showed that for each thickness of In_2S_3 layer there was an optimum thickness of 'In' for which performance parameters were maximum. For 500 nm thick In_2S_3 layer, optimum thickness was 8 nm. By optimum 'In'

diffusion, efficiency and fill factor of the CZTS /In_2S_3 heterojunction were enhanced to 1.51 % and 44 % respectively. To explore the potential of chemical spray pyrolysis technique we fabricated a device having an area of 16 cm^2.

Chapter 5 of the thesis deals with improvement of performance parameters of the CZTS/In_2S_3 heterojunction through the modification of CZTS absorber layer. In order to decrease rate of precipitation, pH of the spray solution was decreased. By analysing the junction properties we optimized suitable pH and then in order to get the suitable Cu/(Zn+Sn) ratio and Zn/Sn ratio, we varied the molarity of 'Cu' and 'Sn' in the precursor solution. For the device fabricated using optimized CZTS layer, efficiency and fill factor of the device improved to 1.85 % and 52 % respectively. By using a 'double layer structure' with different stoichiometry on each layer, the efficiency could be enhanced to 2.52 %. Finally the fabrication of an "all sprayed" thin film solar cell using FTO, instead of ITO, with a conversion efficiency of 1.25 % is presented.

Chapter 6 is the summary of the work, where important conclusions are highlighted. Future prospects of the work are also presented.

Contents

Chapter 1

INTRODUCTION ---------- 01 - 53

1.1 Problems of the energy economy ---------- 01
1.2 Why Solar Energy? ---------- 02
1.3 Thin Film Photovoltaics ---------- 03
1.4 Possible materials ---------- 04
1.5 CZTS thin films ---------- 08
1.5.1 Structural properties ---------- 09
1.5.2 Electrical properties ---------- 11
1.5.3 Optical properties ---------- 12
1.6 CZTS Thin Film Deposition Techniques ---------- 13
1.6.1 Vacuum based approaches ---------- 14
1.6.1.1 Evaporation ---------- 14
1.6.1.2 Sputtering ---------- 16
1.6.1.3 Pulsed Laser Deposition ---------- 21
1.6.2 Non-vacuum techniques ---------- 22
1.6.2.1 Sol-Gel method ---------- 22
1.6.2.2 Spray pyrolysis technique. ---------- 24
1.6.2.3 Electrodeposition ---------- 27
1.6.2.4 Other non-vacuum techniques ---------- 30
1.7 CZTS cell works ---------- 33
References ---------- 41

Chapter 2

THEORY OF SOLAR CELLS ---------- 55 - 70

2.1 Introduction ---------- 55
2.2 Solar radiation ---------- 55
2.3 p-n junctions as solar cell ---------- 56
2.3.1 p-n junction under equilibrium ---------- 57
2.3.2 p-n junction under bias ---------- 58
2.3.3 p-n junction under illumination ---------- 59
2.4 Performance parameters of a solar cell ---------- 62
2.4.1 Open circuit voltage (V_{oc}) ---------- 62
2.4.2 Short circuit current (I_{sc}) ---------- 63
2.4.3 Fill factor (FF) ---------- 65
2.4.4 Efficiency (η) ---------- 65
2.5 Diode parameters of a solar cell. ---------- 67

2.5.1 Series resistance (R_s) ---- 67
2.5.2 Shunt resistance (R_{sh}) ---- 68
2.5.3 Ideality factor (n) ---- 69
2.5.4 Reverse saturation current (I_0) ---- 69
References ---- 70

Chapter 3
PREPARATION AND CHARACTERIZATION OF CU_2ZnSnS_4 ABSORBER LAYER USING CHEMICAL SPRAY PYROLYSIS TECHNIQUE ---- 71 -107

3.1 Introduction ---- 71
3.2 Deposition technique: Chemical spray pyrolysis ---- 72
3.3 Effect of deposition parameters ---- 73
3.3.1 Choice of precursor's ---- 73
3.3.1.1 Deposition of CZTS using various precursors ---- 74
3.3.1.2 Structural studies ---- 74
3.3.1.3 Compositional analysis ---- 77
3.3.1.4 Electrical properties ---- 79
3.3.1.5 Hall measurements ---- 80
3.3.1.6 Morphological studies ---- 81
3.3.1.7 Optical Studies ---- 82
3.3.1.8 Fabrication of junction ---- 84
3.3.1.9 XPS analysis of junction ---- 86
3.3.2 Effect of substrate temperature ---- 87
3.3.2.1 Structural studies ---- 88
3.3.2.2 Optical properties ---- 89
3.3.2.3 Thickness measurement ---- 89
3.3.2.4 Electrical analysis ---- 90
3.3.2.5 Compositional analysis ---- 90
3.3.3 Effect of copper concentration ---- 91
3.3.3.1 Compositional analysis ---- 91
3.3.3.2 Structural analysis using XRD ---- 92
3.3.3.3 Structural analysis using Raman spectra ---- 93
3.3.3.4 Morphological studies ---- 95
3.3.3.5 Optical studies ---- 96
3.3.3.6 Electrical studies ---- 97
3.3.4 Effect of spray rate ---- 98
3.3.4.1 Structural characterization ---- 98
3.3.4.2 Optical studies ---- 99
3.3.4.3 Electrical studies ---- 100
3.4 Conclusions ---- 101
References ---- 103

Chapter 4

FABRICATION OF CZTS/ In_2S_3 SOLAR CELL AND ITS IMPROVEMENT THROUGH MODIFICATION OF In_2S_3 LAYER ---------- 109 -134

4.1 Introduction ---------- 109
4.2 Review of devices employing In_2S_3 buffer layer---------- 110
4.2.1 Spray pyrolysis ----------110
4.2.2 Chemical bath deposition (CBD)----------111
4.2.3 Atomic layer deposition (ALD) ----------112
4.2.4 Physical vapour deposition (PVD) ----------113
4.3 CZTS/In_2S_3 heterojunction using chemical spray pyrolysis technique.---------- 113
4.4 Improvements of CZTS/In_2S_3 cell parameters ---------- 115
4.4.1 Experimental details ----------115
4.4.2 Structural analysis----------116
4.4.3 XPS studies ----------117
4.4.4 Optical studies----------119
4.4.4.1 Optical absorption studies ----------119
4.4.4.2 Photoluminescence studies ----------120
4.4.5 Electrical studies ----------121
4.4.6 Junction trials using pristine as well as 'In' diffused buffer layer ----------122
4.4.7 J-V characteristics of the CZTS/In_2S_3 heterojunction with 'In' diffused buffer layer. ----------122
4.5 Role of buffer layer thickness ---------- 126
4.6 Large area heterojunction ---------- 129
4.7 Conclusions ---------- 131
References ---------- 132

Chapter 5

ENHANCEMENT OF CELL PARAMETERS BY MODIFICATION OF CZTS ABSORBER LAYER---------- 135 - 156

5.1 Introduction ---------- 135
5.2 Effect of starting solution pH on properties of CZTS layer.------- 136
5.2.1 Experimental ----------136
5.2.2 Structural analysis----------137
5.2.3 Optical studies----------138
5.2.4 Compositional analysis ----------139
5.2.5 Electrical studies ----------139
5.2.6 Junction trials----------139
5.3 Effect of 'Cu' concentration ---------- 141
5.3.1 Structural analysis using X-ray diffraction----------141

5.3.2 Structural analysis using Raman spectra.----------142
5.3.3 Compositional analysis. ----------144
5.3.4 Junction studies ----------144
5.4 Effect of 'Sn' concentration ---------- 146
5.4.1 Experimental ----------146
5.4.2 Junction analysis ----------147
5.5 Effect of double layer structure---------- 148
5.5.1 Experimental ----------148
5.5.2 Junction analysis ----------149
5.6 All sprayed FTO/CZTS/In_2S_3 solar cell---------- 153
5.6.1 Experimental ----------153
5.6.2 Junction analysis ----------154
5.7 Conclusions ---------- 155
References ---------- 156

Chapter 6
SUMMARY OF THE PRESENT WORK AND FUTURE PROSPECTS ---------- 157 - 159

Publications

JOURNAL PUBLICATIONS

[1]. "Role of precursor solution in controlling the optoelectronic properties of spray pyrolysed Cu_2ZnSnS_4 thin films*"* , **V. G. Rajeshmon**, C. Sudha Kartha, K. P. Vijayakumar, C. Sanjeeviraja, T. Abe, Y. Kashiwaba, ***Solar Energy*** **85** (2011) 249–255.

[2]. *"*Modification of the optoelectronic properties of sprayed In_2S_3 thin films by indium diffusion for application as buffer layer in CZTS based solar cell*"*, **V.G. Rajeshmon,** N. Poornima, C. Sudha Kartha, K. P. Vijayakumar, ***J. Alloys Compd.*** **553** (2013), 239-244.

[3]. "Reliable and damage-free estimation of resistivity of ZnO thin films for photovoltaic applications using photoluminescence technique*",* N. Poornima, T. V. Vimalkumar, **V. G. Rajeshmon**, C. Sudha Kartha, K. P. Vijayakumar*,* ***International Journal of Photoenergy****,* **2013** (2013) 1-9.

[4]. "Probing the defects in spray deposited CZTS thin films using photoluminescence technique", N. Poornima, **V. G. Rajeshmon**, C. Sudha Kartha, K. P. Vijayakumar; under review in SOLMAT

[5]. "Improvement of performance parameters of sprayed CZTS solar cell using double layer structure for CZTS*"*, **V. G. Rajeshmon**, M. R. Rajeshmenon, C. Sudha Kartha and K. P. Vijayakumar, To be communicated.

CONFERENCE PROCEEDINGS

[1]. *"*Spray pyrolysed Cu_2ZnSnS_4 solar cell using 'Cd' free buffer layer*"* **V. G. Rajeshmon**, C. Sudha Kartha, K. P. Vijayakumar, AIP. Conf. Proc. **1349** (2011) 683-684

[2]. "Effect of variation of tin concentration on the properties of Cu_2ZnSnS_4 thin films deposited using chemical spray pyrolysis", **V. G. Rajeshmon**, Abin

Kuriakose, C. Sudha Kartha, K. P. Vijayakumar, AIP. Conf. Proc. **1512** (2013) 1206-1207.

[3]. *"*Defect analysis of CZTS thin films using photoluminescence technique" N. Poornima, **V. G. Rajeshmon**, C. Sudha Kartha, K. P. Vijayakumar, AIP. Conf. Proc. **1512** (2013) 464-465.

[4]. *"*Preparation and characterization of spray pyrolysed ZnS thin films and the effect chlorine doping*"* Anjaly Jose, **V. G. Rajeshmon**, N. Poornima, C. Sudha Kartha, K.P. Vijayakumar., AIP. Conc. Proc.**1349** (2011) 707-708.

[5]. *"*Modification of optoelectronic properties of sprayed CZTS thin films through spray rate variation" **V. G. Rajeshmon**, C. Sudha Kartha, K. P. Vijayakumar., Accepted for publication in AIP. Conf. Proc.

[6]. *"*Photoluminescence studies on off-stoichiometric defects in sprayed CZTS thin films" N. Poornima, **V. G. Rajeshmon**, C. Sudha Kartha, K. P. Vijayakumar., Accepted for publication in AIP. Conf. Proc.

[7]. *"*Copper doping; an effective method for improving optoelectronic properties of sprayed SnS thin films" Gisa Grace Ninan, **V. G. Rajeshmon**, C. Sudha Kartha, K. P. Vijayakumar., Accepted for publication in AIP. Conf. Proc.

[8]. *"*XPS depth study of sprayed CZTS thin films" D. R. Deepu, **V. G. Rajeshmon**, C. Sudha Kartha, K. P. Vijayakumar., Accepted for publication in AIP. Conf. Proc.

CONFERENCE PRESENTATIONS

International:

[1]. "Effect of 'In' diffusion on the properties of sprayed CZTS/In_2S_3 solar cell", **V. G. Rajeshmon**, C. Sudha Kartha, K P Vijayakumar, ICMAT- 2011, NUS, Singapore.

National:

[1]. *"*Effect of substrate temperature on the properties of spray deposited Cu_2ZnSnS_4 thin films*"* **V. G. Rajeshmon**, C. Sudha Kartha, K. P. Vijayakumar, Proceedings of MRSI-AGM, Feb 10-12 2009.

[2]. *"*Characterization of Cu_2ZnSnS_4 thin films with different copper concentration in the precursor solution*"* **V. G. Rajeshmon**, C. Sudha Kartha, K. P. Vijayakumar NCEMSC-2010, Jan 23-24, 2010.

[3]. *"*Improvisation of the performance parameters of sprayed Cu_2ZnSnS_4/In_2S_3 solar cell*"* **V. G. Rajeshmon**, C. Sudha Kartha, K. P. Vijayakumar, HTFT-2011, Jan 20-21, 2011.

.....ꕥ.....

Chapter 1

INTRODUCTION

1.1 Problems of the energy economy
1.2 Why Solar Energy?
1.3 Thin Film Photovoltaics
1.4 Possible materials
1.5 CZTS thin films
1.6 CZTS Thin Film Deposition Techniques
1.7 CZTS cell works

This thesis is devoted to the development of thin film solar cells using a relatively new, rapidly developing quaternary semiconducting material (viz., Cu_2ZnSnS_4) through spray technique. This semiconductor, commonly known as CZTS, is closely related to the family of materials that have been used for the development of solar cell applications **[1]**. ***It is a compound semiconductor made of copper, zinc, tin and sulfur, which are sufficiently abundant elements; more over none of them is harmful to the environment. At first the influence of various spray parameters like substrate temperature, spray rate, precursor ratio etc., on the opto-electronic properties of CZTS films are studied in detail. Then the fabrication of CZTS/In_2S_3 heterojunctions and various ways to improve the performance parameters are discussed.***

1.1 Problems of the energy economy

Achievement of energy security necessitates diversification of our energy resources. Energy economy of nearly all countries (in particular, that of the industrialized countries) is based on the use of stored energy, mainly fossil energy in the form of coal, oil and natural gas, as well as nuclear energy in the form of the uranium isotope U235 [2].

Ever-increasing prices for petroleum products, projection that petroleum resources would be exhausted in a relatively short period of time and the use of fossil fuel resources for political purposes will adversely affect worldwide economic and social development[3]. The impact of the energy crisis is particularly felt in developing countries like India, where a large percentage of national budget earmarked for development must be diverted to the purchase of petroleum products. For nuclear power plants also there are problems, related to fuel processing and dumping of used fuel. In addition, global warming caused largely by green house gas emission from fossil fuel generating systems is also a major concern [4].

To overcome such perennial problems associated with conventional sources of energy, most countries, including India, have shifted their focus to develop non-conventional renewable sources of energy. Among these the prominent resources are solar, wind, geothermal, biomass and small hydropower.

1.2 Why Solar Energy?

Current trends suggest solar energy will play a vital role in future energy production. Indeed solar energy alone has the capacity to meet all the planet's energy needs for the foreseeable future. The sun deposits ~ 120,000 TW of electromagnetic radiation on the surface of the Earth, far exceeding human needs even in the most aggressive energy demand scenarios. Covering just 0.16 % of the land on Earth with 10 % efficient solar conversion systems would provide 20 TW of power, which is nearly twice the world's present consumption rate of fossil energy (or equivalent of 20,000 1-GW_e nuclear fission plants) [5-7]. These comparisons illustrate the incredible magnitude of the solar resource, providing an energy stream far more potent than present-day human technology can achieve.

A solar energy source provides pollution-free, self-contained, reliable, quiet, long-term, maintenance-free, and year-round continuous and unlimited operation at moderate costs. Despite all these benefits of solar cells and nearly 55 years after their invention, this device is generating only 0.04 % of the world's on-grid electricity, mainly due to the high cost of solar cells, making it beyond the reach of the common consumer. Based on the statistical review of world energy consumption in 2007, 30 % of the electrical energy is generated from coal, 16 % from natural gas, 15 % from water generators, 9 % from oil, 4 % from nuclear reactors, and only 1 % from solar cells [8].

Western countries such as the United States, Germany, Japan, Brazil, Italy, Spain, and many other European countries are turning to electrical power generation from solar cells, because of the high capital investments, radiation, and carbon dioxide emissions associated with coal-based, nuclear-based, gas-based, and oil-based power plants.

1.3 Thin Film Photovoltaics

Photovoltaics (PV) market has been booming, over recent years, with sales almost completely dominated by product based on the use of silicon wafers, similar to those used in microelectronics. The two parameters often cited for terrestrial solar cells are its efficiency and cost. The bottleneck for solar electricity to become a household energy source is mainly the cost. Wafer costs account for over 50 % of the total module cost. One way of eliminating this major cost component is the replacement of wafers by thin films of (compound) semiconductors deposited onto a supporting substrate [9].

The key motivation for thin film solar cells was, and still is, the potential for high speed/high throughput manufacturing and minimum material requirements to reduce cost [10]. Compared to crystalline silicon solar cells much less material is

expended in the case of thin film solar cells. As the absorption coefficient of typical thin film absorber materials is ~100 times higher than crystalline silicon, a 100 times thinner layer of thin film materials can absorb an equivalent amount of energy as crystalline silicon. While crystalline silicon needs 100 cm^3 (100 μm· 1 m· 1 m) material for 1 m^2 solar cell, only 1 cm^3 is needed for thin film material.

In addition, purity and crystal quality requirements on thin film solar cell materials are less stringent than in crystalline silicon solar cells [11]. Thus, thin film solar cells are cheaper to produce than silicon solar cells. Another advantage of the thin film solar cells is that they can be fabricated on flexible materials like metal foils or polyimides, which allows completely new applications. Furthermore, installations of silicon cells require heavy glass protection plates, which reduce residential applications [12].

Yet another advantage is that it is possible to adjust the band gap of thin film materials by varying composition. By this, larger portion of the solar spectrum can be utilized much better and higher efficiency can be achieved, because the theoretical possible efficiency depend strongly on the band gap.

1.4 Possible materials

There are some important criteria to be satisfied by the materials for thin film solar cells. A fundamental qualification is of course a large absorption coefficient, since almost all of the available photons should be absorbed in only a few micrometers. Furthermore, the band gap should be in the range of roughly 1–1.7 eV as per theoretical calculations to reach sufficient efficiency. Quite a lot materials fulfill these conditions (figure 1.1). When it comes to semiconductor the most popular one is of course silicon. In thin film solar cell technology amorphous silicon (a-Si) is one of the suitable material. It is a disordered

material whose properties are significantly different from those of crystalline silicon. For example, the band gap increases from 1.1 eV in crystalline silicon to 1.7 eV in amorphous silicon and the absorption coefficient of a-Si is much higher than that of crystalline silicon.

An approach that is often followed when it becomes necessary to find alternative materials is the principle of isoelectronic or cross substitution [13]. Following the isoelectronic substitution, atoms of the group IV (Si) are substituted by an equal number of cations and anions of group III and V or II and VI respectively to form binary compounds such as GaAs or CdTe. Further compound semiconductor can be formed by substituting half of the group-II element with a group-I and half with a group-III element. A common example for such a I–III–VI compound semiconductor is copper indium selenide ($CuInSe_2$) or replacing partly the indium by gallium to modify the band gap to form copper indium gallium selenide ($CuInGaSe_2$). Various other substitutions are also possible, for example replacing half of the group-III element with a group-II element and half with a group-IV element. Substitution of In/Ga in CIGS with 'Zn' and 'Sn', leads to CZTS ($Cu_2ZnSnSe_4$). But it should be realized that all substituitional compounds will not work. Only those materials which form suitable junctions with other materials and exhibit a photovoltaic effect when exposed to light are suitable for thin film solar cell applications.

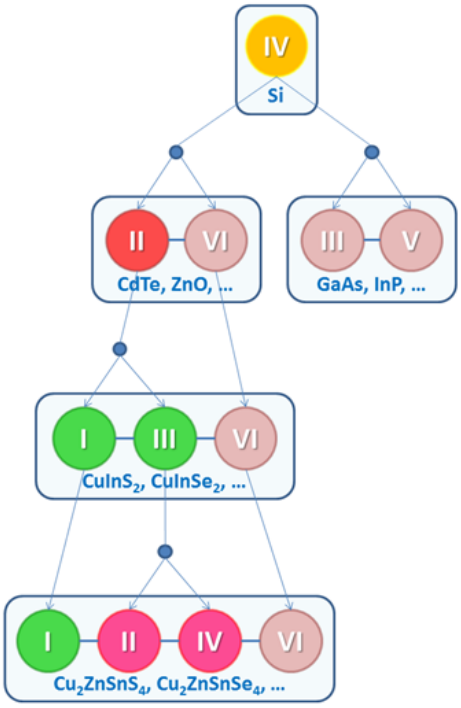

Figure 1.1. Various possible compound semiconductors obtained by gradual substitution of elements from higher and lower groups.

Thin film solar cell technologies emerged in the 1960s with Cu_2S/CdS, which was the first (flexible) thin film solar cell and the first to achieve 10 % efficiency in 1981 [14]. From 1970 through the 1980s, $CuInSe_2$ [15], CdTe [16], and a-Si [17] became the solar cell materials of interest with all the three achieving ~10 % efficiency. In the 1990s, however, performance levels of the thin film solar cells increased with $CuInGaSe_2$ >19 % [18], CdTe> 16 % [19], and a-Si > 10 % (stabilized) [20].

Thin film solar cells based on direct band gap materials such as copper indium (gallium) selenide (CIGS) and cadmium telluride (CdTe) have reached the commercialization stage with highest reported conversion efficiency of 15 % in module production [21]. Cadmium telluride (CdTe) thin film module is currently the least expensive, with module production cost of $ 0.76/Wp [22].

Table 1.1. Confirmed terrestrial cell and sub module efficiencies (η) measured under the global AM1.5 spectrum (1000 W/m^2) at 25 °C (IEC60904-3: 2008, ASTM G-173-03 global) [21].

Classification	η (%)	Area (cm^2)	V_{oc} (mV)	J_{sc} (mA/cm^2)	FF (%)	Description
CIGS	20.4	0.5203	736.3	35.08	78.9	EMPA Flexible CIGS
CdTe	19.6	1.0055	857.3	28.59	80	GE Global research
a-Si	10.1	1.036	886	16.75	67.8	Oerlikon Solar lab.
CZTS	8.5	0.2382	708	16.83	70.9	Toyota Central R&D laboratories
CZTSSe	11.1	0.4496	459.8	34.54	69.8	IBM Solution grown
Organic thin film	11.1	0.159	867	17.81	72.2	Mitsubishi Chemical

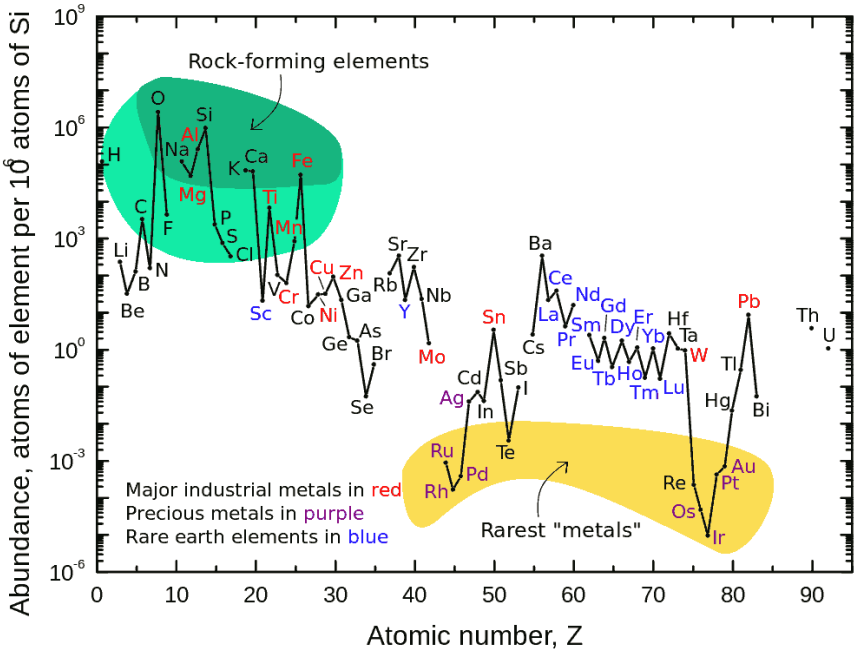

Figure 1.2.Relative abundance of various elements in the earth's crust.

Unfortunately there are drawbacks to both of these technologies. Cadmium is toxic and there are issues around the potential scarcity, and consequent volatility in cost, of both indium (In) and tellurium (Te) [23]. This can be seen in figure 1.2, which shows that tellurium is about as scarce as gold. Indium, whilst somewhat more common, is in great demand for many alternative uses and has seen enormous price volatility over the past 10 years - around a 10-fold increase in price between 2003 and 2009. To overcome the possible future effects of 'In' scarcity on TW-scale consumption, it has been projected that CIGS can be replaced by kesterite CZTS.

1.5 CZTS thin films

Recently considerable work has been done on the quaternary compound semiconductor, Cu_2ZnSnS_4 (CZTS) to make it a good absorber layer for thin film solar cells [24-25] and thermoelectric power generators [26]. CZTS has talented physical properties, such as the direct band gap (~1.5 eV), high optical absorption coefficient ($>10^{-4}$ cm^{-1}), low thermal conductivity etc. CZTS is derived from the CIGS structure by the isoelectronic substitution of two 'In' (or one 'In' and one 'Ga') atoms by one 'Zn' and one 'Sn' atom. As a consequence, CZTS has some similar properties as CIGS. The availability of copper, zinc, tin and sulfur in the earth's crust are 50, 75, 2.2 and 260 ppm respectively. But availability of indium is only 0.049 ppm [27]. i.e., all the constituents of CZTS are abundant in the earth's crust.

Intrinsic point defects in CZTS make its conductivity p-type. Crystal structure of CZTS can tolerate some deviation from stoichiometry [28] making its deposition process easier. Moreover grain boundaries in CZTS thin films are favorable to enhance the minority carrier collection [11].

Theoretical calculations have shown that conversion efficiency as high as 32.2 % [29] is possible for CZTS thin film solar cells with a CZTS layer of few micrometers. Wadia et al. [30] calculated the minimum cost of raw materials for the existing PV technologies and the emerging PV technologies (figure 1.3). Cost of raw material for CZTS PV technology is much lower than that of the three existing thin film PV technologies.

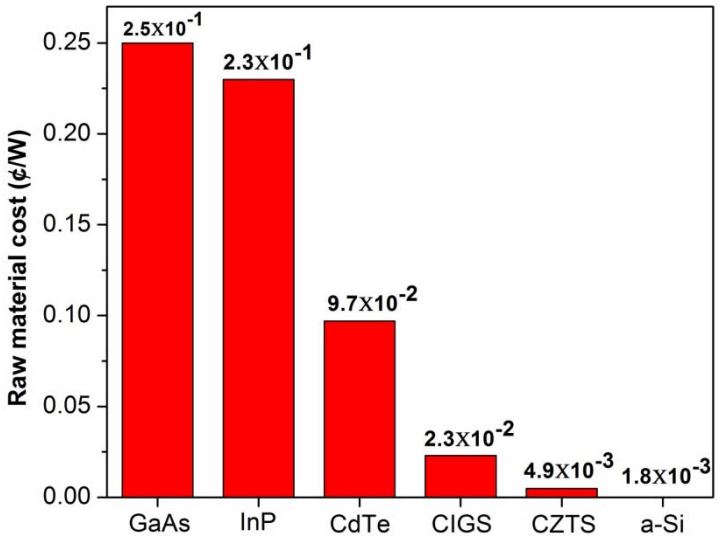

Figure 1.3. Minimum ¢/W (Cent/Watt) for major photovoltaic materials. Here cost of processing the material for PV grade applications is larger and should be evaluated further.

1.5.1 Structural Properties

Crystallographically, CZTS has two principal structures, known as stannite type and kesterite type. These two structures are similar except for the different arrangements of 'Cu' and 'Zn' atoms (figure 1.4). However, CZTS material usually appears in kesterite phase because it is thermodynamically more stable as compared to stannite type [31-32]. Commonly observed X-ray diffraction peaks for this material corresponds to the lattice planes (112), (200), (220/204), and (312/116) with preferred orientation along (112) [33-36]. Peaks corresponding to

(002), (008), (101), (103), (105), (110), (211), (213), (224) and (332) planes were also reported[37-42].

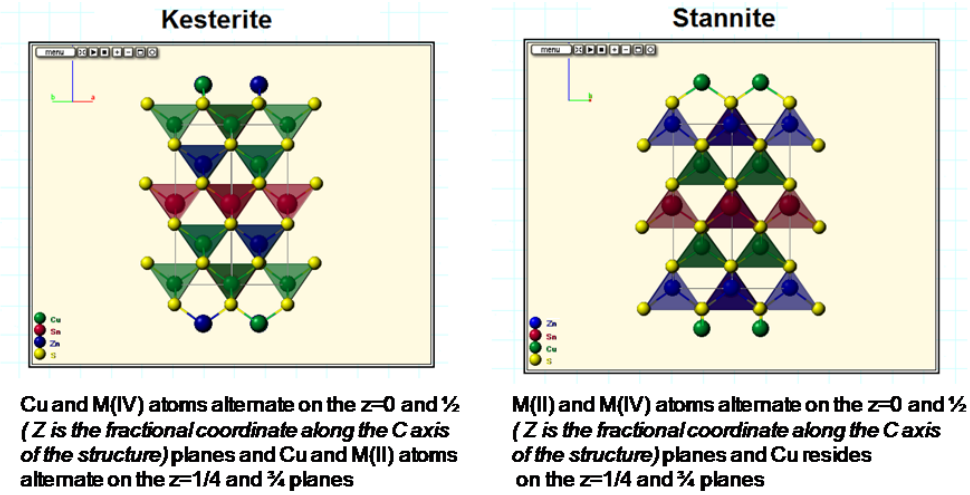

Figure 1.4. Two possible crystal structures of copper zinc tin sulfide (CZTS)

Table 1.2. Lattice data of the kesterite CZTS single crystal

2θ (degrees)	d (Å)	(hkl)	I/I_o (%)
16.338	5.421	002	1
18.205	4.869	101	6
23.101	3.847	110	2
28.530	3.126	112	100
29.675	3.008	103	2
32.989	2.713	200	9
37.025	2.426	202	1
37.966	2.368	211	3
40.758	2.212	114	1
44.996	2.013	105	2
47.331	1.919	220	90
56.177	1.636	312	25
56.858	1.618	303	3
58.969	1.565	224	10
64.177	1.450	314	1
69.229	1.356	008	2
76.442	1.245	332	10

Schäfer and Nitsche [43] reported the detailed lattice data of a CZTS single crystal in 1974 (table 1.2). Thereafter, this data was frequently referred to determine CZTS phase in literatures.

Washio et al. [44] investigated the relationship between composition and kesterite crystal structure of CZTS thin films. They choose three Cu/(Zn+Sn) composition ratios of about 1.2 (non-photovoltaic composition ratio), 1.0 (non-photovoltaic composition ratio), and 0.8 (photovoltaic composition ratio). It was found that when Cu/Zn+Sn ratio is 0.8, 'Cu' substitutes for 'Zn' at the 2d site and/or 'Zn' substitutes for 'Cu' at the 2c site. They claimed that high performance of CZTS thin films in photovoltaic activity is due to the kesterite crystal structure.

The lattice constants for CZTS are a=0.54 nm and c=1.09 nm [45]; from that one can calculate (with the atomic masses of 'Cu', 'Zn', 'Sn' and 'S') density of CZTS, which is ≈ 4.6 g/cm^3 [46]. The quaternary Cu–Zn–Sn–S system is also interesting from the viewpoint of fundamental science, as it further increases the complexity of the defect chemistry and electronic structure, while providing additional opportunities for material optimization by control of stoichiometry and compositional gradients.

1.5.2 Electrical properties

Doping of CZTS material occurs by internal defects. First principle theoretical calculations of the formation energy and the transition energy levels for a series of intrinsic point defects and defect complexes in CZTS shows that 'Cu' atoms sitting on the places of 'Zn' atoms (Cu_{Zn}antisite) causes p-type conductivity which has a lower formation energy and relatively deeper acceptor level compared to the 'Cu' vacancy [47]. All donor defects have higher formation energy, consistent with the experimental verification of p-type conductivity. The

low formation energy of acceptor defects makes n-type doping difficult in CZTS.

Most of the reported resistivity values of CZTS thin films vary from ~10^{-3} Ω.cm to 10^{1} Ω.cm [25, 48-52] but resistivity values as high as 10^{4} Ω.cm were also reported [53]. The hole concentration was reported to vary from 10^{16} cm^{-3} to 10^{21} cm^{-3} [54-57]. Hall effect measurement results showed that hole mobility of CZTS changed from lower than 0.1 to as high as 30 $cm^2.V^{-1}.s^{-1}$, while most published values were in the range of 1 to 10 $cm^2.V^{-1}.s^{-1}$ [56-60]. Lower mobility indicates that the optimized thickness of absorber layer in CZTS thin film solar cells cannot be as large as that for CIGS thin film solar cells.

1.5.3 Optical properties

Theoretically the band gap of stoichiometric kesterite CZTS is calculated to be 1.5 eV by Chen et al. [61]. They have performed hybrid functional calculations (HSE06) at experimental lattice constants, where 25 % of the GGA exchange potential is replaced by screened Fock exchange. The bandgap reported for CZTS prepared from various deposition techniques varied from 1.4 eV to 1.55 eV [57, 62-65]. Very low bandgap of 1.20 eV is also reported due to deviation in stoichiometry [66].

The absorption coefficient of CZTS thin films is greater than 10^{4} cm^{-1} [42, 67]. Zhao et al. [68] theoretically determined high frequency dielectric constant ofCZTS, CISe, CGSe and CZTSe using three different approaches. All the three approaches give the same size order of dielectric constants with ε_∞ (CZTS) < ε_∞ (CISe, CGSe) < ε_∞ (CZTSe). For CZTS the value is about 6.8. The high-frequency dielectric constant, $\varepsilon_\infty = n^2 (\lambda \rightarrow \infty) = A+1$ (A is the fitting parameter in first order Sellmeier's equation) was determined to be 6.92 for CZTS bulk crystals [69]. Seol et al. [62] reported a refractive index value of 2.07 for RF

magnetron sputtered CZTS thin film deposited with 75 mW of RF power and annealed at 400 ^{o}C.

Low temperature photoluminescence spectra were carried out by researchers to find out the recombination mechanism in CZTS thin films. In most of the reports a broad peak centered at ~ 1.2 eV was observed. A model of radiative recombination of an electron with a hole bound to an acceptor level, broadened by potential fluctuations of the valence-band edge, was proposed by Leitaoet al. [70-71]. According to Unold et al. [72], the broad transition peak and its strong blue shift with excitation intensity indicates donor-acceptor pair transitions under the influence of potential fluctuations. Miyamoto et al. [73] observed a broad luminescence between 1.1 and 1.4 eV. Origin of the photoluminescence was attributed to donor-acceptor pair recombination with activation energy of 39 and 59 meV for stoichiometric CZTS and Cu-poor, Zn-rich CZTS respectively.

Photoluminescence (PL) from CZTS bulk single crystals was studied as a function of temperature and excitation intensity by Tanaka et al. [74]. The broad emission between 1.1 and 1.45 eV was attributed to donor-acceptor pair recombination with activation energy of 48 meV. Broad emissions at around 1.45 eV and 1.31 eV were observed by Oishi et al. [75] in the PL spectrum of CZTS thin films measured at 13 K. They assigned the peak at ~ 1.45 eV to the donor-acceptor pair transition. Time-resolved PL data illustrates that lifetime of free carriers in CZTS thin film was lower than 1 ns [76], much lower than that of CIGS device which is beyond 50 ns [77].

1.6 CZTS Thin Film Deposition Techniques

The increasing awareness of CZTS as a potentially ideal candidate as photovoltaic absorber material is mainly due to the abundance and variety of

routes that have been developed for thin-film deposition. To determine the most promising technique for the fabrication of thin film solar cells, the overriding criteria are that the deposition can be completed at low cost while maintaining high deposition or processing rate with high yield and reproducibility. There exists a wide variety of vacuum and non-vacuum based techniques. For each of these deposition techniques, one key barrier toward a reliable and low-cost process is the complexity for preparing single phase films. A second common theme generally encountered is the challenge of compositional control during deposition of the film. Despite these challenges, reasonably successful film deposition and device fabrication has been demonstrated for CZTS using both vacuum and non-vacuum deposition techniques.

1.6.1 Vacuum based approaches

The potentially high uniformity of vacuum deposition methods, together with their capacity to deliver precisely timed elemental fluxes, provides good opportunity for fabrication of high quality thin film devices. These techniques involve deposition of constituent atoms of the CZTS compound on a substrate either by sputtering or by evaporation/co-evaporation of the target sources under optimized pressure and temperature.

1.6.1.1 Evaporation

Evaporation is a well-known technique in the development of thin film solar cells. Based on the success of evaporated CIGS materials [78], initially evaporation was selected as the principal deposition technique for CZTS thin films too. From 1996 onwards Prof. Katagiri's group worked extensively on CZTS thin films deposited using electron beam (EB) evaporation followed by sulfurization. In the first report they deposited precursors, Cu/Sn/Zn stacked layers ('Zn' on bottom of stack), by EB evaporation [53]. In order to obtain

CZTS films they sulfurized precursors at 500 ^{o}C in N_2+ H_2S (5 %) atmosphere. The films obtained were p-type with a bandgap of 1.45 eV and absorption coefficient greater than 10^4 cm^{-1}. Grain size of the films is extremely large (~3 μm) compared with the film thickness of 1.9 μm. They obtained very high value of resistivity of the order of 10^4 Ω.cm. In another report during the same year they reported an even high value for resistivity of the order of 10^5 Ω.cm, by increasing the hold time for sulfurization [79].

In 2001, Katagiri et al. [80] reported the preparation of CZTS using ZnS as precursor for 'Zn', while precursors for 'Sn' and 'Cu' were same as earlier work. Use of ZnS instead of 'Zn' increased the adhesion of the CZTS film and they could bring down the resistivity to 3.9×10^2 Ω.cm. In another report they tried different thickness of precursor layers and found that resistivity of the films decreased from 10^4 to 10^{-2} Ω.cm, when Cu/(Zn+Sn) ratio increased from 0.9 to 1.1 [39].

In 2005, Katagiri et al. [81] prepared CZTS thin films by varying Cu/(Zn+Sn) ratio from 0.49 to 1.18. They reported that the band gap energy increased and the absorption of the tail region decreased with increase in Cu/(Zn+Sn) ratio up to 0.9. For CZTS films whose Cu/(Zn+Sn) ratio was over 0.94, absorption of the tail region was extremely elevated due to the presence of binary phases of 'Cu' and 'S'. They concluded that CZTS films with Cu/(Zn+Sn) ratio from 0.8 to 0.9 are suitable as absorbers. In the same year, same group [82] has shown that the ordering of precursors can improve the surface morphology of the films.They fabricated films using the modified precursor with the stacking order of Sn/Cu/ZnS. From SEM micrographs they found that the surface morphology was much improved using the new order of precursors.

In 2006, Tanaka et al. [83] prepared CZTS thin films by co-evaporation of elemental sources. Larger and densely packed grains were formed as substrate

temperature increased. Oishi et al. [75] deposited CZTS films on 'Si' substrates by multisource evaporation. They confirmed the tetragonal structure of films from RHEED patterns. Broad emissions at ~ 1.45 eV and 1.31 eV were observed in the PL spectrum measured at 13 K. The peak at ~1.45 eV was assigned to the donor–acceptor pair transition. Multistage evaporation technique is used for the deposition of CZTS thin films by Weber et al. [84]. They investigated two different stage sequences: (A) using Cu_2SnS_3 as precursor to react with Zn-S and (B) using ZnS as precursor to react with Cu-Sn-S. Both sequence results in formation of CZTS, while SEM micrographs reveal that films of sample type B are denser and have larger crystallites than for sample type A. In 2011, near stoichiometric single phased polycrystalline CZTS thin films were prepared by fast coevaporation process [85]. They showed that Cu-rich growth conditions lead to the segregation of a CuS secondary phase. Nearly stoichiometric CZTS thin films were prepared by sulfurization of simultaneously evaporated Cu/Zn/Sn metal alloy films.

In 2012, Xinkun et al. [60] deposited Sn/Cu/ZnS precursors, by evaporation, on soda lime glass at room temperature, and then polycrystalline thin films of CZTS were produced by sulfurizing the precursors in a sulfur atmosphere at 550 ^{o}C for 3 hour. Carrier concentration, resistivity and mobility of the deposited film are found to be 6.98×10^{16} cm^{-3}, 6.96 Ω.cm and 12.9 $cm^2.V^{-1}.s^{-1}$ respectively. Recently CZTS thin films were prepared by flash evaporation followed by annealing in 'Ar' atmosphere [86]. The desired kesterite composition for solar cell applications was achieved by using a Zn-rich compound as the evaporation source plus a thermal treatment at 620 °C in 'Ar' atmosphere.

1.6.1.2 Sputtering

Sputtering has been extensively used by researchers to deposit high quality thin films. Various sputtering technologies such as argon beam, ion beam, DC,

RF, hybrid and reactive magnetron sputtering have been employed for the deposition of CZTS thin films [87]. In the case of CZTS thin films, there are two different approaches: a single step without sulfurization and a two step, deposition of metallic precursors Cu–Zn–Sn/Cu–Zn–Sn–Cu or Cu–ZnS–SnS, followed by a sulfurization.

The first reported CZTS material was made by atom beam sputtering, using pressed and sintered targets produced from synthesized powders, in 1988 by Ito and Nakayama [57]. A sharp peak resulting from (112) plane of the stannite type CZTS appeared for the film deposited at 90 ^{o}C. Hall effect measurement estimated that deposited film had mobility lower than 0.1 $cm^2.V^{-1}.s^{-1}$ and carrier concentration higher than 5×10^{19} cm^{-3}.

Seol et al. [62] deposited CZTS thin films using RF magnetron sputtering technique without substrate heating. Effects of sputtering power and annealing temperature on the properties of CZTS thin films were checked. It was found that the atomic ratio of the thin films deposited between 50 W and 100 W was appropriate. The as-deposited films were amorphous and annealed in the atmosphere of 'Ar'+'S'. With the increase of annealing temperature crystallinity of CZTS thin films was improved and sheet resistance decreased rapidly.

Tanaka et al. [51] for the first time used vacuum based hybrid sputtering to deposit CZTS thin films on a quartz glass substrate. Films were fabricated by the sequential deposition of metal elements and annealing in 'S' flux, varying the substrate temperature from 300 to 500 ^{o}C. Film thickness decreased with increase in substrate temperature. Single phase, stoichiometric CZTS film with stannite structure was obtained at 400 ^{o}C. However, composition of the thin films became Zn-poor at and above 450 ^{o}C. Resistivity, carrier concentration and Hall mobility of the films at 400 ^{o}C were 0.13 Ω.cm , 8×10^{18} cm^{-3} and 6 $cm^2.V^{-1}.s^{-1}$ respectively.

In 2006, Zhang et al. [25] successfully prepared CZTS thin films through sulfurization ofion beam sputtered precursors. Their results show that electrical and optical properties of the prepared films have strong dependence on atomic ratio of the constituents. By optimizing the precursor preparation conditions they obtained low resistivity of ~ 0.156 Ω.cm.

Prof. Katagiri, after doing extensive pioneering work on CZTS employing evaporation based approaches, deposited sputtered CZTS thin films in 2007 [88]. Targets of 'Cu', ZnS and SnS were simultaneously sputtered by RF sources. The finished precursor was automatically transferred to the annealing chamber without being exposed to atmosphere and annealed at 580 ℃ for 3 hours in an atmosphere ofN_2+H_2S (20 %). The deposited film was 2.5 μm thick and having a band gap value of 1.45 eV. The film was Cu-poor and slightly Zn-rich and S-rich (Cu/Zn+Sn: 0.87, Zn/Sn: 1.15, S/metal: 1.17).

In 2009, Fernandes et al. [89] reported preparation of CZTS thin films using sulfurization of (DC magnetron) sputtered Cu/Zn/Sn precursor layers. They got CZTS films having a thickness of 1.5 μm and with the preferential growth orientation along (112) plane. They confirmed the existence of CZTS from the presence of Raman peaks at 338-339 cm^{-1}, 288 cm^{-1} and 256–257 cm^{-1}. In the same year they reported effect of changing precursor's deposition on the morphological and structural properties of CZTS films [90]. From the results the best precursor sequence for the CZTS growth was found to be Mo/Zn/Sn/Cu. The 'Cu' layer on top reduces the loss of 'Zn' and 'Sn'. This allows for a better composition control of the CZTS. In yet another report they reported Raman scattering study of CZTS thin films prepared using DC-magnetron sputtering [42]. Same group reported preparation and characterization of CZTS based solar cells in 2010 [55]. CZTS absorber layer was obtained by sulfurization of DC

magnetron sputtered Zn/Sn/Cu precursor layers. They reported a carrier concentration value of 1.5×10^{17} cm^{-3} for the deposited CZTS layer.

Leitao et al. [71] investigated the optical and structural properties of CZTS thin films grown by sulfurization of DC magnetron sputtered metallic precursors. They reported band gap value of 1.51 eV. The PL revealed an asymmetric broad band with a maximum intensity at 1.24 eV. In a report came in Physical Review B, Leitao et al. [70] studied the structural, optical, electrical and morphological properties of CZTS thin films. A broad and asymmetric band, with peak energy at 1.24 eV, was observed in PL measurements and a model of radiative recombination of an electron with a hole bound to an acceptor level, broadened by potential fluctuations of the valence-band edge, was proposed.

Salome et al. [91] studied incorporation of 'Zn' into a CTS film in the elemental and sulfide forms to get CZTS and influence of H_2 during sulfurization of the CTS films was also studied. They showed that sulfurization of CTS+ZnS under an atmosphere containing H_2 improves significantly the diffusion of 'Zn' into the CTS layer and also prevents losses of 'Zn' by evaporation.

In 2012, Fernandes et al. [92] proposed an AC response equivalent circuit model to describe the admittance measurements of CZTS thin film solar cell grown by sulfurization of stacked metallic precursors. Study of the back contact resistance allowed the estimation of a back contact barrier of 246 meV. Later the same group showed that by increasing the sulfurization time of metallic precursors there is an improvement in both the in-depth homogeneity of composition and the structural and morphological properties of the films [93]. With increasing sulfurization time they obtained a lower free carrier concentration, a wider space charge region and higher conduction activation energy.

From the electrical conductivity and photoconductivity studies on sputtered CZTS it was found that high temperature conductivity is dominated by band conduction and nearest neighbor hopping [94]. However at low temperatures Mott variable-range hopping (VRH) and Efros–Shklovskii VRH were observed. Sousa et al. [95] reported the preparation of CZTS films using a hybrid method, combining RF-magnetron sputtering and evaporation, for the preparation of CZTS films.

Recently in 2010, Yoo et al. [96] fabricated CZTS thin films through sulfurization of RF-sputtered stacked metallic films. Three types of Cu–Zn–Sn metallic films, i.e., Cu-rich (CR), Cu-correct (CC) and Cu-poor (CP) precursor films were sputtered. The $Cu_{2-x}S$ phase was observed in the CR and CC-CZTS films, whereas it was not seen in the CP-CZTS films. All CZTS films exhibited (112) orientation dominant growth, which were confirmed through XRD and Raman scattering measurements. In 2011, same group compared properties of CZTS thin films prepared via spray pyrolysis and sulfurization of metallic precursors deposited through sputtering [97]. The sprayed films were not observed to be grown well with good crystallinity, compared with CZTS films made by sulfurization of stacked metallic films. But they found that application of additional sulfurization to sprayed CZTS films induced great improvement of crystallinity to the level of the sulfurized metallic films.

Mamose et al. [98] prepared CZTS thin films by simultaneous sputtering of metallic targets followed by sulfurization under elemental sulfur atmosphere in a sealed tube. Under high sulfur vapor pressure (1.5 atm) with rapid reaction period, films with good adhesion and large crystal grains were achieved.

Chalapathy et al. [99] deposited CZTS thin films by sulfurization of DC-sputtered Cu/Zn/Sn/Cu precursors in sulfur atmosphere. Films obtained after annealing at 560 and 580 ^{o}C for 30 min exhibited the kesterite structure. Results

showed that sulfurization temperature had strong influence on microstructure and distribution of elements in the films. Shin et al. [100] reported effect of ordering of precursors on properties of CZTS films. Stacked precursor thin films were prepared from 'Cu', SnS_2 and ZnS targets at room temperature with different stacking orders of Cu/SnS_2/ZnS/glass, ZnS/Cu/SnS_2/glass and SnS_2/ZnS/Cu/glass. The stacked precursor thin films were sulfurized in mixed N_2 (95 %)+H_2S (5 %) atmosphere at 550 ^oC for 10 min. From the results the stacking order Cu/SnS_2/ZnS/glass is adjudged so as to obtain good quality CZTS films.

In 2012, Platzer-Bjorkman et al. [101] reported the preparation of CZTS thin films by sulfurization of co-sputtered metallic and sulfur containing precursor films. Larger grains were obtained for films prepared from metallic precursors while more uniform films with fewer voids were obtained for sulfur containing precursors. Khalkar et al. [102] deposited CZTS thin films using co-sputtering technique. Effect of working pressure, target powers, and annealing conditions were studied. Amal and Kim [103] prepared kesterite CZTS by sulfurization of a sputtered Cu–Zn–Sn alloy precursor. The film sulfurized at 550 °C exhibited a dense morphology with no pores.

Ericson et al. [104] prepared reactively sputtered Cu–Zn–Sn–S precursor films and recrystallized by rapid thermal processing to generate CZTS layers. They studied effect of film properties on substrate heating and composition. Recently, Watjen et al. [105] studied effects of annealing at the Mo/CZTS interface. Solar cells based on CZTS absorber layers were deposited using reactive sputtering of precursor layer followed by a short anneal. It was found that during annealing secondary phases were formed in the film and MoS_2 was formed on the interface.

1.6.1.3 Pulsed Laser Deposition

First report on CZTS prepared using pulsed laser deposition (PLD) was in 2006. Sekiguchi et al. [64] deposited CZTS thin films epitaxially on GaP

substrates using PLD. The bandgap of the films was found to be 1.5 eV and films were nearly stoichiometric. In 2007, Moriya et al. [106] prepared CZTS thin films using PLD. Film was Sn- rich and the band gap was 1.5 eV. Next year same group prepared CZTS precursor using PLD and then annealed in N_2+H_2S (5 %) atmosphere [52].

In 2010, Pawar et al. [107] prepared polycrystalline CZTS thin films through PLD at room temperature. Study of laser incident energy revealed that structural, morphological and optical properties were improved up to incident energy of 2.5 J/cm^2. Sun et al. [108] deposited CZTS thin films on heated Mo-coated glass substrates using PLD. Band gap of the films varied from 1.53 to 1.98 eV depending on substrate temperature. From EDAX results all the films were Cu-rich and S-deficient. Recently, Surgina et al. [109] reported the growth of CZTS thin films by reactive PLD in H_2S atmosphere and further annealed in N_2 atmosphere. The films were close to stoichiometric and as prepared films had a bandgap of 1.27 eV which increased up to 1.5 eV upon annealing.

1.6.2 Non-vacuum techniques

Vacuum equipments are often expensive and only applicable to high-value niche markets. Core of the development of any new technology is the cost-effectiveness. The best way to further reduce the cost of photovoltaics is the complete avoiding of vacuum technology. There are a lot of non-vacuum techniques suitable for the deposition of CZTS thin films.

1.6.2.1 Sol-Gel method

It is one of the catalysts preparation methods; It is a homogeneous process resulting in continuous transformation of a solution into hydrated solid precursor. This method has several promising advantages over the conventional

techniques. It offers better control of the texture, composition, homogeneity and structural properties of the final solids.

Tanaka et al. [110], for the first time, prepared CZTS thin films by sulfurizing precursors deposited by sol-gel method. They prepared films by annealing oxyhydrate precursors deposited by the sol-gel method in an N_2+H_2S atmosphere. The films showed XRD peaks attributed to CZTS and had almost stoichiometric chemical composition and a direct band gap of 1.49 eV. Next year same group tried to improve transmittance in IR region and to eliminate voids in the CZTS films by pre-annealing the precursors in air or in N_2+H_2 (5 %) atmosphere before annealing of precursors in H_2S contained atmosphere[66]. In 2009, same group reported fabrication of CZTS thin film solar cell via non-vacuum method [111-112]. They used CZTS films prepared over 'Mo' coated glass substrates by sulfurizing precursors deposited by sol-gel technique as the absorber layer.

Yeh et al. [113] prepared CZTS films by sol-gel spin coating deposition. They avoided usual sulfurization process. Film with a nearly stoichiometric composition was prepared at synthesizing temperature of 280 ^oC. Absorption coefficient and the optical energy gap of the deposited films were 2.9×10^4 cm^{-1} and 1.5 eV respectively. In 2011, Tanaka et al. [114] studied the properties of CZTS thin films deposited by sol–gel sulfurization. They found that as Cu/(Zn+Sn) ratio of the sol–gel solution decreased, the grains in the CZTS thin films became larger. Band gap of the films shifted to higher energies as Cu/(Zn+Sn) ratio of the CZTS film decreased.

Same group also reported effect of H_2S concentration used for sulfurization [115]. CZTS thin film prepared with an H_2S concentration of 3 % had grains in the order of 1 μm in size, which were larger than those of films prepared at other

H_2S concentrations. In 2011, Jiang et al. [116] prepared CZTS thin films by spin-coating the sol-gel precursor followed by annealing in a nitrogen atmosphere. Band gap and absorption coefficient of the films were 1.51 eV and 10^4 cm^{-1} respectively. Recently, Park et al. [117] deposited sol-gel processed CZTS thin films without sulfurization. The grain size was up to 1 μm and the Cu/(Zn+Sn) and Zn/Sn ratios were 0.93 and 1.07 respectively.

1.6.2.2 Spray pyrolysis technique.

Spray pyrolysis is a process in which a thin film is deposited by spraying a solution on to a pre-heated substrate, where the constituents react to form the required chemical compound. It is the most popular technique due to its simplicity, cost-effectiveness and ability to control the structure at molecular level. There is virtually no restriction on substrate material and its surface, any support having high temperature tolerance will be a suitable substrate.

The first report on spray deposited CZTS came in 1996. Nakayama and Ito [50] deposited polycrystalline stannite CZTS films on glass substrates. As deposited films were sulfur deficient while it becomes stoichiometric on annealing at 550 ^oC in an 'Ar' flow containing H_2S. Stoichiometric film showed resistivity of 2×10^2 Ω.cm. Five years later Madarasz et al. [118] prepared CZTS thin films on glass substrates by varying substrate temperature from 225 ^oC to 350 ^oC. The XRD profiles correspond to the zincblende superstructure of the stannite type CZTS. Kamoun et al. [119] reported preparation of CZTS thin films by varying substrate temperature from 280 ^oC to 360 ^oC. They prepared films by spraying precursor solution for duration of 30 and 60 min. All the films exhibited kesterite structure with preferential orientation along the (112) direction. Annealing at 550 ^oC showed an improvement in optical properties.

In 2009, Kumar et al. [120] studied effect of substrate temperature on the properties of CZTS thin films prepared using chemical spray pyrolysis technique. Films deposited at T_s= 290 ^oC were found to contain Cu_2SnS_3 and Cu_xS as the secondary phases while at T_s= 330 ^oC, Cu_xS was found to be the secondary phase. At T_s= 450 ^oC, ZnS appears as the secondary phase. Polycrystalline CZTS thin films, with amorphous ZnS being present to a small extent, could be obtained in the substrate temperature range 370-410 ^oC. In another report they studied effect of starting solution pH on the properties of spray deposited films [121]. Polycrystalline, non-stoichiometric CZTS thin films with kesterite structure could be obtained when solution pH is 3.0. Films deposited from a solution having pH = 4.5, contain Cu_xS and ZnS along with CZTS. Films deposited with solution pH = 5.5 contain only binary sulfides. In 2010, same group studied effect of copper salt and thiourea concentrations on the formation of CZTS thin films [49]. Near-stoichiometric CZTS films with kesterite structure could be obtained with solution containing 0.009 M copper salt, 0.0045 M zinc salt, 0.005 M tin salt and 0.05 M thiourea.

Prabhakar et al. [65] studied effect of substrate temperature on the properties of CZTS thin films prepared using ultrasonic spray pyrolysis technique. XRD patterns showed that best crystallinity was obtained for 340 ^oC as substrate temperature. Band gap energy of 1.54 eV was obtained for the grown CZTS films. Next year same group reported effect of sodium incorporation on the properties of sprayed CZTS thin films [122]. They deposited films on soda lime and 'Na' free borosilicate glass substrates through ultrasonic spray pyrolysis. Sodium enhanced the grain size and the (112) texture of the CZTS films. Number of holes was also found to increase significantly due to the influence of sodium diffusion. In 2011, they fabricated CZTS based solar cell with an absorber layer thickness 2.1 μm [123]. Substrate temperature during

deposition was 340 ^{o}C and copper ion concentration in the spray solution was 0.019 M.

Yoo et al. [97] have done a comparative study of CZTS film growth using two different methods, viz., spray pyrolysis and sulfurization of Cu–Zn–Sn metallic films. They showed that application of additional sulfurization to sprayed CZTS films induced great improvement of crystallinity to the level of the sulfurized metallic films. Arba et al. [124] reported the growth of CZTS thin films by spray pyrolysis at the substrate temperatures 375 ^{o}C and 425 ^{o}C. Both the films were polycrystalline with kesterite structure. In 2012, Das et al. [125] prepared CZTS thin films using spray pyrolysis. They studied effect of substrate temperature and molarity of the precursors. As-deposited CZTS films were H_2S treated and annealed under 'Ar' atmosphere. The annealed films showed significant improvement in structural, optical, morphological and electronic properties.

Patel et al. [126] deposited thin films of CZTS on glass substrates at 320 ^{o}C, using spray pyrolysis, under a non-equilibrium condition (by varying 'Zn', 'Sn' and 'S' precursor concentrations) and without additional sulfurization. The optical bandgap of stoichiometric CZTS was 1.45 eV and Hall mobility in the range 87–92 $cm^2.V^{-1}.s^{-1}$ was observed for 'S' and 'Zn' enriched films. Same group reported fabrication of spray pyrolysed CZTS based solar cell in 2013 [127]. The effective minority carrier lifetime of 263 μs was confirmed by diffused monochromatic LED excitation induced OCVD fitting.

Huang et al. [128] prepared CZTS films by ultrasonic spray pyrolysis on FTO (SnO_2:F on glass) substrates. Effect of substrate temperatures on the phases, morphologies and photo-electrochemical properties of CZTS film was investigated. The samples deposited at 400–450 ^{o}C showed highest cathode photocurrent. The conduction band of CZTS was found to be higher than the H^+

reduction potential, and hence they claimed that it is an appropriate photocathode material for solar hydrogen production.

Seboui et al. [129] studied the effect of substrate temperature on sprayed CZTS deposited over Pyrex substrates. XRD analysis, optical measurements, and electrical studies revealed that CZTS thin film deposited at the highest temperature T_s =280 ^oC has the best crystallinity, the lowest resistivity, and the ideal band gap (Eg~1.5 eV). Shinde et al. [130] reported effect of thickness on the properties of spray pyrolysed CZTS thin films. Band gap varied in the range 1.6–1.67 eV, depending on film thickness. Electrical conductivity and contact angle enhanced with film thickness.

Recently, Gurieva et al. [131] reported the deposition of CZTS thin films using spray pyrolysis. They added a small quantity of C_2H_5OH to the precursor solution to improve its stability. On annealing they could improve the crystallinity of the films. Aono et al. [132] analyzed spray pyrolysed CZTS thin films using XPS depth profile technique. The composition on surfaces of the as grown CZTS films was Cu-poor and near stoichiometric compositions of 'Zn', 'Sn' and 'S'. In contrast to the surface, Cu-rich and Zn-poor compositions were obtained in the films. Rodriguez et al. [133] reported the compositional optimization of thin film deposition of CZTS onto Mo/glass substrates for low-cost solar cell applications, using pneumatic spray pyrolysis technique in air ambient. They investigated influence of both, starting solution precursor's concentrations and further annealing conditions on the properties of the films.

1.6.2.3Electrodeposition

Electrodeposition is the application of metallic coatings to metallic or other conductive surfaces by electrochemical processes. It is a low cost preparation technique used for the deposition of different semiconductor thin

films. It has been extensively used for fabrication of CdTe as well as CIGS absorber layers [134-135]. CZTS thin films can be prepared using this technique either by sequential electroplating of precursors or by single step electrodeposition of precursors, followed by sulfurization/annealing.

Feasibility of this new technique for depositing CZTS thin films was first studied by Scragg et al. [136] in 2008. The deposition process consists of the electrodeposition of metallic precursors followed by annealing in sulfur vapor. Polycrystalline films of about 1 μm thickness with grain size in the range 0.2–0.5 μm could be deposited. Later they reported on electrodeposited CZTS films by photo-electrochemical methods, which showed that the films were p-type with doping densities of the order of 10^{16} cm^{-3} and a band gap of 1.49 eV [137]. In 2010, they prepared solar cell with 3.2 % efficiency using electrodeposited CZTS absorber layer [138].

Araki et al. [38] prepared CZTS thin films by sulfurizing precursors deposited by electroplating. The precursors (Cu/Sn/Zn stacked layers) were deposited using electroplating sequentially onto 'Mo' coated glass substrates. Aqueous solutions containing copper sulfate for 'Cu' plating, tin sulfate for 'Sn' plating and zinc sulfate for 'Zn' plating were used as the electrolytes. X-ray diffraction peaks attributable to CZTS were detected in thin films sulfurized at temperatures above 400^{o}C.Zhang et al. [34] deposited CZTS thin films on 'Ag' substrates by the electrochemical atomic layer epitaxy (EC-ALE) method. Chan et al. [139] deposited CZTS thin films by ionic liquid electrodeposition technique. Sulfurization of the stacked layers was achieved in elemental sulfur vapor at 450 °C for 2 hours. In 2010, again they reported the preparation of kesterite CZTS using the same technique [59].

In 2009, Kurihara et al. [140] synthesized CZTS thin films by sequentially electrodepositing layers of 'Cu', 'Sn', and 'Zn' from unstirred baths and subsequently annealing the stacked precursors in sulfur atmosphere. Control of the flux of ions to the deposition surface allowed uniform layers of material to be deposited and this also resulted in films of uniform composition. Ennaoui et al. [141] fabricated CZTS absorbers by solid-state reaction in H_2S atmosphere of electrodeposited Cu–Zn–Sn precursors. The ternary alloys were deposited in one step from a cyanide-free alkaline electrolyte containing Cu (II), Zn (II) and Sn (IV) metal salts on 'Mo' coated glass substrates.

Pawar et al. [35] deposited CZTS thin films on 'Mo' coated and ITO coated glass plates. The polycrystalline CZTS thin films with kesterite crystal structure were obtained after annealing as-deposited thin films at 550 ^{o}C in 'Ar' atmosphere for 1 hour. The deposited films were nearly stoichiometric and photoactive. Same group later studied effect of complexing agent on properties of electrodeposited CZTS thin films [142]. Film prepared without complexing agent showed wellcovered surface morphology on the substrate with some cracks on the surface of the film whereas those prepared using complexing agent, exhibited uneven and slightly porous and some over grown particles on the surface of the films.

Ma et al. [143] showed that surface morphology of electrodeposited CZTS was greatly influenced by change in the pH of the 'Zn' electroplating solution. At a pH of 9, an irregular hollow column type CZTS was formed, resulting in the highest CZTS electrode photocurrent. Fontane et al. [144] characterized electrodeposited CZTS layers using in depth resolved Raman scattering and auger electron spectroscopy. Jeon et al. [145] employed two different techniques for the electrodeposition of CZTS layers: a potentiostatic method and a pulsed potential electrodeposition method. Near stoichiometric CZTS thin films were

prepared using potentiostatic deposition method. The samples deposited through pulsed potential methods showed wire-like CZTS nanostructures. Cui et al. [67] employed single step electrodeposition process for the preparation of CZTS layer followed by post annealing treatment at 550 ^{o}C for 60 min in the atmosphere of N_2+H_2S (5 %).

Bhattacharya et al. [146] performed cyclic voltammetric measurements to understand electrochemical behavior of the metal salts in ionic liquid solutions. Electrodeposited CZTS absorber layers were fabricated by annealing stacked Cu/Sn/Zn layers in the tube furnace in the presence of elemental sulfur. Recently, Iljina et al. [147] showed that thiocyanate ions (CNS^{-}) can be used as a suitable complexing agent for the electrodeposition of CZTS from aqueous solutions. The sulfur concentration in the as-deposited layers was dependent on the duration of deposition. Mkawi et al. [148] deposited CZTS layers on flexible 'Cu' substrates using sequential electrodeposition method. Films showed p-type conductivity, with a carrier concentration between 9.56×10^{16} $cm^{-3}$and 3.66×10^{17} cm^{-3}, depending on the composition of the precursor mixture.

1.6.2.4 Other non-vacuum techniques

Hydrothermal method is another non-vacuum method that does not require any expensive precursors or equipment and can be readily adopted for industrial production processes. It possesses remarkable reliability and selectivity as well as high efficiency at low temperature. Liu et al. [149] introduced hydrothermal method for preparing CZTS nanocrystals with an average size of 5–6 nm using simple Cu (II), Zn (II), Sn (II) inorganic salt and thiourea as precursor. They could synthesize kesterite CZTS having band gap of 1.47 eV at 180 ^{o}C. Verma et al. [150] synthesized nanocrystalline CZTS powder again through hydrothermal process, using thiourea as sulfur precursor. They got kesterite CZTS of particle size 4-5 nm.

Zhou et al. [151] reported a simple and low cost screen printing approach for the preparation of CZTS absorber layers. Microparticles of CZTS prepared using wet ball milling and sintering methods, were dispersed in isopropanol. Separately, ethyl cellulose was dissolved in isopropanol. The screen printable paste was then made by mixing both solutions with small quantity of terpinol and deposited onto 'Mo' coated polyimide substrates. Band gap, sheet resistance, carrier concentration, and Hall mobility of the screen printed CZTS layers were 1.49 eV, $2.42\times10^{3}\ \Omega/\square$, $3.81\times10^{18}\ cm^{-3}$, and 12.61 $cm^{2}.V^{-1}.s^{-1}$ respectively.

Wangperawong et al. [33,152] deposited SnS and ZnS on 'Mo' coated SLG substrates through chemical bath deposition (CBD) in which 'Cu' ions were incorporated into the precursor films via ion exchange technique. These CZTS precursor films were then annealed in H_2S atmosphere at 500 ^{o}C. They could produce compositionally uniform microcrystalline CZTS with kesterite structure and band gap of 1.45 eV.

Cao and Shen [37] used a relatively simple and convenient solvothermal route for the deposition of CZTS nanoparticles. Nanoparticles with diameters of about 5–10 nm were obtained at the temperature of 180 ^{o}C. Band gap of as synthesized CZTS nanoparticles was about 1.5 eV. Recently, Pal et al. [153] reported preparation of highly crystalline CZTS nanocrystals with controlled Cu/(Zn+Sn) ratio. They obtained films with particle size less than 10 nm.

Mau and Kim [154] successfully deposited CZTS thin films by sulfurizing dip coated precursors. Precursor films were obtained by several cycles of dipping and air-jet cutting to rinse the film and make it flat, followed by drying at 200 ^{o}C for 15 min. Films had a band gap of ~ 1.5 eV and absorption coefficient higher than $10^{4}\ cm^{-1}$. Rajesh et al. [155] deposited CZTS thin films

using simple sol-gel dip coating method. They used zinc nitrate and copper nitrate for the first time as precursor material for the preparation of CZTS films.

Guo et al. [156] for the first time reported synthesis of CZTS nanoparticles and its use as absorber layer in solar cell using CZTS nanocrystalline drop casting approach. X-ray diffraction pattern showed that as synthesized particles belonged to kesterite CZTS phase. EDAX analysis showed that nanoparticles were slightly Cu-rich. In another report same group explained the fabrication of 7.2 % efficient solar cell using CZTS absorber layer prepared using the same technique [157]. Xin et al. [158] reported an efficiency of 7.37 % for dye sensitized solar cell constructed using CZTS nanoparticles. They synthesized CZTS nanoparticles using similar approach as that of Guo et al. [156]. Sheinhagen et al. [159] prepared CZTS nanocrystals by high temperature arrested precipitation of copper acetyl acetonate, zinc acetate, tin chloride dihydrate and elemental sulfur in oleyamine at 280 ^{o}C for 1 hour under inert atmosphere. These nanocrystals were slightly Sn-rich and S-deficient and had band gap of 1.3 eV.

Shinde et al. [160] reported a novel chemical successive ionic layer adsorption and reaction (SILAR) technique for CZTS thin film formation by sequential reaction on SLG substrate surface. Films were then annealed in vacuum at 400 ^{o}C. X-ray diffraction studies showed formation of kesterite structure of CZTS films. Mali et al. [161] reported fabrication of CZTS thin film based solar cells using similar approach. CZTS thin films were formed by sequential immersion of substrate into the solutions of cationic and anionic precursors. As deposited films were dried in oven at 60 ^{o}C for 30 min. Same group later reported an efficiency of 1.85 % on a solar cell based on CZTS prepared from SILAR technique [162]. Recently, Guan et al. [163] prepared CZTS films by sulfurizing (Cu, Sn) S/ZnS structured precursors prepared by

combination of the successive ionic layer absorption and reaction method and the chemical bath deposition method, respectively.

Lin et al. [164] proposed a new route to prepare CZTS thin films by spin coating of the precursor inks composed of Cu_3SnS_4 and ZnS nanoparticles and annealing in Ar/H_2S atmosphere. Swami et al. [165] prepared CZTS films by spin coating of solution prepared by dissolving of copper (II) chloride, zinc (II) chloride, tin (IV) chloride and thiourea in 2-Methoxyethanol. X-ray diffraction studies showed formation of kesterite phase with peaks corresponding to (112), (220) and (312) planes.

Washio et al. [166] fabricated CZTS based thin films by sulfurizing oxide precursor thin films synthesized through the open atmosphere type chemical vapor deposition (OACVD) method. $Cu(C_5H_7O_2)_2$, $Zn(C_5H_7O_2)_2$ and $Sn(C_5H_7O_2)_2$ were used as raw materials. The oxide precursor thin films were sulfurized at 520–560 ^oC in 5 % (vol) H_2S balanced with N_2. Formed CZTS based thin films included oxygen with composition ratio of $O/(S + O) = 0.17–0.27$.

1.7 CZTS cell works

Wagner et al. [167] reported the development of first $(I)_2(II)(IV)(VI)_4$ solar cell in 1977. An n-type CdS thin film was evaporated on vapor transportation-grown Cu_2CdSnS_4 single crystal substrate to form the p-n junction. Authors have mentioned that due to the large series resistance fill factor is 30 % and efficiency is limited to 1.6 %. The first CZTS solar cell was developed in 1988 by Ito and Nakazawa [57]. A heterojunction solar cell with an open circuit voltage of 165 mV was achieved by depositing cadmium tin oxide on CZTS thin film. Later the same group enhanced the voltage up to 265 mV by annealing the same device [168].

Katagiri et al. [53] reported their first work on CZTS thin film solar cell in 1997. They prepared CZTS thin films on 'Mo' coated glass plates by

sulfurization of EB evaporated precursors. Fabricated solar cells, Al/ZnO/CdS/CZTS/Mo/SLG, showed a conversion efficiency of 0.66 %. The low efficiency was attributed to the degraded fill factor due to the high resistance of window layer.

In 2001, Katagiri et al. [80] improved the efficiency of EB evaporated CZTS based solar cell to 2.62 % using CdS buffer layer deposited using CBD technique, together with transparent conductive ZnO:Al films deposited by RF-magnetron sputtering. In another report they claimed the highest open circuit voltage of 735 mV on CZTS based solar cell [39]. In 2003, same group examined the effect of addition of 'Na' by fabricating CZTS cell using Na_2S/Mo/SiO_2/SLG substrate. The device showed an efficiency of 5.45 % and a fill factor of 60 % [169]. By optimizing the material composition, Jimbo et al. [88], enhanced the efficiency of CZTS solar cell to 5.74 %. Material composition of their CZTS sample was Cu/(Zn+Sn)=0.87 and Zn/Sn=1.15. They claimed that for better performance CZTS film should be Cu-lean and Zn-rich type.

In 2008, Katagiri et al. [170] reported an efficiency of 6.8 % on a CZTS cell by soaking the CZTS layer (on 'Mo' coated soda lime glass substrate) in deionized water (DIW) after forming the CZTS layer. It was found that DIW soaking had the effect of preferential etching, which eliminated selectively metal oxide particles in the CZTS layer. Araki et al. [40] deposited six kinds of precursors with different stacking sequences on 'Mo' coated borosilicate glass substrates using EB evaporation. The deposited precursors were then sulfurized at 560 ^{o}C for 2 hour in N_2+S_2 vapor to form CZTS thin films and the solar cell device based on this CZTS film exhibited conversion efficiency of 1.79 %. Moriya et al. [52] fabricated thin film solar cell based on CZTS absorber layer deposited by PLD with ZnO:Al (n-type) as window layer and CdS as buffer layer. The device showed a conversion efficiency of 0.66 %. In another report they claimed an efficiency of 1.74 % on a

CZTS thin film solar cell prepared by PLD[106]. Scragg et al. [137] reported fabrication of thin film solar cell using electrodeposited CZTS absorber. The device showed open circuit voltage of 295 mV, short circuit current density of 8.7 mA/cm^2, fill factor of 32 % and efficiency of 0.8 %.

In 2009, Araki et al. [38] prepared CZTS thin films by sulfurizing electrodeposited precursors. A photovoltaic cell using CZTS thin film produced through sulfurizing an electroplated Sn-rich precursor at 600 ^{o}C exhibited efficiency of 0.98 %. Araki et al. [41] introduced for the first time a one step process of co-electrodeposition for the metal precursors. The solar cell based on CZTS thin film yielded a conversion efficiency of 3.16 % for an active area of 0.15 cm^2. Ennaoui et al. [141] achieved an efficiency of 3.4 % and fill factor of 41 % on an electrodeposited CZTS thin film solar cell with chemical bath deposited CdS buffer layer and a sputtered i-ZnO/ZnO:Al bilayer. The best performance was obtained for Cu-poor samples. Tanaka et al. [112] prepared thin film solar cell having the structure Al/ZnO:Al/CdS/CZTS/Mo/SLG in which all the semiconductor layers were prepared under non-vacuum condition. In their work CZTS absorber was deposited using sol-gel method. They reported a conversion efficiency of 1.01 % under an illumination of AM 1.5 (100 mW/cm^2). Same group later enhanced the efficiency to 1.61 % by varying the dipping time for the CdS deposition [111].

In 2009, Steinhagen et al. [159] reported a synthetic method for producing CZTS nanocrystals. PV devices fabricated with these CZTS nanocrystals exhibited power conversion efficiencies up to 0.23 %. Guo et al. [156] reported synthesis of CZTS nanoparticles and its use as absorber layer in solar cell using CZTS nanocrystalline drop casting approach. CZTS nanoparticles films were prepared by drop casting of CZTS nanoparticles onto 'Mo' coated SLG substrates. These films were then selenized under selenium vapor at 450 and 500 ^{o}C. The

solar cell constructed using the film selenized at 450 ^{o}C exhibited an efficiency of 0.74 %.

In 2010, Scragg et al. [138] made large improvements to the microscopic and macroscopic uniformity of electrodeposited stacked elemental precursors. Precursors with the stacking order Cu/Sn/Cu/Zn were produced, and sulfurized to form CZTS films. The best device produced achieved an efficiency of 3.2 %. Wang et al. [171] fabricated CZTS solar cell, using thermal evaporated CZTS absorber layer, having efficiency up to 6.8 % with absorber layer thickness less than 1 μm. It was found that on decreasing the thickness from 1200 nm to 650 nm efficiency improved from 2.44 % to 6.81 %. Zhou et al. [151] reported a simple and low cost screen printing approach for the preparation of CZTS absorber layers. Solar cell based on screen printed CZTS layers with structure polyimide/Mo/CZTS/CdS/Al:ZnO/Al exhibited an efficiency of 0.49 %.

In 2011, Moholkar et al. [172] reported the preparation of CZTS thin film solar cell using PLD. The device exhibited open-circuit voltage (V_{oc}) of 585 mV, short-circuit current (J_{sc}) of 6.74 mA/cm^2, fill factor (*FF*) of 51 %, and conversion efficiency of 2.02 %. They later enhanced the power conversion efficiency to 3.14% [173]. The deposited CZTS thin films were annealed in 95 % N_2+5 % H_2S atmosphere at 400 ^{o}C for 1 hour. The fabricated CZTS thin film based solar cells of configuration glass/Mo/CZTS/CdS/Al:ZnO/Al exhibited V_{oc}=565 mV, J_{sc}=8.76 mA/cm^2, *FF*=55 %. Schubert et al. [85] reported a different route, a fast (16 min) co-evaporation of all elements in a single stage process. CZTS thin films were deposited on 'Mo' coated SLG substrates at 550 ^{o}C by thermal evaporation of 'Cu', 'Sn' and ZnS source materials. The KCN etched CZTS thin films were then processed to form a thin film solar cell device of configuration SLG/Mo/CZTS/CdS/Al:ZnO/Ni/Al. This device showed a conversion efficiency of 4.1 %.

In 2011, Mamose et al. [98] deposited 'Cu', 'Zn' and 'Sn' metals simultaneously by sputtering to obtain the CZTS precursor films. CZTS precursor films were then sulfurized at 590 ^{o}C for 7 min to form CZTS thin films. CZTS thin films were then used as absorber layer in the solar cell device which exhibited an efficiency of 3.7 %. Chalapathy et al. [99] deposited CZTS absorber on 'Mo' coated SLG substrates using metal precursors with the Cu/Zn/Sn/Cu sequence by DC sputtering. The CZTS precursors were then sulfurized in sulfur vapor to form the film. The configuration of Al/Al:ZnO/i-ZnO/CdS/CZTS/Mo/ glass showed a power conversion efficiency of 4.59 % for 0.44 cm^2 area. Tanaka et al. [114] deposited CZTS thin films by sol–gel sulfurization. The solar cell fabricated using CZTS thin film with Cu/(Zn+Sn) ratio 0.80 exhibited an efficiency of 2.03 %. Wangperawong et al. [33] used chemical bath deposition and ion exchange to incorporate copper, zinc, tin and sulfur into a thin film precursor stack. The stack was then sulfurized to form CZTS film. The solar cell based on this CZTS thin film with an architecture of SLG/Mo/CZTS/CdS/Al:ZnO/Al had an efficiency of 0.16 %. Xin et al. [158] reported an efficiency of 3.62 % for dye sensitized solar cell constructed using CZTS nanoparticles.

In 2012, Washio et al. [166] reported a novel approach for CZTS thin film based solar cell using oxide precursors by an open atmosphere chemical vapour deposition (OACVD). The fabricated solar cells with structure SLG/Mo/CZTS/CdS/Al:ZnO/Al yielded an efficiency of 6.03 %. Moholkar et al. [174] fabricated CZTS thin film solar cell, using PLD, by varying the Cu/(Zn+Sn) ratio. Device grown using Cu/(Zn + Sn) = 1.1 had the best conversion efficiency of 4.13 % with V_{oc} = 700 mV, J_{sc} = 10.01 mA/cm^2 and FF = 59 %. Shinde et al. [160] reported a novel chemical successive ionic layer adsorption and reaction (SILAR) technique for deposition of CZTS thin film. The photo-electrochemical solar cell (PEC) constructed using annealed CZTS thin film exhibited an

efficiency of 0.12 %. Mali et al. [161] reported fabrication of CZTS thin film based solar cells using similar approach. CZTS thin films were formed by sequential immersion of substrate into the solutions of cationic precursors (Cu^{2+}, Zn^{2+}, Sn^{2+}) and anionic (S^{2-}) precursors. CZTS thin films with different number of cycles were obtained and PEC cells were formed. The best PEC cell formed using CZTS thin films with 40 cycles exhibited conversion efficiency of 0.396 %. Same group of researchers later on improved the efficiency of CZTS thin film based solar cell using similar approach to 1.85 % [162].

In 2012, Woo et al. [175] reported fabrication of high quality CZTS absorber layer with thickness of 2.8–3.0 μm using air stable non toxic solvent based inks. As fabricated device exhibited total area efficiency of 5.14 %. Bhattacharya et al. [146] reported the deposition of electrodeposited CZTS absorber layers by annealing stacked Cu/Sn/Zn layers in tube furnace in presence of elemental sulfur. Absorber material used for device fabrication has very low carrier concentration and hence the device had only 1.7 % efficiency. Patel et al. [126] deposited CZTS thin films using spray pyrolysis technique. Solar cell fabricated using the sprayed CZTS thin film with superstrate structure of glass/SnO_2:F/CdS/CZTS/graphite showed conversion efficiency of 0.154 %. Das et al. [125] fabricated spray pyrolysed CZTS based solar cell using CdS as buffer layer. They reported an open circuit voltage of 280 mV and short circuit current density of 3.1 mA/cm^2. S. Ahmed et al. [176] fabricated several electrodeposited CZTS solar cells with champion efficiencies ranging from 6.7 % to 7.3 %. They made devices with an electrodeposited CuZnSn precursor that is sulfurized at 585 °C for 12 min.

In 2013, Cho et al. [177] prepared CZTS thin films using precursor solution paste. By applying air annealing and a subsequent sulfurization process polycrystalline CZTS film were synthesized. A solar cell device with this CZTS film as absorber layer showed efficiency of 3.02 %. Ericson et al. [104] prepared

reactively sputtered Cu–Zn–Sn–S precursor films and recrystallized by rapid thermal processing to generate CZTS absorber layers. Grain size in the annealed films seems to increase with higher copper content and higher precursor deposition temperature. The best device showed an efficiency of 4.5 %. Fernandes et al. [93] studied effect of sulfurization time on device properties of DC- sputtered CZTS based solar cell. Three different time intervals, 10 min, 30 min and 60 min, at maximum sulfurization temperature were considered. Highest performance were obtained for a device prepared at least time (ie., 10 min) and maximum efficiency obtained were 0.54 %. Sousa et al. [95] employed a hybrid method, combining RF-magnetron sputtering with evaporation, for the deposition of metallic precursors and compared two approaches to sulfurization. One series of precursors was sulfurized in a tubular furnace directly exposed to a sulfur vapor and the other one sulfurized in the same furnace but inside a graphite box where sulfur pellets have been evaporated. Conversion efficiency of 2.4 % and 1.1 % were obtained for the devices fabricated using direct sulfur flux and that using graphite box respectively.

In 2013, a few works on sprayed CZTS solar cell were reported. Patel et al. [127] fabricated CZTS/CdS solar cell entirely by a spray pyrolysis process. The solar cell exhibited open-circuit voltage of 157.25 mV, short-circuit current density of 3.024 mA/cm^{-2} and fill factor of 24.77 % with irradiance of 200 W/m^{-2} from the white LED source. Rodriguez et al. [133] reported fabrication of CZTS solar cell using pneumatic spray pyrolysis. For a device having CZTS/CdS/i-ZnO/ZnO:Al structure they obtained an efficiency of 0.49 %.

In 2013, Shin et al. [178] deposited CZTS thin films over 'Mo' coated soda lime glass plates using thermal evaporation and a device having structure Glass/Mo/CZTS(600 nm)/CdS(90-100 nm)/i-ZnO(80 nm)/ZnO:Al(450 nm)/Ni-Al/MgF_2(100 nm) was fabricated. Under simulated AM 1.5 Global spectrum and

100 mW/cm^2 (AM 1.5 sun) illumination they obtained an efficiency of 8.4 %. This is the highest efficiency reported for pure sulfide CZTS prepared by any method. Table 1.3 and table 1.4 gives the performance parameters of thin film solar cells based on vacuum deposited CZTS absorber layer and non-vacuum deposited CZTS absorber layer respectively.

Table 1.3. Record efficiencies and other performance parameters of thin film solar cells using CZTS absorber prepared by various vacuum based approaches.

Method of CZTS preparation	η (%)	V_{oc} (mV)	J_{sc} (mA/cm^2)	FF (%)	Reference
'Ar' beam sputtering	…….	265	0.1	…..	[168]
DC- sputtering	4.59	545	15.44	55	[99]
RF- sputtering	6.77	610	17.9	62	[170]
Co-evaporation	4.1	541	13	60	[85]
EBevaporation	4.53	629	12.53	58	[81]
Thermal evaporation	8.4	661	19.5	66	[178]
Pulsed laser deposition	4.13	700	10.1	59	[174]

Table 1.4. Record efficiencies and other performance parameters of thin film solar cells using CZTS absorber prepared by various non-vacuum based approaches.

Method of CZTS preparation	η (%)	V_{oc} (mV)	J_{sc} (mA/cm^2)	FF (%)	Reference
Spray pyrolysis	0.49	173	10.1	28.2	[133]
Screen printing	0.49	386	4.76	27	[151]
CBD	0.16	210	2.4	….	[33]
SILAR	0.396*	280	0.63	62	[161]
Sol-gel	2.03	575	9.69	36	[114]
CVD	6.03	658	16.5	55	[166]
Electrodeposition	7.3	567	22	58	[176]

*Measurement was done at 30 mW/cm^2 illumination at room temperature.

References

[1]. **A. Luque and S. Hegedus.***Handbook of photovoltaic science and engineering.* Chichester : Wiley, 2003.

[2]. **Peter Wurfel.***Physics of Solar Cells: From Principles to New Concepts.* Weinheim : Wiley, 2005.

[3]. **M. I. Khan, A. Kumar, A. Sharma and P. V. Singh.** 2013, JECET, Vol. 2, p. 46.

[4]. **G. D. Rai.***Non-Conventional energy sources.* New Delhi : Khanna, 2002.

[5]. **R. F. Service.** 2005, Science, Vol. 309, p. 548.

[6]. **http://www.sc.doe.gov/bes/reports/files/SEU_rpt.pdf, Report ofthe Basic Energy Sciences Workshop on Solar Energy Utilization, US-DOE, April 18–21.** 2005.

[7]. **R. Eisenberg and D. G. Nocera.** 2006, Inorg. Chem, Vol. 45, p. 6799.

[8]. **A. R. Jha.***Solar Cell Technology and Applications.* Boca Raton : Auerbach, 2010.

[9]. **M. A. Green.** 2007, J Mater Sci: Mater Electron, Vol. 18, p. 15.

[10]. **Lewis Fraas and Larry Partain.***Solar cells and their applications.* New Jersey : Wiley, 2010.

[11]. **J. B. Li, V. Chawla and B. M. Clemens.** 2012, Adv Mater, Vol. 24, p. 720.

[12]. **F. Kessler and D. Rudmann.** 2004, Solar Energy, Vol. 77, p. 685.

[13]. **B. R. Pamplin.** 1960, Nature, Vol. 188, p. 136.

[14]. **R. B. Hall, R. W. Birkmire, J. E. Phillips and J. D. Meakin.** 1981, Appl. Phys. Lett., Vol. 38, p. 925.

[15]. **R. A. Mickelsen and W. S. Chen.** 1981, In Conf. Rec. 15th IEEE Photovoltaic Specialist Conf., p. 800.

[16]. **Y. S. Tyan and E. A. Perez-Albuerne.** 1982, In Conf. Rec. 16th IEEE Photovoltaic Specialist Conf., p. 794.

[17]. **A. Catalano, R. V. D ' Aiello, J. Dresner, B. Faughnan, A. Firester, J. Kane, H. Schade, Z. E. Smith, G. Swartz and A. Triano.** 1982, In Conf. Rec. 16th IEEE Photovoltaic Specialist Conf., p. 1421.

[18]. **I. Repins, M. A. Contreras, B. Egaas, C. DeHart, J. Scharf, C. L. Perkins, B. To and R. Noufi.** 2008, Prog. Photovoltaics , Vol. 16 (3), p. 235.

[19]. **X. Wu, J. C. Keane, R. G. Dhere, C. DeHart, A. Duda, T. A. Gessert, S. Asher, D . H. Levi and P. Sheldon.** 2001, Proceedings of the 17th European Photovoltaic Solar Energy Conference, p. 995.

[20]. **J. Meier, J. Sitznagel, U. Kroll, C. Bucher, S. Fay, T. Moriarty and A. Shah.** 2004, Thin Solid Films, Vols. 451-452, p. 518.

[21]. **M. A. Green, K. Emery, Y. Hishikawa, W. Warta and E. D. Dunlop.** 2013, Prog. Photovolt: Res. Appl., Vol. 21, p. 1.

[22]. **First Solar. First Solar Web Site, Available at: http://www.firstsolar.com/en/recycling.php [accessed october 2010].** 2010.

[23]. **C. Candelise, J. F. Speirs and R. J. K. Gross.** 2011, Renew. Sustain. Energy Rev., Vol. 15, p. 4972.

[24]. **L. A. Wahab, M. B. El-Den, A. A. Farrag, S. A. Fayek and K. H. Marzouk.** 2009, J. Phys. Chem. Solids, Vol. 70, p. 604.

[25]. **J. Zhang, L. Shao, Y. Fu and E. Xie.** 2006, Rare metals, Vol. 25, p. 315.

[26]. **M. Liu, F. Huang, L. Chen and I. Chen.** 2009, Appl. Phys. Lett., Vol. 94, p. 202103.

[27]. **M. I. Hossain.** 2012, Chalcogenide Lett., Vol. 9, p. 231.

[28]. **L. Choubrac, A. Lafond, C. Guillot-Deudon, Y. Moëlo and S. Jobic.** 2012, Inorg. Chem. , Vol. 51, p. 3346.

[29]. **W. Shockley and H. J. Queisser.** 1961, Jpn. J. Appl. Phys., Vol. 32, p. 510.

[30]. **C. Wadia, A.P. Alivisatos and D. Kammen.** 2009, Environ. Sci. Technol., Vol. 43, p. 2072.

[31]. **S. Schorr.** 2007, Thin Solid Films, Vol. 515, p. 5985.

[32]. **T. Maeda, S. Nakamura and T. Wada.** 2009, In: Mater. Res. Soc. Symp. Proc., p. 1165.

[33]. **A. Wangperawong, J. S. King, S. M. Herron, B. P. Tran, K. Pangan-Okimoto and S. F. Bent.** 2011, Thin Solid Films, Vol. 519, p. 2488.

[34]. **X. Zhang, X. Shi, W. Ye, C. Ma and C. Wang.** 2009, Appl. Phys. A, Vol. 94, p. 381.

[35]. **S. M. Pawar, B. S. Pawar, A. V. Moholkar, D. S. Choi, J. H. Yun, J. H. Moon, S. S. Kolekar and J. H. Kim.** 2010, Electrochemica Acta, Vol. 55, p. 4057.

[36]. **Y. Zhou, W. Zhou, Y. Du, M. Li and S. Wu.** 2011, Mater. Lett., Vol. 65, p. 1535.

[37]. **M. Cao and Y. Shen.** 2011, J. Crystal Growth, Vol. 318, p. 1117.

[38]. **H. Araki, Y. Kubo, A. Mikaduki, K. Jimbo, W. Maw, H. Katagiri, M. Yamazaki, K. Oishi and A. Takeuchi.** 2009, Sol. Energy Mater. Sol. Cells, Vol. 93, p. 996.

[39]. **H. Katagiri, N. Ishigaki, T. Ishida and K. Saito.** 2001, Jpn. J. Appl. Phys., Vol. 40, p. 500.

[40]. **H. Araki, A. Mikaduki, Y. Kubo, T. Sato, K. Jimbo, W. Maw, H. Katagiri, M. Yamazaki, K. Oishi and A. Takeuchi.** 2008, Thin Solid Films, Vol. 517, p. 1457.

[41]. **H. Araki, Y. Kubo, K. Jimbo, W. Maw, H. Katagiri, M. Yamazaki, K. Oishi and A. Takeuchi.** 2009, Phys. Status Solidi (c), Vol. 6, p. 1266.

[42]. **P. A. Fernandes, P. M. P. Salome and A. F. da Cunha.** 2011, J. Alloys Compd., Vol. 509, p. 7600.

[43]. **W. Schafer and R. Nitsche.**1974, Mat. Res. Bull., Vol. 9, p. 645.

[44]. **T. Washio, H. Nozaki, T. Fukano, T. Motohiro, K. Jimbo and H. katagiri.** 2011, J. Appl. Phys., Vol. 110, p. 074511.

[45]. **S. R. Hall, J. T. Szymanski and J. M. Stewart.** 1978, In: Canadian Mineralogist , Vol. 16, p. 131.

[46]. **D. R. Lide.***Handbook of Chemistry and Physics. 79th.* s.l. : CRC press, 1998-1999.

[47]. **S. Chen, J. Yang, X. G. Gong, A. Walsh and S. Wei.** 2010, Phys. Rev. B, Vol. 81, p. 245204 (1).

[48]. **J. Zhang and L. Shao.** 2009, Sci. China Ser. E:Tech. Sci., Vol. 52, p. 269.

[49]. **Y. B. Kishore Kumar, P. uday Bhaskar, G. Suresh babu and V. Sundara raja.** 2010, Phys. Status Solidi A , Vol. 207, p. 149.

[50]. **N. Nakayama and K. Ito.** 1996, Appl. Surf. Sci., Vol. 92, p. 171.

[51]. **T. Tanaka, T. Nagatomo, D. kawasaki, M. Nishio, Q. Guo, A. Wakahara, A. Yoshida and H. Ogawa.** 2005, J. Phys. Chem. Solids, Vol. 66, p. 1978.

[52]. **K. Moriya, K. Tanaka and H. Uchiki.** 2008, Jpn. J. Appl. Phys., Vol. 47, p. 602.

[53]. **H. Katagiri, N. Sasaguchi, S. Hando, S. Hoshino, J. Ohashi and T. Yokota.** 1997, Sol. Energy Mater. Sol. Cells, Vol. 49, p. 407.

[54]. **T. K. Chaudhari and D. Tiwari.** 2012, Sol. Energy Mater. Sol. Cells, Vol. 101, p. 46.

[55]. **P. A. Fernandes, P. M. P. Salome, A. F. da Cunha and B. Schubert.** 2010, Thin Solid Films, Vol. 519, p. 7382.

[56]. **V. G. Rajeshmon, C. Sudha Kartha, K. P. Vijayakumar, C. Sanjeeviraja, T. Abe and Y. Kashiwaba.** 2011, Sol. Energy, Vol. 85, p. 249.

[57]. **K. Ito and T. Nakazawa.** 1988, Jpn. J. Appl. Phys., Vol. 27, p. 2094.

[58]. **F. Liu, Y. Li, K. Zhang, B. Wang, C. Yan, Y. Lai, Z. Zhang, J. Li and Y. Liu.** 2010, Sol. Energy Mater. Sol. Cells, Vol. 94, p. 2431.

[59]. **C. P. Chan, H. Lam and C. Surya.** 2010, Sol. Energy Mater. Sol. Cells, Vol. 94, p. 207.

[60]. **W. Xinkun, L. Wei, C. Shuying, L. Yunfeng and J. Hongjie.** 2012, J. Semicond., Vol. 33, p. 022002.

[61]. **S. Chen, X. G. Gong, A. Walsh and S. Wei.** 2009, Appl. Phys. Lett., Vol. 94, p. 041903.

[62]. **J. Seol, S. Lee, J. Lee, H. Nam and K. Kim.** 2003, Sol. Energy mater. Sol. Cells, Vol. 75, p. 155.

[63]. **K. Moriya, J. Watabe, K. Tanaka and H. Uchiki.** 2006, Phys. status solidi (c), Vol. 3, p. 2848.

[64]. **K. Sekiguchi, K. Tanaka, K. Moriya and H. Uchiki.** 2006, Phys. status solidi (c), Vol. 3, p. 2618.

[65]. **T. Prabhakar and J. Nagaraju.** s.l. : Proceedings of the IEEE 35th Photovoltaic Specialist Conference,Hawaii, USA, 2010. p. 1964.

[66]. **K. Tanaka, N. Moritake, M. Oonuki and H. Uchiki.** 2008, Jpn. J. Appl. Phys., Vol. 47, p. 598.

[67]. **Y. Cui, S. Zuo, J. Jiang, S. Yuan and J. Chu.** 2011, Sol. Energy Mater. Sol. Cells, Vol. 95, p. 2136.

[68]. **H. Zhao and C. Persson.** 2011, Thin Solid Films, Vol. 519, p. 7508.

[69]. **S. Levcenko, G. Gurieva, M. Guc and A. Nateprov.** 2009, Moldavian Journal of the Physical Sciences , Vol. 8, p. 173.

[70]. **J. P. Leitao, N. M. Santos, P. A. Fernandes, P. M. P. Salome, A. F. da Cunha, J. C. Gonzalez, G. M. Ribeiro and F. M. Matinaga.** 2011, Phys. Rev. B, Vol. 84, p. 024120.

[71]. **J. P. Leitao, N. M. Santos, P. A. Fernandes, P. M. P. Salome, A. F. da Cunha, J. C. Gonzalez and F. M. Matinaga.** 2011, Thin Solid Films, Vol. 519, p. 7390.

[72]. **T. Unold, S. Kretzschmar, J. Just, O. Zander, B. Schubert, B. Marsen, H. Schock, H. Berlin and H. Platz.** 2011. Proceedings 37th IEEE PVSC 2011 (Seattle, USA). p. 002820.

[73]. **Y. Miyamoto, K. Tanaka, M. Oonuki, N. Moritake and H. Uchiki.** 2008, Jpn. J. Appl. Phys., Vol. 47, p. 596.

[74]. **K. Tanaka, Y. Miyamoto, H. Uchiki, K. Nakazawa and H. Araki.** 2006, Phys. status solidi (a), Vol. 203, p. 2891.

[75]. **K. Oishi, G. Saito, K. Ebina, M. Nagahashi, K. Jimbo, W. Maw, H. Katagiri, M. Yamazaki, H. Araki and A. Takeuchi.** 2008, Thin Solid Films, Vol. 517, p. 1449.

[76]. **B. Shin, K. Wang, O. Gunawan, K. B. Reuter, S. J. Chey, N. A. Bojarczuk, T. Todorov, D. B. Mitzi and S. Guha.** 2011. Proceedings 37th IEEE PVSC2011 (Seattle, USA). p. 002510.

[77]. **B. Ohnesorge, R. Weigand, G. Bacher, A. Forchel and W. Riedl.** 1998, Appl. Phys. Lett., Vol. 73, p. 1224.

[78]. **M. Kemell, M. Ritala and M. Leskela.** 2005, Crit. Rev. Solid State Mater. Sci., Vol. 30, p. 1.

[79]. **H. Katagiri, M. Nishimura, T. Onozawa, S. Maruyama, M. Fujita, T. Sega and T. Watanabe.** 1997. Proceedings of the Power Conversion Con ference-Nagaoka. p. 1003.

[80]. **H. Katagiri, K. Saitoh, T. Washio, H. Shinohara, T. Kurumadani and S. Miyajima.** 2001, Sol. Energy Mater. Sol. Cells, Vol. 65, p. 141.

[81]. **T. Kobayashi, K. Jimbo, K. Tsuchida, S. Shinoda, T. Oyanagi and H. Katagiri.** 2005, Jpn. J. Appl. Phys., Vol. 44, p. 783.

[82]. **H. Katagiri.** 2005, Thin Solid Films, Vols. 480-481, p. 426.

[83]. **T. Tanaka, D. Kawasaki, M. Nishio, Q. Guo and H. Ogawa.** 2006, Phys. Status Solidi (c), Vol. 3, p. 2844.

[84]. **A. Weber, H. Krauth, S. Perlt, B. Schubert, I. Kotschau, S. Schorr and H. W. Schock.** 2009, Thin Solid Films, Vol. 517, p. 2524.

[85]. **B. A. Schubert, B. Marsen, S. Cinque, T. Unold, R. Klenk, S. Schorr and H. W. Schock.** 2011, Prog. Photovolt. Res. Appl., Vol. 19, p. 93.

[86]. **R. Caballero, V. Izquierdo-Roca, J. M. Merino, E. J. Friedrich, A. Climent-Font, E. Saucedo, A. Perez-Rodriguez and M. Leon.** 2013, Thin Solid Films, Vol. 535, p. 62.

[87]. **M. P. Suryawanshi, G. L. Agawane, S. M. Bhosale, S. W. Shin, P. S. Patil, J. H. Kim and A. V. Maholkar.** 2013, Materials Technology, Vol. 28, p. 98.

[88]. **K. Jimbo, R. Kimura, T. Kamimura, S. Yamada, W. Maw, H. Araki, K. Oishi and H. Katagiri.** 2007, Thin Solid Films, Vol. 515, p. 5997.

[89]. **P. A. Fernandes, P. M. P. Salome and A. F. da Cunha.** 2009, Thin Solid Films, Vol. 517, p. 2519.

[90]. **P. A. Fernandes, P. M. P. Salome and A. F. da Cunha.** 2009, Semicond. Sci. Technol., Vol. 24, p. 105013.

[91]. **P. M. P. Salome, J. Malaquias, P. A. Fernandes, M. S. Ferreira, J. P. Leitao, A. F. da Cunha, J. C. Gonzalez, F. N. Matinaga, G. M. Ribeiro and E. R. Viana.** 2011, Sol. Energy Mater. Sol. Cells, Vol. 95, p. 3482.

[92]. **P. A. Fernandes, A. F. Sartori, P. M. P. Salome, J. Malaquias, A. F. da Cunha, M. P. F. Graca and J. C. Gonzalez.** 2012, Appl. Phys. Lett., Vol. 100, p. 233504.

[93]. **P. A. Fernandes, P. M. P. Salome, A. F. Sartori, J. Malaquias, A. F. da Cunha, B. Schubert, J. C. Gonzalez and G. M. Ribeiro.** 2013, Sol. Energy Mater. Sol. Cells, Vol. 115, p. 157.

[94]. **J. C. Gonzalez, G. M. Ribeiro, E. R. Viana, P. A. Fernandes, P. M. P. Salome, K. Gutierrez, A. Abelenda, F. M. Matinaga, J. P. Leitao and A. F. da Cunha.** 2013, J. Phys. D: Appl. Phys., Vol. 46, p. 155107.

[95]. **M. G. Sousa, A. F. da Cunha, P. M. P. Salome, P. A. Fernandes, J. P. Teixeira and J. P. Leitao.** 2013, Thin Solid Films, Vol. 535, p. 27.

[96]. **H. Yoo and J. Kim.** 2010, Thin Solid Films, Vol. 518, p. 6567.

[97]. **H. Yoo and J. Kim.** 2011, Sol. Energy Mater. Sol. Cells, Vol. 95, p. 239.

[98]. **N. Mamose, M. T. Htay, T. yudasaka, S. Igarashi, T. Seki, S. Iwano, Y. Hashimoto and K. Ito.** 2011, Jpn. J. Appl. Phys., Vol. 50, p. 01BG09.

[99]. **R. B. V. Chalapathy, G. S. Jung and B. T. Ahn.** 2011, Sol. Energy Mater. Sol. Cells, Vol. 95, p. 3216.

[100]. **S. W. Shin, S. M. Pawar, C. Y. Park, J. H. Yun, J. H. Moon, J. H. Kim and J. Y. Lee.** 2011, Sol. Energy Mater. Sol. Cells, Vol. 95, p. 3202.

[101]. **C. Platzer-Bjorkman, J. Scragg, H. Flammersberger, T. Kubart and M. Edoff.** 2012, Sol. Energy Mater. Sol. Cells, Vol. 98, p. 110.

[102]. **A. Khalkar, K. Lim, S. Yu, S. P. Patole and J. Yoo.** 2013, Int. J. Photoenergy, Vol. 2013, p. 690165.

[103]. **M. I. Amal and K. H. Kim.** 2013, Thin Solid Films, Vol. 534, p. 144.

[104]. **T. Ericson, J. J. Scragg, T. Kubart, T. Torndahl and C. Platzer-Bjorkmam.** 2013, Thin Solid Films, Vol. 535, p. 22.

[105]. **J. T. watjen, J. J. Scragg, T. Ericson, M. Edoff and C. Platzer-Bjorkman.** 2013, Thin Solid Films, Vol. 535, p. 31.

[106]. **K. Moriya, K. Tanaka and H. Uchiki.** 2007, Jpn. J. Appl. Phys., Vol. 46, p. 5780.

[107]. **S. M. Pawar, A. V. Malhokar, I. K. Kim, S. W. Shin, J. H. Moon, J. I. Rhee and J. H. Kim.** 2010, Current Appl. Phys., Vol. 10, p. 565.

[108]. **L. Sun, J. He, H. Kong, F. Yue, P. Yang and J. Chu.** 2011, Sol. Energy Mater. Sol. Cells, Vol. 95, p. 2907.

[109]. **G. D. Surgina, A. V. Zenkevich, I. P. Sipaylo, V. N. Nevolin, W. Drube, P. E. Teterin and M. N. Minnekaev.** 2013, Thin Solid Films, Vol. 535, p. 44.

[110]. **K. Tanaka, N. Moritake and H. Uchiki.** 2007, Sol. Energy Mater. Sol. Cells, Vol. 91, p. 1199.

[111]. **N. Moritake, Y. Fukui, M. Oonuki, K. Tanaka and H. Uchiki.** 2009, Phys. Status solidi (c), Vol. 6, p. 1233.

[112]. **K. Tanaka, M. Oonuki, N. Moritake and H. Uchiki.** 2009, Sol. Energy Mater. Sol. Cells, Vol. 93, p. 583.

[113]. **M. Y. Yeh, C. C. Lee and D. S. Wuu.** 2009, J. Sol-Gel Sci. Technol. , Vol. 52, p. 65.

[114]. **K. Tanaka, Y. Fukui, N. Moritake and H. Uchiki.** 2011, Sol. Energy Mater. Sol. Cells, Vol. 95, p. 838.

[115]. **K. Maeda, K. Tanaka, Y. Fukui and H. Uchiki.** 2011, Sol. Energy Mater. Sol. Cells, Vol. 95, p. 2855.

[116]. **M. Jiang, Y. Li, R. Dhakal, P. Thapaliya, M. Mastro, J. D. Caldwell, F. Kub and X. Yan.** 2011, J. Photonics for energy, Vol. 1, p. 019501.

[117]. **H. Park, Y. H. Hwang and B. Bae.** 2013, J. Sol-Gel Sci. Technol., Vol. 65, p. 23.

[118]. **J. Madarasz, P. Bombicz, M. Okuya and S. Kaneko.** 2001, Solid State Ionics, Vols. 141-142, p. 439.

[119]. **N. Kamoun, H. Bouzouita and B. Rezig.** 2007, Thin Solid Films, Vol. 515, p. 5949.

[120]. **Y. B. Kishore Kumar, G. Suresh Babu, P. Uday Bhaskar and V. Sundara Raja.** 2009, Sol. Energy Mater. Sol. Cells, Vol. 93, p. 1230.

[121]. **Y. B. Kishore Kumar, G. Suresh Babu, P. Uday Bhaskar and V. Sundara Raja.** 2009, Phys. Status Solidi (a), Vol. 206, p. 1525.

[122]. **T. Prabhakar and J. Nagaraju.** 2011, Sol. Energy Mater. Sol. Cells, Vol. 95, p. 1001.

[123]. **T. Prabhakar and J. Nagaraju.** 2011. 37th IEEE Photovoltaic Specialists Conference (PVSC).

[124]. **Y. Arba, M. Rafi, B. Hartiti, A. Ridah and P. Thevenin.** 2011, M. J. Condensed Matter, Vol. 13, p. 100.

[125]. **S. Das, C. Frye, P. G. Muzykov and K. C. Mandal.** 2012, ECS transactions, Vol. 45, p. 153.

[126]. **M. Patel, I. Mukhopadhyay and A. Ray.** 2012, J. Phys. D: Appl. Phys. , Vol. 45, p. 445103.

[127]. **M. Patel, I. Mukhopadhyay and A. Ray.** 2013, Semicond. Sci. Technol., Vol. 28, p. 055001.

[128]. **S. Huang, W. Luo and Z. Zou.** 2013, J. Phys. D: Appl. Phys., Vol. 46, p. 235108.

[129]. **Z. Seboui, Y. Cuminal and N. K. Turki.** 2013, J. Renewable Sustainable Energy, Vol. 5, p. 023113.

[130]. **N. M. Shinde, R. J. Deokate and C. D. Lokhande.** 2013, Journal of Analytical and Applied Pyrolysis, Vol. 100, p. 12.

[131]. **G. Gurieva, M. Guc, L. I. Bruk, V. Izquierdo-Roca, A. P. Rodriguez, S. Schorr and E. Arushanov.** 2013, Phys. Status Solidi (c), p. 1.

[132]. **M. Aono, K. Yoshitake and H. Miyazaki.** 2013, Phys. Status Solidi (c), p. 1.

[133]. **M. E. Rodriguez, M. Placidi, O. V. Galan, V. Izquierdo-Roca, X. Fontane, A. Fairbrother, D. Sylla, E. Saucedo and A. P. Rodriguez.** 2013, Thin Solid Films, Vol. 535, p. 67.

[134]. **D. R. Johnson.** 2000, Thin Solid Films, Vol. 361, p. 321.

[135]. **S. Taunier, J. Sicxkurdi, P. Grand, A. Chomond, O. Ramdani, L. Parissi, P. Panheleux, N. Naghavi, C. Hubert and M. Benfarah.** 2005, Thin Solid Films, Vol. 480, p. 526.

[136]. **J. J. Scragg, P. J. Dale and L. M. Peter.** 2008, Electrochemistry Communications, Vol. 10, p. 639.

[137]. **J. J. Scragg, P. J. Dale, L. M. Peter, G. Zoppi and I. Forbes.** 2008, Phys. Status Solidi (b), Vol. 245, p. 1772.

[138]. **J. J. Scragg, D. M. Berg and P. J. Dale.** 2010, J. Electroanalytical Chem., Vol. 646, p. 52.

[139]. **C. P. Chan, H. Lam and C. Surya.** s.l. : IEEE, 2009. 14th OptoElectronics and Communications Conference. .

[140]. **M. Kurihara, D. Berg, J. Fischer, S. Siebentritt and P. J. Dale.** 2009, Phys. Status Solidi (c), Vol. 6, p. 1241.

[141]. **A. Ennaoui, M. Lux-steiner, A. Weber, D. Abou-Ras, I. Kotschau, H. W. Schock, R. Schurr, A. Holzing, S. Jost, R. Hock, T. Vob, J. Schulze and A. Kirbs.** 2009, Thin Solid Films, Vol. 517, p. 2511.

[142]. **B. S. Pawar, S. M. Pawar, S. W. Shin, D. S. Choi, C. J. Park, S. S. Kolekar and J. H. Kim.** 2010, Appl. Surf. Sci., Vol. 257, p. 1786.

[143]. **G. Ma, T. Minegishi, D. Yokoyama, J. Kubota and K. Domen.** 2011, Chem. Phys. Lett., Vol. 501, p. 619.

[144]. **X. Fontane, L. C. Barrio, V. I. Roca, E. Saucedo, A. P. Rodriguez, J. R. Morante, D. M. Berg, P.J. Dale and S. Siebentritt.** 2011, Appl. Phys. lett., Vol. 98, p. 181905.

[145]. **M. Leon, T. Shimizu and S. Shingubara.** 2011, Matterials Letters, Vol. 65, p. 2364.

[146]. **R. N. Bhattacharya and J. Y. Kim.** 2012, The open Surface Science Journal, Vol. 4, p. 19.

[147]. **J. Iljina, R. Zhang, M. Ganchev, T. Raadik, O. Volobujeva, M. Altosaar, R. Traksmaa and E. Mellikov.** 2013, Thin Solid Films, Vol. 537, p. 85.

[148]. **E. M. Mkawi, K. Ibrahim, M. K. M. Ali and A. S. Muhammed.** 2013, Int. j. Electrochem. Sci., Vol. 8, p. 359.

[149]. **W. Liu, B. Guo, C. Mak, A. Li, X. Wu and F. Zhang.** 2013, Thin Solid Films, Vol. 535, p. 39.

[150]. **S. Verma, V. Agarwal, K. Jain, R. Pasricha and S. Chand.** 2013, Int. j. Photoenergy, Vol. 2013, p. 1.

[151]. **Z. Zhou, Y. Wang, D. Xu and Y. Zhang.** 2010, Sol. Energy Mater. Sol. Cells, Vol. 94, p. 2042.

[152]. **A. Wangperawong, J. S. King, S. M. Herron, B. P. Tran, K. Pangan-Okimoto and S. F. Bent.** s.l. : IEEE, 2010. 35th Photovoltaic Specialists Conference (PVSC).

[153]. **M. Pal, N. R. Mathews, R. S. Gonzalez and X. Mathew.** 2013, Thin Solid Films, Vol. 535, p. 78.

[154]. **T. T. Mau and K. H. Kim.** 2012, Journal of Ceramic Processing Research, Vol. 13, p. 301.

[155]. **G. Rajesh, N. Muthukumarasamy, E. P. Subramaniam, S. Agilan and D. Velaudhapillai.** 2013, J. Sol-Gel Sci. Technol., Vol. 66, p. 288.

[156]. **Q. Guo, H. W. Hillhouse and R. Agrawal.** 2009, J. Am. Chem. Soc., Vol. 131, p. 11672.

[157]. **Q. Guo, G. M. Ford, W. C. Yang, B. C. Walker, E. A. Stach, H. W. Hillhouse and R. Agrawal.** 2010, J. Am. Chem. Soc., Vol. 132, p. 17384.

[158]. **X. Xin, M. He, W. Han, J. Jung and Z. Lin.** 2011, Angew. Chem. Int. Ed., Vol. 50, p. 11739.

[159]. **C. Steinhagen, M. G. Panthani, V. Akhavan, B. Goodfellow, B. Koo and B. A. Korgel.** 2009, J. Am. Chem. Soc., Vol. 131, p. 12554.

[160]. **N. M. Shinde, D. P. Dubal, D. S. Dhawale, C. D. Lokhande, J. H. Kim and J. H. Moon.** 2012, Mater. Res. Bull., Vol. 47, p. 302.

[161]. **S. S. Mali, P. S. Shinde, C. A. Betty, P. N. Bhosale, Y. W. Oh and P. S. Patil.** 2012, J. Phys. Chem. Solids, Vol. 73, p. 735.

[162]. **S. S. Mali, B. M. Patil, C. A. Betty, P. N. Bhosale, Y. W. Oh, S. R. Jadkar, R. S. Devan, Y. R. Ma and P. S. Patil.** 2012, Electrochim. Acta, Vol. 66, p. 216.

[163]. **H. Guan, H. Shen, C. Gao and X. He.** 2013, J Mater Sci: Mater Electron., Vol. 24, p. 2667.

[164]. **X. Lin, J. Kavalakkatt, K. Kornhuber, S. Levcenko, M. Lux-Steiner and A. Ennaoui.** 2013, Thin Solid Films, Vol. 535, p. 10.

[165]. **S.K. Swami, A. Kumar and V. Dutta.** 2013, Energy Procedia, Vol. 33, p. 198.

[166]. **T. Washio, T. Shinji, S. Tajima, T. Fukano, T. Motohiro, K. Jimbo and H. Katagiri.** 2012, J. Mater. Chem., Vol. 22, p. 4021.

[167]. **S. Wagner and P.M. Brfdenbaugh.** 1977, J. Crystal Growth, Vol. 39, p. 151.

[168]. **K. Ito and T. Nakazawa.** Sydney, Australia : s.n., 1989. Proc. 4th Int. Conf. on 'Photovoltaics science and engineering'. p. 341.

[169]. **H. Katagiri, K. Jimbo, K. Moriya and K. Tsuchida.** Osaka, Japan : s.n., 2003. 3rd World Conference on Photovoltaic Energy Conversion. p. 2874.

[170]. **H. Katagiri, K. Jimbo, S. Yamada, T. Kamimura, W. S. Maw, T. Fukano, T. Ito and T. Motohiro.** 2008, Appl. Phys. Express, Vol. 1, p. 041201.

[171]. **K. Wang, O. Gunawan, T. Todorov, B. Shin, S. J. Chey, N. A. Bojarczuk, D. Mitzi and S. Guha.** 2010, Appl. Phys. Lett., Vol. 97, p. 143508.

[172]. **A. V. Moholkar, S. S. Shinde, A. R. Babar, K. U. Sim, Y. B. Kwon, K. Y. Rajpure, P. S. Patil, C. H. Bhosale and J. H. Kim.** 2011, Solar Energy, Vol. 85, p. 1354.

[173]. **A. V. Moholkar, S. S. Shinde, A. R. Babar, K. U. Sim, H. K. Lee, K. Y. Rajpure, P. S. Patil, C. H. Bhosale and J. H. Kim.** 2011, J. Alloys Compd., Vol. 509, p. 7439.

[174]. **A. V. Moholkar, S. S. Shinde, G. L. Agawane, S. H. Jo, K. Y. Rajpure, P. S. Patil, C. H. Bhosale and J. H. Kim.** 2012, J. Alloys Compd., Vol. 544, p. 145.

[175]. **K. Woo, Y. Kim and J. Moon.** 2012, Energy Environ. Sci., Vol. 5, p. 5340.

[176]. **S. Ahmed, K. B. Reuter, O. Gunawan, L. Guo, L. T. Romankiw and H. Deligianni.** 2012, Adv. Energy Mater., Vol. 2, p. 253.

[177]. **J. W. Cho, A. Ismail, S. J. Park, W. Kim, S. Yoon and B. K. Min.** 2013, ACS Appl. Mater. Interfaces, Vol. 5, p. 4162.

[178]. **B. Shin, O. Gunawan, Y. Zhu, N. A. Bojarczuk, S. J. Chey and S. Guha.** 2013, Prog. Photovolt: Res. Appl., Vol. 21, p. 72.

.....ooo.....

Chapter 2

THEORY OF SOLAR CELLS

2.1. Introduction
2.2. Solar radiation
2.3. p-n junctions as solar cell
2.4. Performance parameters of a solar cell
2.5. Diode parameters of a solar cell.

2.1 Introduction

Invention of p-n junction in around 1950 formed the basis of discovery of crystalline 'Si' solar cell by Pearson in 1954. A solar cell, or photovoltaic cell, is a semiconductor device consisting of p-n junction diode, which in the presence of sunlight is capable of generating electrical energy. A single cell can produce voltage of the order of 1 V and current of the order of few mA. Since the voltage and current are too small for most applications, cells should be inter connected to produce required voltage and current; this can be in series & parallel to form modules as per the power requirement. A solar module generally contains about 30 cells to generate typically dc output of 15 V and 1.5 A. Solar array is a set of solar modules electrically connected and mounted on a supporting structure. Intensive research is going on to obtain good performance solar cells at lab scale and then extend these results to industrial scale.

2.2 Solar radiation

Solar radiation is the electromagnetic radiation emitted by the Sun. Almost all biological as well as physical cycles in the Earth system are driven by solar radiation reaching the Earth. The Sun's total radiation output is approximately equivalent to that of a blackbody at 5776 K. Solar constant (I_{sc}) is the amount of

solar radiation received outside the Earth's atmosphere on surface normal to the incident radiation per unit time and per unit area and its value is 1367 Wm^{-2}.

The radiation coming directly from the Sun received at the Earth's surface is called "direct solar radiation". Quantity of scattered radiation coming from all other directions is called "diffuse solar radiation". Sum of both components as received on a horizontal surface is called "global solar radiation".

Solar radiation is partially absorbed during its passage through the atmosphere. "Air mass" coefficient can be used to help characterize the solar spectrum after solar radiation has travelled through the atmosphere. The spectrum outside the atmosphere is designated as AM 0 and that on the surface of the earth for normal incidence by AM 1. A typical spectrum for moderate climates is AM 1.5, which corresponds to an angle of incidence of solar radiation of 48.2° relative to the surface normal. The AM 1.5 conditions represent a satisfactory energy weighted average for terrestrial applications.

2.3 p-n junctions as solar cell

In order to convert light energy in to electrical energy, first we need to increase the potential energy of the carriers and then the carriers should be separated. The first one could be achieved by using semiconducting material, which possesses energy bands separated from each other by means of an energy gap. On absorption of a photon, difference in energy bands results in increase in the potential energy of electrons. Now in order to separate the charge carriers, an asymmetry in electronic structure in the semiconductor device is required. A combination of p-type semiconductor and n-type semiconductor has such an asymmetry which provides 'built in electric field' at the junction. When a p-n junction is illuminated electron hole pairs will be

created. Due to the built in field across the junction electrons will flow from p-side to n-side and holes will flow from n-side to p-side resulting in the separation of the charge carriers.

2.3.1 p-n junction under equilibrium

When two layers of semiconductor material of opposite carrier types are intimately joined, exchange of charge takes place so that the Fermi level becomes the same in both layers. Electrons from the n-type material diffuse in to the p-type material and holes diffuse from the p-side to n-side. Due to this diffusion process the region close to the junction becomes almost completely depleted of mobile charge carriers. Gradual depletion of the charge carriers gives rise to 'space charge' created by the charge of the (stationary) ionized donor and acceptor atoms that is not compensated by the mobile charges any more. This region of the space charge is called the "space-charge region" or "depleted region". Regions outside the depletion region, in which the charge neutrality is conserved, are denoted as the "quasi-neutral" regions.

The space charge region at the junction causes internal electric field across the junction which makes the carriers drift in a direction opposite to that of diffusion current. At equilibrium, drift current balances the diffusion current and the net current becomes zero. At equilibrium the electrochemical potential, [which describes an average energy of electrons and is represented by the Fermi energy], is constant. i.e., under equilibrium Fermi level has a constant position in the band diagram. Figure 2.1 shows the energy band diagram of p-n junction at equilibrium.

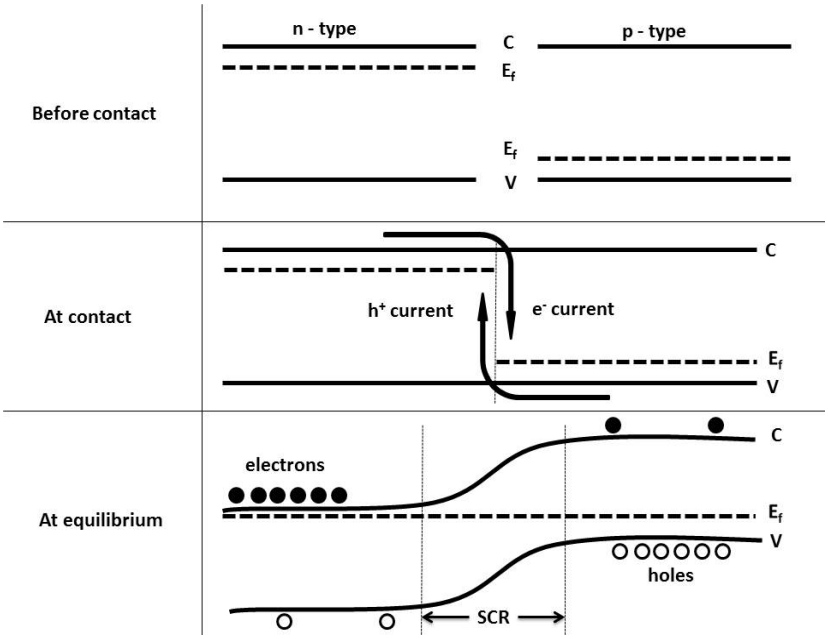

Figure 2.1. p-n junction under equilibrium condition

The energy gap between Fermi level and the conduction/valence band must be the same in the quasi neutral regions and is the same as in isolated n and p type semiconductors. In the space charge region, conduction/valence bands are not represented by straight lines any more but they are curved, which indicates the presence of an electric field. Presence of the internal electric field inside the p-n junction means that there is an electrostatic potential difference, V, across the space-charge region. Since n-side has lost electrons, and p-side has acquired electrons, n-side becomes positive relative to the p-side.

2.3.2 p-n junction under bias

When an external voltage V_a is applied across the junction, the potential across the junction becomes $V+V_a$. When the applied external voltage is positive with respect to the potential of the n-type region, the applied voltage will increase the potential difference across the p-n junction. This is known as

'reverse biased' condition.The potential barrier across the junction is increased under reverse-bias voltage, which results in a wider space-charge region. When the applied external voltage is negative with respect to the potential of the n-type region, the applied voltage will decrease the potential difference across the p-n junction. This is known as 'forward biased' condition. Potential barrier across the junction is decreased under forward-bias and the space charge region becomes narrower.

Shockley equation describes current voltage behaviour of an ideal p-n junction diode. Total current I in a diode is given by

$$I = I_0\left(e^{\frac{qVa}{kT}} - 1\right) \text{----------(2.1)}$$

Where I_0 is the reverse saturation current, V_a the applied voltage, k Boltzmann constant, T absolute temperature & q electronic charge. The reverse saturation current (I_0) is very important since it incorporates material parameters like diffusion coefficient (D), diffusion length (L), carrier life time (τ) and intrinsic carrier concentration n_i.

$$I_0 = qA\left(\frac{D_n n_i^2}{L_n N_A} + \frac{D_p n_i^2}{L_{np} N_D}\right) \text{----------(2.2)}$$

2.3.3 p-n junction under illumination

From the solar cell point of view, it is more important to study the behaviour of p-n junction under light. When the junction is illuminated, additional electron-hole pairs are created both in space charge region and quasi neutral region. Carriers created in the space charge region are readily swept out by the electric field at the junction (Electrons moves towards n-side and holes towards p-side). Now among the carriers created at the quasi neutral region,

those within the diffusion length can reach the junction region and will be 'pulled out' to other side. Only minority carriers will cross the junctions as they have to go 'down the hill' in terms of energy. Electrons from p-side will come to the n-side and holes from the n-side flow towards the p-side. In this way there is a net increase in the negative charge at n-side and net increase in the positive charge at p-side. This causes a potential to appear across the p-n junction due to light falling on it and is known as photovoltaic effect.

The direction of current flow, under illumination, is from n-side to p-side. This current is known as light generated current (I_L). Under open circuit condition, which means there is no external contact between the n-type and the p-type regions, no net current can flow inside the p-n junction. It means that the current resulting from the flux of photo-generated and thermally-generated carriers has to be balanced by the opposite recombination current. Recombination current will increase through lowering of the electrostatic potential barrier across the depletion region. The electrostatic-potential barrier across the junction is lowered by an amount V_{oc}, known as open circuit voltage.

Under illumination, when the n-type and p-type regions are short circuited, whole of the photo generated current will flow through the external circuit. Under the short circuited condition, electrostatic potential barrier is not changed, but from a strong variation of the quasi Fermi levels inside the depletion region one can determine that the current is flowing inside the semiconductor.

When resistive load is connected between the terminals of the illuminated p-n junction, the junction experiences both optical and electrical bias. Now, only a fraction of the photo-generated current will flow through the external circuit. The electrochemical potential difference between the n-type and p-type regions will be lowered by the voltage drop over the load. This in turn lowers the

electrostatic potential over the depletion region which results in an increase of the recombination current. The net current flowing through the load is determined as the sum of the light generated current and the recombination current. The voltage drop at the load can be simulated by applying a forward-bias voltage to the junction. Equation 2.1, which describes the behaviour of the junction under applied voltage, can be modified to describe the net current of the illuminated p-n junction

$$I = I_0\left(e^{\frac{qVa}{kT}} - 1\right) - I_L \text{ ----------(2.3)}$$

The dark and illuminated I-V characteristics of the p-n junction are represented in figure 2.2. The illuminated I-V characteristic of the p-n junction is the same as the dark I-V characteristic, but it is shifted down by the light generated current I_{sc}.

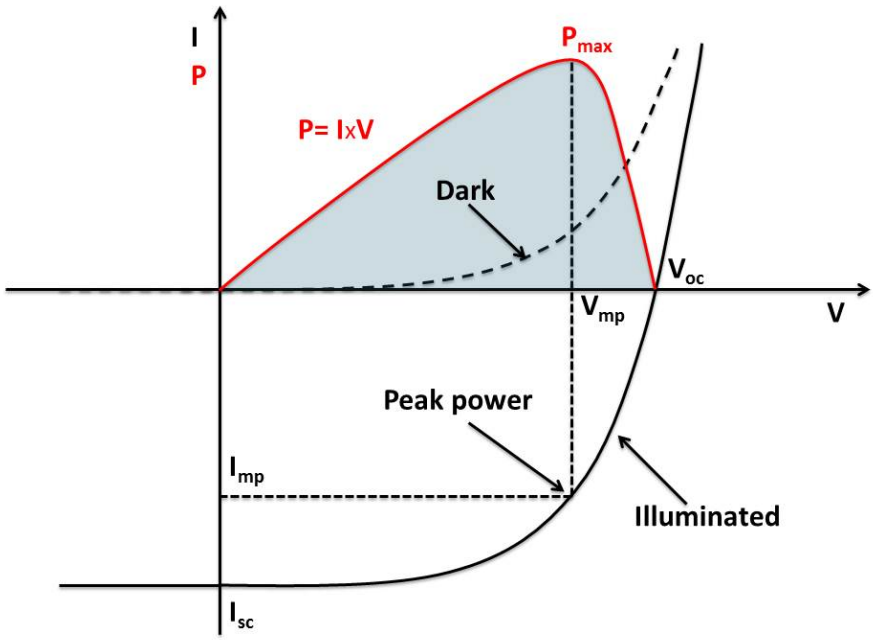

Figure 2.2. DarK and illuminated I-V characteristics of a solar cell

2.4 Performance parameters of a solar cell

The characteristic equation of a solar cell, which relates solar cell parameters to the output current and voltage, is given by

$$I = I_L - I_0\left(e^{\frac{q(V-IR_s)}{nkT}} - 1\right) - \frac{V - IR_s}{R_{sh}} \quad \text{----------(2.4)}$$

Where, I_L is the light-generated current, q is the electron charge, k is the Boltzmann constant, T is the temperature, R_{sh} is the shunt resistance, R_s is the series resistance, n is the diode ideality factor and I_0 is the reverse saturation current of the cell. R_{sh}, R_s, n and I_0 are known as diode parameters of the cells.

Performance of a solar cell is monitored through four performance parameters viz., open circuit voltage (V_{oc}), short circuit current (I_{sc}), fill factor (FF) and efficiency (η) of the cell.

2.4.1 Open circuit voltage (V_{oc})

Open circuit voltage (V_{oc}) is the maximum voltage that is available from a solar cell. It is the voltage between the terminals of the cell when no current is drawn. The V_{oc} is corresponding to the amount of forward bias of a p-n junction due to light generated current (at this voltage I_L becomes equal and opposite to forward bias diffusion current of a p-n junction diode). V_{oc} depends on light generated current and by assuming the shunt resistance is high enough to neglect the final term of the characteristic equation, V_{oc} is given by

$$V_{oc} \approx \frac{nkT}{q} ln\left(\frac{I_L}{I_0} - 1\right) \quad \text{----------(2.5)}$$

Thus for higher V_{oc}, the I_0 should be lower. Since I_0depends on the recombination in the solar cell, V_{oc} is actually a measure of the amount of recombination in the device. The lowest value of I_0 is obtained when the

recombination rate is equal to the thermal equilibrium recombination rate. In this case, the maximum possible V_{oc} for 'Si' solar cell is 0.85 V. V_{oc} of a solar cell depends also on the band gap of the material. According to Shockley–Queisser limit max V_{oc} will always be less than the band gap as shown in figure 2.3. The dotted line shows maximum V_{oc} is always below the bandgap.

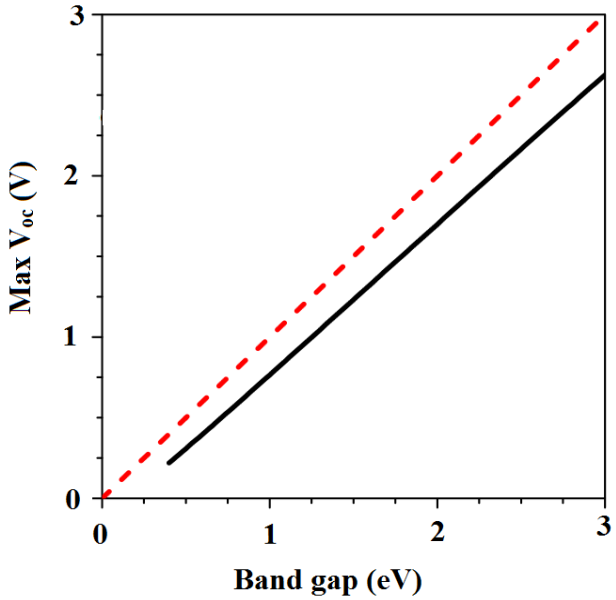

Figure 2.3. Solid curve: The limit for V_{oc} in the Shockley-Queisser model

2.4.2 Short circuit current (I_{sc})

Short circuit current (I_{sc}) is the maximum current produced by a solar cell when its terminals are short circuited and it depends on the number of incident photons; this is determined by the spectrum of the incident light and the area of the solar cell. In order to remove the dependence of the I_{sc} on the solar cell area, the short-circuit current density (J_{sc}) is often used to describe the maximum current delivered by a solar cell.

We can relate J_{sc} to the incident spectrum using quantum efficiency (QE), which is the probability that an incident photon of energy E will deliver one electron to the external circuit.

$$J_{sc} = q\int b_s(E)QE(E)dE \quad \text{----------(2.6)}$$

Where $b_s(E)$ is the incident photon flux density and q is the electronic charge. Maximum current that the solar cell can deliver strongly depends on the optical properties (band gap, absorption coefficient & reflection coefficient) of the solar cell material. J_{sc} also depends on the collection probability of the solar cell, which depends mainly on the surface passivation and the minority carrier lifetime.

J_{sc} of the solar cell depends strongly on the band gap of the absorber material. A material with large band gap will absorb less number of photons as compared to the materials with low band gap. Therefore, J_{sc} will increase with decrease in band gap energy. Figure 2.4 shows a plot of the possible J_{sc} from an absorber as a function of band gap. 'Si' has band gap of 1.1 eV, and the corresponding upper limit to J_{sc} is about 46 mA/cm^2. For 'Si' solar cell maximum J_{sc}achieved so far in the lab scale is 42.7mA/cm^2.

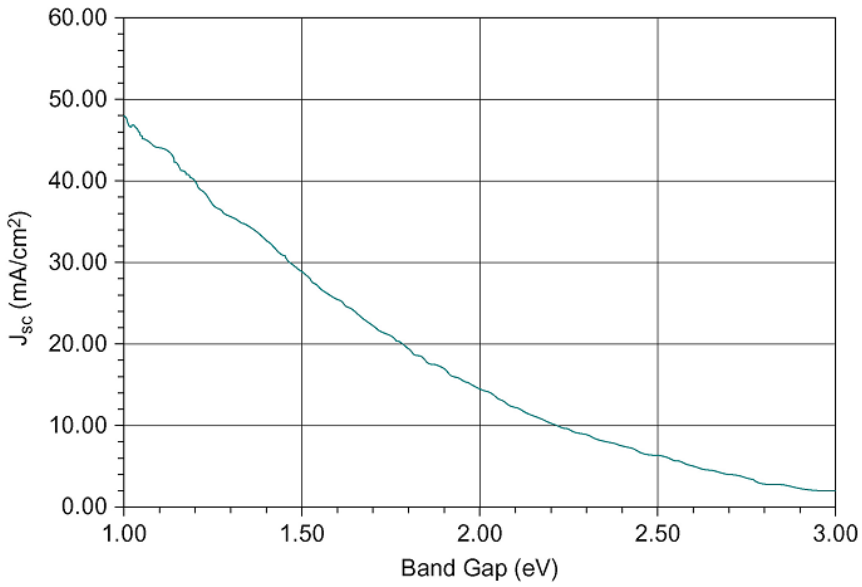

Figure 2.4. J_{sc}vs. absorber band gap for an AM 1.5 spectrum of light

2.4.3 Fill factor (*FF*)

Fill factor (*FF*), is a parameter which, in conjunction with V_{oc} and I_{sc}, determines the maximum power from a solar cell. It is defined as the ratio of the maximum power from the solar cell to the product of V_{oc} and I_{sc}. Graphically, the *FF* is the measure of "squareness" of the solar cell characteristics

$$FF = \frac{V_m J_m}{V_{oc} J_{sc}} \text{ ---------- (2.7)}$$

FF is the most important parameter which determines the efficiency of solar cell, since for the same V_{oc} and J_{sc} , *FF* determines the maximum power that can be obtained from a solar cell as given by the equation.

$$P_{\max} = V_{oc} J_{sc} FF \text{ ---------- (2.8)}$$

In ideal case, its value can be 100 % corresponding to square I-V curve. But it is not feasible to have square I-V. There are always some losses which reduces value of *FF*. The best values of *FF* that can be obtained for a solar cell can be written as a function of V_{oc}.

$$FF = \frac{\nu_{oc} - \ln(\nu_{oc} + 0.72)}{\nu_{oc} + 1} \text{ ----------(2.9)}$$

Where $\nu_{oc} = \frac{qV_{oc}}{kT}$ is normalized voltage. Good solar cells typically will have *FF* values of about 80 %.

2.4.4 Efficiency (η)

Solar cell efficiency is the ratio of the power output to the power input. It is the most commonly used parameter to compare the performance of solar cells. Cell efficiency depends on spectrum and intensity of incident sunlight and also on temperature of solar cell. So usually solar cell efficiencies are measured under

standard test conditions (STC). STC specifies temperature of 25 °C and irradiance of 1000 W/m^2 with AM 1.5 spectrum.

$$\eta = \frac{V_{oc} J_{sc} FF}{P_{in}} \quad \text{----------} \quad (2.10)$$

J_{sc} of solar cell decreases with band gap and V_{oc} increases with band gap; hence there should be an optimum band gap for which the efficiency of a solar cell would be maximum. Shockley–Queisser limit refers to the calculation of the maximum theoretical efficiency of a solar cell made from a single p-n junction. It was first calculated by William Shockley and Hans Queisser [1]. The calculation places maximum solar conversion efficiency around 33.7 % assuming a single p-n junction with band gap of 1.4 eV (using an AM 1.5 solar spectrum). Variation of conversion efficiency as function of band gap is shown in figure 2.5.

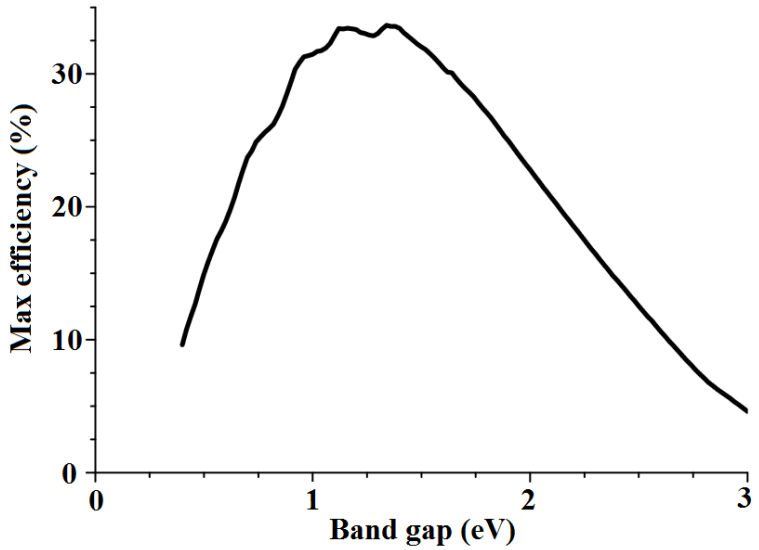

Figure 2.5. Maximum conversion efficiency of a single junction cell vs. band gap.

2.5 Diode parameters of a solar cell.

Values of the performance parameters solely depend on the diode parameters of cell at given illumination intensity and temperature. The four diode parameters of a cell are series resistance (R_s), shunt resistance (R_{sh}), ideality factor (n) and reverse saturation current (I_0). Many analytical methods have been developed to determine one or more of the diode parameters [2].

2.5.1 Series resistance (R_s)

The series resistance R_s of solar cell is important parameter that mainly affects the *FF*. Series resistance is the sum of resistances due to all components that comes in the path of the current [3]. This includes base, emitter, semiconductor-metal contact resistance and resistance of metal contact. The main impact of series resistance is to reduce the fill factor, although excessively high values may also reduce the short-circuit current. For an ideal solar cell series resistance should be zero.

Series resistance does not affect the solar cell at open-circuit voltage since the overall current flow through the solar cell, and therefore through the series resistance is zero. However, near the open-circuit voltage, the IV curve is strongly affected by the series resistance. A straight forward method of estimating series resistance from solar cell is to find slope of the I-V curve at the open-circuit voltage point.

As the series resistance increases, more and more voltage drop occurs within the cell and its I-V starts to deviate from the low R_s case (figure 2.6). For very high value of R_s, one gets nearly straight line with reduced I_{sc}. But V_{oc} remains the same, as in open circuit no current flows, and voltage drop in the cell is zero.

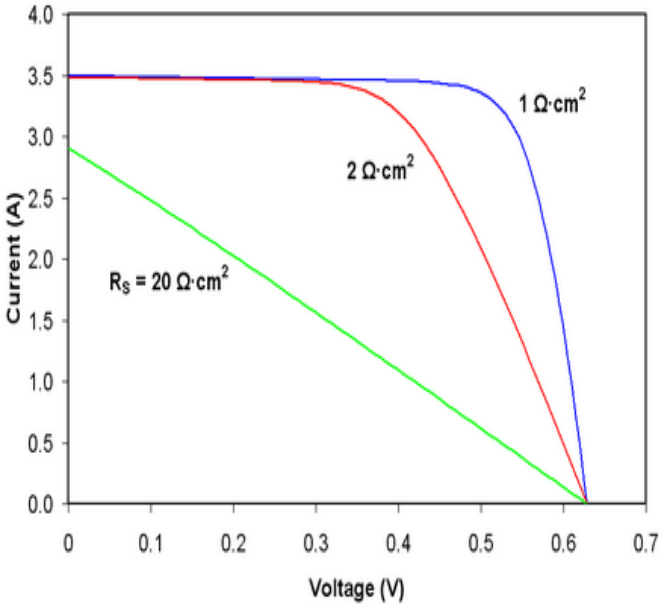

Figure 2.6. Effect of series resistance on the I-V characteristics of a solar cell

2.5.2 Shunt resistance (R_{sh})

Parallel or shunt resistance arises from the leakage of current through the cell, around the edges of the device and between contacts of different polarity [4].

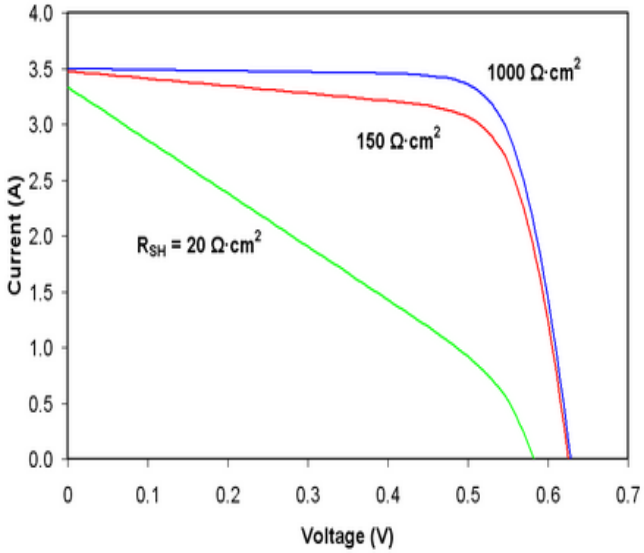

Figure 2.7.Effect of shunt resistance on the I-V characteristics of a solar cell

Low shunt resistance causes power losses in solar cells by providing an alternate current path for the light-generated current. As shunt resistance decreases, the current diverted through the shunt resistor increases for a given level of junction voltage. The result is that the voltage-controlled portion of the I-V curve begins to sag toward the origin (figure 2.7), producing a significant decrease in the terminal current I and slight reduction in V_{oc}. Very low values of R_{sh} will produce a significant reduction in V_{oc}.

2.5.3 Ideality factor (*n*)

The ideality factor (n) of a diode is measure of how closely the diode follows the ideal diode equation. The forward current in *p-n* junction is dominated by diffusion of minority carriers injected into the neutral regions of the junction. This type of current gives an ideality factor of 1. Recombination of carriers in the space charge region, mediated by recombination centers located near the intrinsic Fermi level, results in an ideality factor of 2 [5]. In fact, defects drive the recombination process. More defects leads to more space charge recombination. If there were no defects present, total diode current would be diffusion current and n would be 1. This would be the "ideal" diode case. More defects drive n up to 2 (the "non-ideal" case). Value of n can be estimated directly from the current-voltage (I-V) data by calculating the slopes of the straight-line regions of dark Log I vs. V. In heterojunctions, tunneling through barriers may give rise to 'n' values greater than 2. The effect of an ideality factor greater than 1 is to reduce the *FF* of the solar cell.

2.5.4 Reverse saturation current (I_0)

Reverse saturation current (I_0) is a measure of the leakage of carriers across the p-n junction in reverse bias. This leakage is the result of carrier recombination in the neutral regions on either side of the junction.

References

[1]. **W. Shockley and H. J. Queisser.** 1961, J. Appl. Phys., Vol. 32, p. 510.

[2]. **F. Khan, S. N. Singh and M. Husain.** 2010, Semicond. Sci. Technol., Vol. 25, p. 015002.

[3]. **C. S. Solanki.***SOLAR PHOTOVOLTAICS Fundamentals, Technologies and Applications.* New Delhi : PHI Learning Private Limited, 2009.

[4]. **Jenny Nelson.***The Physics of Solar Cells.* London : Imperial College Press, 2003.

[5]. **J. M. Shah, Y. L. Li, T. Gessmann and E. S. Schubert.** 2003, J. Appl. Phys., Vol. 94, p. 2627.

.....ꕥ.....

Chapter 3

PREPARATION AND CHARACTERIZATION OF Cu_2ZnSnS_4 ABSORBER LAYER USING CHEMICAL SPRAY PYROLYSIS TECHNIQUE

3.1. Introduction
3.2. Deposition technique: Chemical spray pyrolysis
3.3. Effect of various deposition parameters
3.4. Conclusions

3.1 Introduction

Nowadays intense research is going on all over the world for developing low cost, eco-friendly thin film solar cells using earth-abundant materials. Cu_2ZnSnS_4 (CZTS) is a relatively new and strong contender in this direction. It has the optimum band gap of 1.5 eV, suitable for an absorber layer and high absorption coefficient (> 10^4 cm^{-1}). It can be deposited in thin film form using various vacuum and non-vacuum based approaches [1-11]. Of all the possible routes, devices with evaporated CZTS absorber have touched a maximum conversion efficiency of 8.4 % [12]. Despite the high efficiency, use of vacuum technique and cadmium based buffer layer are the major drawbacks for this cell.

Aim of present work is the development of CZTS based solar cell using cost-effective deposition technique and cadmium free buffer layer. Hence for the present study we selected chemical spray pyrolysis (CSP) as the deposition technique. CSP is simple and low cost technique widely used for the deposition of thin films. Moreover, easiness of doping and possibility of large area deposition make this technique more popular and specifically suitable for depositing thin film solar cells.

As we mentioned in chapter 1, there are several groups currently working on spray deposition of CZTS. But only very few reached the level of device fabrication using this technique. Prabhakar et al. [13] reported the fabrication of CZTS/ZnS solar cell on FTO coated glass substrates using ultrasonic spray pyrolysis with conversion efficiency of 1.16 %. Taking into consideration of present need for low cost energy, we intend to work towards the development of CZTS absorber layer using spray pyrolysis technique and subsequently CZTS based solar cells.

3.2 Deposition technique: Chemical spray pyrolysis

There are various processes by which one can deposit thin films. They can be broadly classified as physical and chemical processes. Among these, the chemical processes are relatively economical and easier than the physical processes. There is no ideal process to prepare the compound semiconductors in thin film form which will satisfy all the possible requirements. Among the various chemical processes (viz. chemical vapour deposition, chemical spray pyrolysis, chemical bath deposition, sol-gel etc.), chemical spray pyrolysis is the most popular one due to its simplicity, cost-effectiveness and ability to control the stoichiometry. A large variety of thin films from a group of inorganic, organic and polymer materials can be deposited onto variety of substrates such as soda glass, quartz, pyrex, sapphire, silicon wafer etc. There is virtually no restriction on substrate material, any substrate having high temperature tolerance can be used.

Spray pyrolysis is a process in which thin film is deposited by spraying solution on to a pre-heated substrate, where the constituents react to form required chemical compound. Despite the simplicity of spray pyrolysis process, it has number of advantages,

1) It is a non-vacuum technique and does not require any high quality targets and/or substrates.

2) Stoichiometry can be easily controlled by merely changing the concentration of precursors in the starting solution.

3) Doping can be easily done, by adding the soluble salt of dopant into the precursor solution.

4) There are virtually no restrictions on substrate materials dimensions or on its surface profile. Deposition over large area is possible.

5) By changing composition of the spray solution during the spray process, films having gradient in composition across the thickness can be deposited.

3.3 Effect of various deposition parameters

In the case of spray deposition, property of the deposited films depends on several parameters of which the major ones are substrate temperature, spray rate and ratio of precursors. In this chapter, we will describe how we optimized each of these parameters for obtaining good quality absorber layer. Our initial aim is to find out the right choice of precursors for obtaining good quality CZTS absorber layer.

3.3.1 Effect of precursor Choice

Precursors used were water soluble salts of 'Cu', 'Zn', 'Sn' and 'S'

'Cu'-precursor: The widely used precursor for copper for depositing CZTS and CIS thin films using spray pyrolysis is $CuCl_2.2H_2O$ [11, 14-25]. Hence it is used in the present case also.

'Zn'-precursor: There are reports on using two different precursors for Zn viz. $Zn(CH_3COO)_2.2H_2O$ and $ZnCl_2.2H_2O$ for spray pyrolytic deposition of CZTS [15, 20, 26-27]. Hence both the precursors are tried.

'Sn'-precursor: Similar to the case of 'Zn'-precursor, two different compounds viz. stannous chloride ($SnCl_2.2H_2O$) and stannic chloride ($SnCl_4.5H_2O$) were reported as precursor for 'Sn' [11, 16-17,21] and hence both these precursors are tried.

'S'-precursor: The water soluble organic compound $CS(NH_2)_2$ (thiourea) is used as the precursor for sulfur.

3.3.1.1 Experimental

As mentioned before, we used two different precursors for tin viz., stannous chloride ($SnCl_2$) and stannic chloride ($SnCl_4$) and two for zinc viz. zinc chloride ($ZnCl_2$) and zinc acetate ($Zn(CH_3COO)_2$). Aqueous solution, containing cupric chloride (0.02 M), zinc acetate/zinc chloride (0.0125 M), stannous chloride /stannic chloride (0.0125 M) and thiourea (0.15 M), was sprayed at the rate of 8 ml/min onto the substrate kept at 623 K using compressed air (pressure~1.5 bar) as carrier gas. Concentration of thiourea was 3 times larger than that was required to maintain stoichiometry (0.05 M), to compensate for the loss of sulfur during pyrolysis. The samples were named as follows

CZ-A – stannous chloride and zinc chloride
CZ-B – stannous chloride and zinc acetate
CZ-C – stannic chloride and zinc acetate
CZ-D – stannic chloride and zinc chloride

In order to know the best combination of precursors for getting 'device quality' CZTS absorber layer, deposited films were analyzed as follows.

3.3.1.2 Structural studies

Analysis of films using X-ray diffraction (XRD) can provide valuable insights about crystalline structure and secondary phases. Every crystalline substance gives a

diffraction pattern; the same substance always gives the same pattern and in a mixture of substances each produces its own pattern independent from others. XRD pattern of a pure substance is, therefore, fingerprint of the substance.

Geometrical conditions, which must be satisfied for diffraction to occur in a crystal, were first established by Bragg. When monochromatic x-rays impinge upon the atoms in a crystal lattice, each atom acts as a source of scattering. The crystal lattice acts as series of parallel reflecting planes. Intensity of the reflected beam at certain angles will go high when the path difference between two reflected waves from two consecutive parallel planes is an integral multiple of λ. This condition is called Bragg's law and is given by the relation

$$n\lambda = 2d\sin\theta \quad \text{.....(3.1)}$$

where n is the order of diffraction, λ is the wavelength of the x-rays, d is the spacing between consecutive parallel planes and θ is the 'glancing angle'[28].

X-ray diffraction studies give whole range of information about crystal structure, orientation, average crystalline size and stress in the films. Experimentally obtained diffraction patterns of the sample are compared with standard powder diffraction files published by "International Centre for Diffraction Data (ICDD)" formerly known as "Joint Committee on Powder Diffraction Standards (JCPDS)".

Lattice parameters of the crystallographic systems in the present study can be calculated using the following relation with (hkl) parameters and inter planar spacing 'd'.

$$\frac{4\,Sin^2\theta}{\lambda^2} = \frac{h^2+k^2}{a^2} + \frac{l^2}{c^2} \quad \text{.....(3.2)}$$

where *h, k* and *l* are the Miller indices of the plane. X-ray diffraction measurements of the films in the present studies were carried out using Rigaku X-ray diffractometer. The filtered Cu K_α (λ =1.5418 Å) radiation was used for recording the diffraction pattern.

Choice of precursor plays an important role in the structure of sprayed thin films [29-33]. X-ray diffractograms of the CZTS films deposited using different precursor solutions are given in figure 3.1. All the films show preferential orientation along (112) plane. Crystallite size of the films increased considerably when the precursor of tin changes from stannous chloride to stannic chloride. But choice of zinc precursor does not make significant change in crystallite size of the films. For CZTS films prepared using stannic chloride precursor, there are peaks corresponding to the Cu_xS phase, which is not that much pronounced in stannous chloride based films.

From the XRD peaks, lattice constants were calculated using equation 3.2. The 2θ values chosen for the calculation were 28.45 ^{o} corresponding to (112) plane and 47.36 ^{o} corresponding to (220) plane. The obtained lattice constants were $a = 0.5424 nm$ and $c = 1.086 nm$ which are in good agreement with the reported single crystal data, $a = 0.5427 nm$ and $c = 1.0848 nm$. Values of crystallite size was calculated using Scherrer formula (table 3.1)

$$D = \frac{0.9\lambda}{\beta \cos\theta} \quad \text{.....(3.3)}$$

where D is the grain size, λ is the wavelength of Cu-K_α line and β is the full width at half maximum.

Table 3.1. FWHM and Crystallite size of CZTS films deposited using various precursors

Sample name	FWHM (degrees)	Crystallite size (nm)
CZ-A	0.40	20
CZ-B	0.45	18
CZ-C	0.23	35
CZ-D	0.26	31

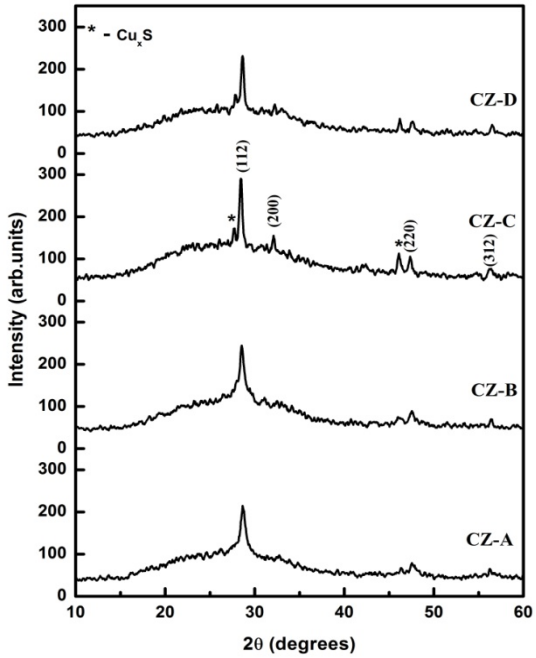

Figure 3.1. X-ray diffractograms of CZTS samples prepared with different precursors.

3.3.1.3 Compositional analysis

Compositional analysis of the CZTS samples was done using Energy Dispersive X-ray Analysis (EDAX),which makes use of X-ray spectrum (emitted by the sample on bombarding with focused beam of electrons) to obtain the localized chemical composition. All elements from atomic number 4 (Be) to 92 (U) can be detected in principle; however all instruments are not

equipped for 'light' elements (Z < 10). Qualitative analysis involves identification of lines in the spectrum and is fairly straightforward owing to the simplicity of X-ray spectra. Quantitative analysis (determination of the concentrations of the elements present) entails measuring 'line intensity' for each element in the sample and then calibrating with standards of known composition.

From the EDAX studies done on precursor varied samples (table 3.2), it was found that copper concentration was low in all the films as it was in the precursor solution. In most of the works reported in spray pyrolysed CZTS films, the sulfur content is low [11,14]. Nakayama and Ito [34] were able to increase sulfur content in spray deposited film to 48 at. % by adding 30 vol. % ethanol to the solvent. But we could deposit films in which sulfur content was quite close to the stoichiometric value. It could be observed that the film CZ-C was nearly stoichiometric with Cu/(Zn+Sn) ratio of 0.91, Zn/Sn ratio of 0.88 and S/metal ratio of 1.01. However the composition of all other films showed large deviation from stoichiometry. Chlorine was present in both the samples in almost same proportion, irrespective of the precursor solutions chosen. Though the reason is quite obscure, we could observe that the Zn/Sn ratio in CZ-A and CZ-B was much lower than that of other two films.

Table.3.2. Elemental composition of CZTS films prepared using different precursors

Sample	Cu (at.%)	Zn (at.%)	Sn (at.%)	S (at.%)	Cl (at.%)	$\frac{Cu}{Zn+Sn}$	$\frac{S}{Metal}$	$\frac{Zn}{Sn}$
CZ-A	23.4	7.1	17.8	48.7	3	0.94	1.01	0.40
CZ-B	22.4	7.4	19.5	47.9	2.8	0.83	0.97	0.38
CZ-C	23.1	11.8	13.5	48.9	2.6	0.91	1.01	0.88
CZ-D	22.5	11.4	15.4	47.5	3.2	0.84	0.96	0.74

3.3.1.4 Electrical properties

Conductivity type of the films can be found out using hot probe technique (otherwise known as thermoelectric probe method). In this method conductivity type is determined by the sign of thermal EMF or 'Seebeck voltage' generated by thermal gradient between two probes kept in contact with the sample surface of which one is hot and the other is cold. In a voltmeter (positive terminal connected to the hot probe and negative terminal to the cold probe) which is kept in contact with an n-type material, a positive voltage is detected. For a p-type material, the voltage detected is negative [35]. Hot probes are usually effective in resistivity range of 10^{-3} to 10^{3} Ω.cm. In the present work conductivity type is evaluated using hot probe method at room temperature. All CZTS films exhibited p-type conductivity regardless of the choice of precursor.

Electrical resistivity of the films was measured using 'two probe method' with the electrode in planar geometry. Measurements were done by giving electrical contacts using silver amalgam in the form of two end contacts. The dark resistivity is given by

$$\rho = \frac{Vlt}{Id} \text{ ---------- (3.4)}$$

Where V is the applied voltage, I is the measured current, l is the length of the electrodes, d is the distance between the electrodes and t is the thickness of the film. In all our resistivity measurements, we kept electrode length and distance between two electrodes as 5 mm so that resistivity is the product of sheet resistance (V/I) and thickness (t) of the film.

Room temperature resistivity of CZTS samples was calculated using two probe method. There is not much variation in resistivity when the zinc precursor changes. But the resistivity decreases by two orders of magnitude just by

changing the precursor from stannous to stannic chloride. The values obtained were of the order of 10^{-1} Ω.cm and 10^{-3} Ω.cm for films based on stannous and stannic chloride respectively. There have been reports about controlling the resistivity by varying substrate temperature [11]. However, variation in resistivity by this order, solely due to a change in precursor, has not been reported earlier.

3.3.1.5 Hall measurements

Hall Effect is a technique that can give lot of information about the conduction properties of semiconductors. Mobility and carrier concentration can be obtained from the Hall coefficient in conjunction with the resistivity. Mobility is pertinent to the understanding of solar cells since such things as 'carrier life time' and 'short circuit current density' of the solar cells are related to this parameter of semiconductors.

Hall Effect occurs when material carrying current is subjected to magnetic field perpendicular to the direction of the current; if the current is flowing in the x-direction and the magnetic field is applied in the z-direction, the potential gradient will appear across the sample in the y-direction. This transverse potential gradient is found to be proportional to product of the current density in the sample and the applied magnetic field; the constant of proportionality is called the "Hall coefficient." The Hall voltage V_H, is given by

$$V_H = \frac{R_H I B}{d} \quad \text{----------} \quad (3.5)$$

Where, d is the sample dimension in the direction of magnetic field B, R_H is the hall coefficient and $I$is the current through the sample [35].

Hall measurements described in this thesis were done using four probe van der Pauw configuration with AC modulation of magnetic field at room temperature employing Ecopia (model No HMS-5300; magnetic field= 0.57 T)

capable of current measurement in the range 1nA- 20 mA. Measurements (table 3.3) were performed on all the samples which indicated that samples prepared using stannic chloride precursor was far better in terms of carrier concentration and mobility. Resistivity values obtained from Hall measurement system (using van der Pauw method) were in good agreement with that obtained from two probe method. Positive value of Hall coefficient indicated that both samples are p-type.

Table 3.3. Carrier concentration, Mobility, Hall coefficient and Resistivity of the CZTS samples prepared with different precursors.

Sample name	Carrier conc. (cm^{-3})	Mobility (cm^2/Vs)	Resistivity ($\Omega.cm$)	Hall coefficient (cm^3/C)
CZ-A	9.31×10^{18}	1.63	4.10×10^{-1}	6.71×10^{-1}
CZ-B	1.03×10^{19}	1.98	3.07×10^{-1}	6.06×10^{-1}
CZ-C	0.83×10^{21}	2.21	3.43×10^{-3}	7.57×10^{-3}
CZ-D	1.03×10^{21}	1.74	3.49×10^{-3}	6.08×10^{-3}

3.3.1.6 Morphological Studies

Scanning electron microscopy (SEM) uses focused electron probe to extract structural and chemical information point-by-point from a region of interest in the sample [35]. Use of electrons has two main advantages over optical microscopes: much larger magnifications (> 100,000 X) are possible since electron wavelength is much smaller than photon wavelength and the depth of field is much higher. Image in an SEM is produced by scanning the sample with the focused electron beam and detecting secondary and/or back scattered electrons. High spatial resolution of SEM makes it powerful tool to characterize wide range of specimens at the nanometer to micrometer scales. In the present work JEOL, JSM-840 was employed to characterize the films.

As seen from X-ray diffraction studies, there is not much variation between the structures of the films with change in zinc precursor. But there is

clear change in structure with respect to tin precursor**.** Figure 3.2 depicts the SEM images of CZTS thin films CZ-B and CZ-C. The micrographs indicate that there are no well-defined grains in the film CZ-B. Grains are larger and densely packed in film CZ-C indicating that grain growth is enhanced due to a change in precursor solution.

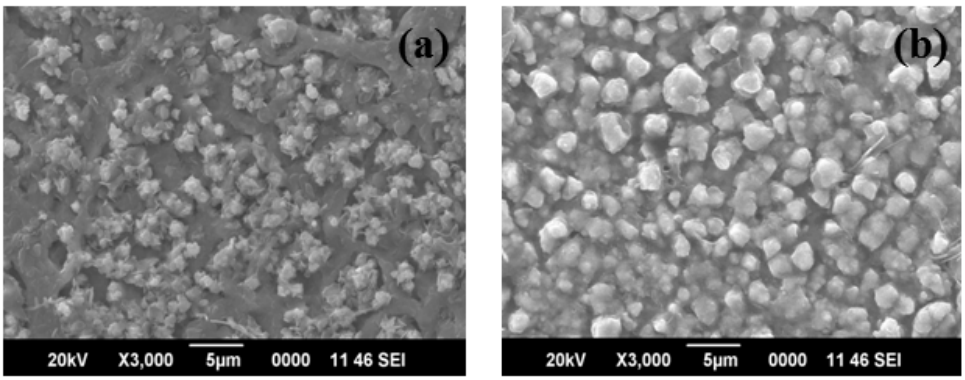

Figure 3.2. SEM micrograph of CZTS films prepared using different precursors (a) film CZ-B (b) film CZ-C.

Grain size values (1 to 2 μm) match perfectly well with the reported values. It is well known that larger size of grains in absorber layer contribute to better conversion efficiency in polycrystalline solar cells, and hence, large grain growth is required for the fabrication of high-performance photovoltaic devices.

3.3.1.7 Optical Studies

Optical absorption of the films has been studied in the wavelength range 190-2500 nm without accounting for reflection and transmission losses. Variation of absorbance with wavelength is analyzed to find out nature of the transition and the band gap of the films. Nature of the transition and optical band gap depends on the well known relation

$$\alpha = \frac{A(h\upsilon - E^{g})^{n}}{h\upsilon} \text{ ---------- (3.6)}$$

Where E_g is the separation between bottom of the conduction band and top of the valence band, hυ is the photon energy and n is a constant. Value of n depends on the probability of transition; it takes values as 1/2, 3/2, 2 and 3 for direct allowed, direct forbidden, indirect allowed and indirect forbidden transitions, respectively. Thus, if the plot of $(\alpha h\upsilon)^2$ versus hυ is linear, the transition is directly allowed.

In the present work, band gap of films was measured using optical absorbance of the films. Spectrum was recorded using UV-ViS-NIR Spectrometer (JASCO V 570 model). The results were combined with thickness to estimate the band gap for each sample [36]. Band gap of the films is determined by extrapolating the linear region of the $(\alpha h\upsilon)^2$ versus hυ (photon energy) curve to the intercept of the hυ axis, as can be seen in figure. 3.3.

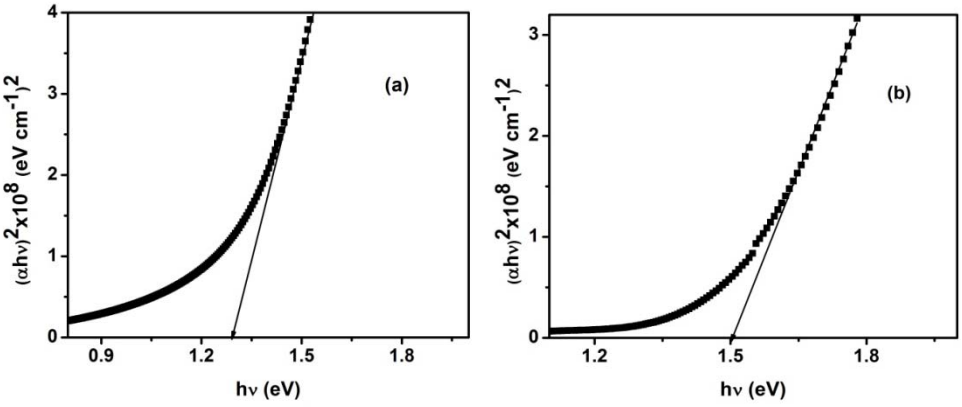

Figure 3.3. Absorption spectra of CZTS films prepared using different precursors (a) film CZ-B (b) film CZ-C.

It was observed that film CZ-B have much lower band gap (~1.30 eV) as compared to film CZ-C (~1.50 eV). This may be due to the deviation of chemical composition from stoichiometry[37]. However the band gap of sample CZ-C is fairly close to the optimum value for a solar cell absorber. Absorption coefficient in the visible region was $>10^4$ cm^{-1}. These values are in good

agreement with the reported values [38-39]. No signature of Cu_xS phase could be obtained from the absorption spectra. Thus from the optical and electrical characterizations, stannic chloride was adjudged as the precursor of tin which yielded samples with properties ideal for device purpose. In the case of zinc, both precursors gave almost similar results; but due to the ease of dissolving, we selected zinc acetate as the precursor for zinc for further studies.

3.3.1.8 Fabrication of Junction

In this section we report fabrication of heterojunction using CZTS as absorber layer and In_2S_3 as buffer layer. Glass plates coated with ITO (thickness 2000 Å, optical transmission 82 % and electrical resistivity 2.25×10^{-4} Ω cm; Geomatec, Yokohama, Japan) are used as the substrates. ITO serves as bottom electrode and metallic silver, deposited over the CZTS/In_2S_3 junction using vacuum evaporation, serves as top contact.

In order to ascertain our observations that stannic chloride based CZTS films are candidates with ideal properties for absorber layer, junctions were fabricated with CZTS films CZ-B and CZ-C as absorber layers. For preparing these p-n junctions, films of CZTS (samples CZ-B and CZ-C) were deposited over ITO coated glass substrates kept at 350 ^oC which was followed by the deposition of In_2S_3 layer (In:S ratio 2:8) above it using CSP technique at the same substrate temperature. Silver electrodes of area 5 mm^2 were vacuum evaporated for top contact, at 2×10^{-5} Torr. These cells were illuminated in the 'front wall mode' using tungsten halogen lamp, (intensity of 100 mW/cm^2). Infrared filter along with water jacket was used to ensure that there was no heating of the device during measurement. *J-V* characteristics of the cells were recorded using SMU with the help of Metric's Interactive Characterization Software (ICS).

For the cells prepared using CZ-B, the junction was quite good; but sensitivity to light was negligible whereas for cells prepared using CZ-C, we got open-circuit voltage (V_{oc}) of 380 mV and short-circuit current density (J_{sc}) of 2.4 mA/cm^2. *J-V* curves under illumination, for cells prepared using CZ-B and CZ-C are shown in figure 3.4. Even though carrier concentration is quite commendable, mobility is quite low as in the published reports [40-41]. This might be the reason for low value of J_{sc}. For comparison,V_{oc} and J_{sc} values obtained for both the junctions have been tabulated in table 3.4.

Table 3.4.Cell parameters of CZTS based solar cell deposited using various precursors

Cell using CZTS film	V_{oc} (mV)	J_{sc} (mA/cm^2)
CZ-B (Cell A)	91	0.41
CZ-C (Cell B)	380	2.40

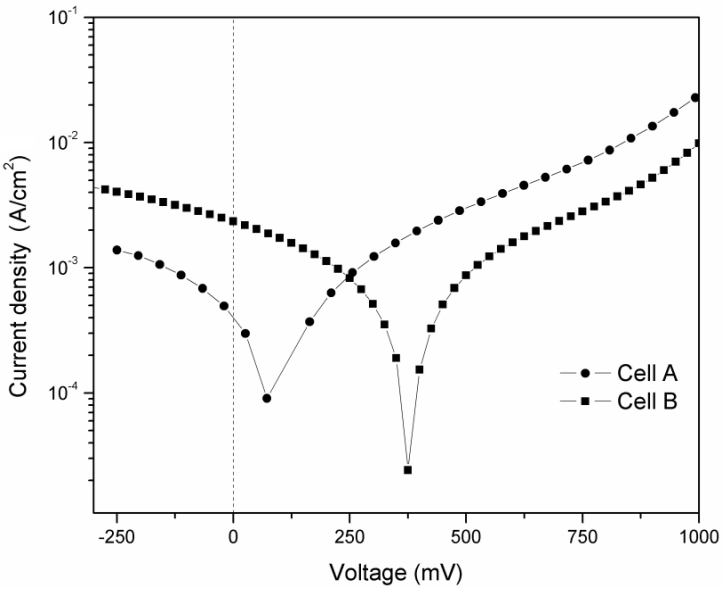

Figure.3.4.Semi logarithmic plot of illuminated *J-V* characteristics of cell prepared using film CZ-B (Cell A) and film CZ-C (Cell B).

3.3.1.9 XPS analysis of Junction

Surface analysis by X-ray photoelectron spectroscopy (XPS) involves irradiation of the solid in vacuo with monoenergetic soft X-rays and sorting the emitted electrons by energy. The spectrum obtained is a plot of the number of emitted electrons per energy interval versus their kinetic energy. Since the mean free path of the electrons is very small, the electrons which are detected originate from only the top few atomic layers. Quantitative data can be obtained from the peak heights or areas and identification of chemical states often can be made from the exact positions and seperations of the peaks [42].

In the present study XPS spectra of the samples were recorded using an ULVAC-PHI unit (model: ESCA 5600 CIM) employing argon ion sputtering (Voltage= 3 kV, Raster size = 3×3 mm^2, pressure 10^{-8} mbar). Al K_α X-ray (1486.6 eV) with a beam diameter of 0.8 mm and power of 400 W was used as the incident beam.

From the XPS 'depth profiling' of the junction (figure 3.5), the binding energy values obtained for Cu $2p_{1/2}$, Cu $2p_{3/2}$, Zn $2p_{3/2}$, Sn $3d_{3/2}$, Sn $3d_{5/2}$ and S $2p_{1/2}$ electrons were 952, 933, 1022, 495, 487 and 162 eV respectively, which matches closely with values already reported [43]. Atomic concentrations of 'Cu', 'Zn', 'Sn' and 'S' were in agreement with those obtained from EDAX measurements. Binding energies of indium indicated formation of indium sulfide (444.9 and 452.9 eV for In $3d_{5/2}$ and In $3d_{3/2}$, respectively). It could be observed that 'Cu' diffused into the In_2S_3 layer which may be due to the high diffusion coefficient of 'Cu' [44]. Due to this diffusion, there is a gradient in concentration of 'Cu' towards the junction which helps in the formation of resistive layer near the junction and a more conducting layer near the collection electrode. Resistive layer near the junction is useful to reduce the leakage current.

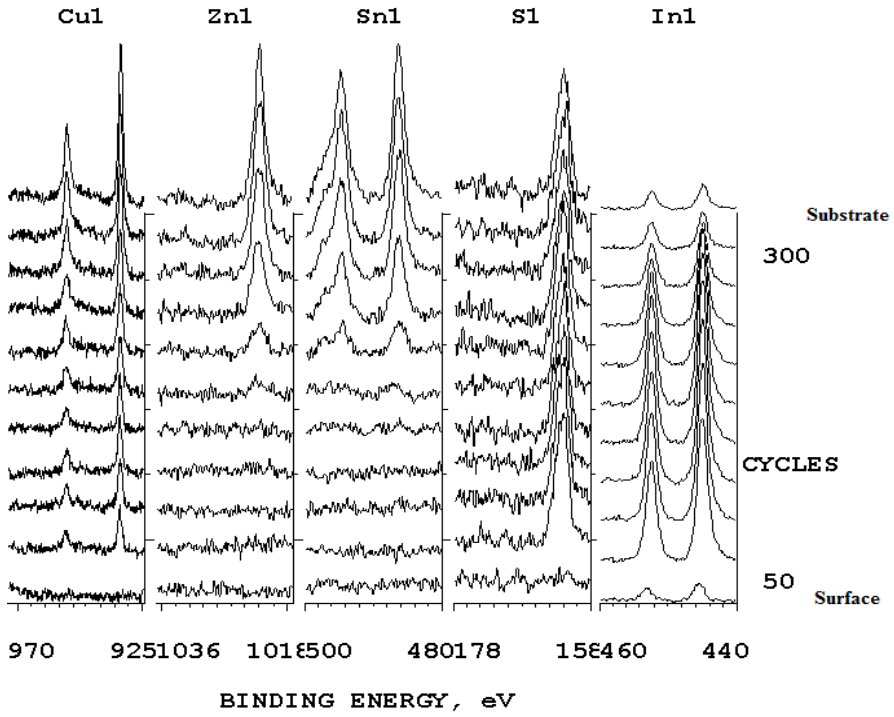

Figure.3.5. XPS depth profile of the Cu_2ZnSnS_4/In_2S_3 Junction.

3.3.2 Effect of substrate temperature

In the case of spray pyrolytic deposition, there is a characteristic substrate temperature for which good quality film is obtained. In order to find out the optimum temperature, films were prepared by varying substrate temperature from 300 to 400 ^oC, in steps of 25 ^oC. Samples were named as C300, C325, C350, C375 and C400. Precursors used for copper, zinc, tin and sulphur were copper chloride ($CuCl_2$ $2H_2O$), zinc acetate ($Zn(CH_3COO)_2$), stannic chloride ($SnCl_4$ $5H_2O$) and thiourea ($CS(NH_2)_2$) respectively. The precursors were dissolved in water and sprayed on to the preheated soda lime glass (SLG) substrates. Concentration of $CuCl_2.2H_2O$, $Zn(CH_3COO)_2$, $SnCl_4.5H_2O$ and $CS(NH_2)_2$ in the spray solution was 0.02, 0.0125, 0.0125 and 0.15 M respectively and spray rate was 8 ml/min; volume of spray solution used for each

spray was 140 ml. In all the cases, distance between spray head and substrate was maintained at 20 cm.

3.3.2.1 Structural Studies

X-ray diffractograms of the CZTS films prepared at different substrate temperatures are shown in figure 3.6.

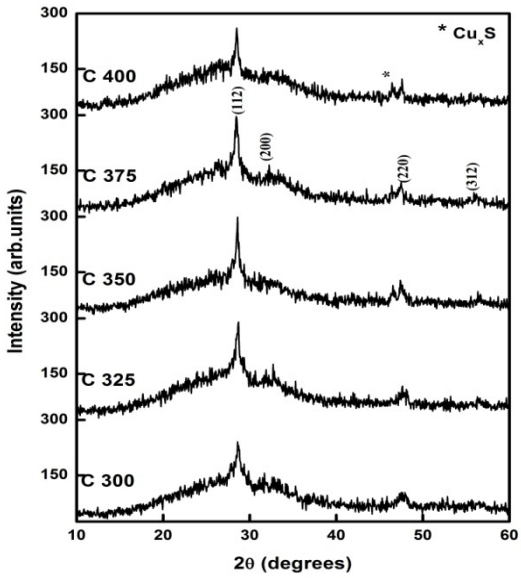

Figure. 3.6. X-ray diffractograms of CZTS samples prepared at different temperatures

Peaks corresponding to the (112), (200), (220) and (312) planes of CZTS, characteristic of the 'kesterite' structure could be seen in all films. The 'd' values coincided with that of CZTS (JCPDS card no. 26-0575) with preferential orientation along the (112) plane. Peaks in XRD pattern become more intense and the 'full width at half maximum' reduce to minimum up to a substrate temperature of 350 ^{o}C, indicating clear improvement in crystallinity. Beyond 350 ^{o}C, "retracing phenomenon" is observed. Crystallite size of the films (calculated using Scherrer formula) increased from 24 to 31 nm for 350 ^{o}C and then decreased. Kamoun et al. [45] also reported that best crystallinity was observed

at substrate temperature of 340 ^oC for spray pyrolysed CZTS thin films. Peaks corresponding to secondary phase of Cu_xS (JCPDS card no. 42-0564) could also be seen in the figure.

3.3.2.2 Optical properties

Band gap of the films was determined by extrapolating linear region of $(\alpha h\upsilon)^2$ versus $h\upsilon$ (photon energy) curve to intercept $h\upsilon$ axis (figure. 3.7). Indeed band gap decreased from 1.66 to 1.42 eV for 350 ^oC. Like grain size, band gap also showed a "retracing nature" beyond 350 ^oC. This range of values is in good agreement with the reported direct band gap of CZTS [2]. No signature of Cu_xS phase could be obtained from the absorption spectra.

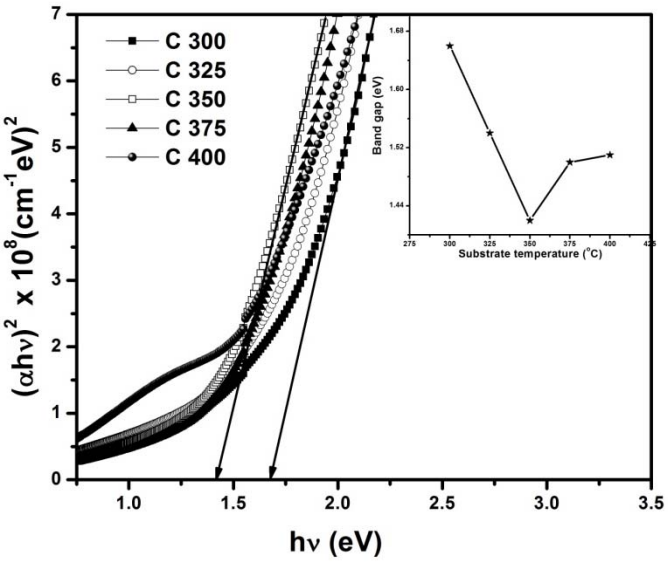

Figure 3.7.$(\alpha h\upsilon)^2$ vs. $h\upsilon$ graph of CZTS samples prepared at different substrate temperatures.

3.3.2.3 Thickness measurement

Thickness of the films has a crucial role in the properties of thin films. Various techniques are available to measure film thickness which are basically divided in to optical and mechanical methods, and are usually non destructive; but

sometimes it can be destructive in nature. Stylus profilometer is an advanced tool for thickness measurement of both thin and thick films. It is capable of measuring thickness even below 100 Å. The instrument can also be used to profile/measure topography, 'waviness', as well as surface roughness in the sub micrometer range [46].

In the present work, thickness of the samples was measured using Dektak 6M Stylus profiler. It was found that thickness (table 3.5) decreased with substrate temperature. In spray pyrolysed films, it was already observed that higher substrate temperatures yielded thinner films [47]. Also the films become less rough as temperature increases, due to the higher nucleation rates at elevated substrate temperatures.

3.3.2.4 Electrical analysis

All CZTS films exhibited p-type conductivity regardless of substrate temperature and resistivity was ~10^{-2} Ω.cm. Resistivity also decreased up to substrate temperature of 350 ^{o}C and then increased. Thickness, roughness and resistivity of the films are tabulated in table 3.5.

Table. 3.5. Thickness, roughness and resistivity of the samples prepared at different substrate temperatures

Sample Name	Thickness (nm)	Roughness (nm)	Resistivity (Ω.cm)
C300	1670	230	8.7×10^{-2}
C325	1565	195	2.8×10^{-2}
C350	1430	160	1.8×10^{-2}
C375	1350	130	3.1×10^{-2}

3.3.2.5 Compositional analysis

It was found that the CZTS film deposited at 350 ^{o}C was nearly stoichiometric with Cu/(Zn+Sn) ratio 0.91, Zn/Sn ratio 1.01 and S/metal ratio 0.88. For stoichiometric sample, all these ratios should be 1. Our next aim is to

obtain a stoichiometric, single phase CZTS film. For that we deposited films with different concentration of copper in the precursor solution.

3.3.3 Effect of copper concentration

For this study, substrate temperature was fixed at 350°C.Precursors used for copper, zinc, tin and sulphur were copper chloride ($CuCl_2$.2H2O), zinc acetate ($Zn(CH_3COO)_2$), stannic chloride ($SnCl_4.5H_2O$) and thiourea ($CS(NH_2)_2$) respectively. These precursors were dissolved in water and sprayed on to preheated soda lime glass (SLG) substrates. Concentration of $CuCl_2.2H_2O$ was varied from 0.01 M to 0.03 M in steps of 0.005 M while the concentrations of$(Zn(CH_3COO)_2)$, $SnCl_4.5H_2O$ and $CS(NH_2)_2$ in the spray solution were 0.01, 0.01 and 0.12 M respectively. Spray rate, volume and distance between spray head and substrate heater were maintained at the same values as in the earlier study.

3.3.3.1 Compositional analysis

In order to confirm whether we could achieve stoichiometry through the variation of copper concentration, compositional analysis using EDAX was done. For each sample measurement was taken from different points on the surface and their mean values are taken. As expected, copper incorporation in the film increased with the increase in copper concentration in the precursor solution. Results of the measurements are tabulated in table 3.6.

Table 3.6. Elemental composition of CZTS films prepared by varying the copper concentration

Sample	Cu (at.%)	Zn (at.%)	Sn (at.%)	S (at.%)	$\frac{Cu}{Zn+Sn}$	$\frac{Zn}{Sn}$	$\frac{S}{Metal}$
C-0.01	20.6	17.5	13.2	48.7	0.67	1.33	0.95
C-0.015	25.2	13.2	12.4	49.2	0.98	1.06	0.97
C-0.02	26.0	13.4	16.3	44.3	0.87	0.82	0.80
C-0.025	30.2	10.3	12.3	47.2	1.33	0.84	0.89
C-0.03	33.2	8.8	8.2	49.8	1.95	1.07	0.99

For 0.015 M copper, we got almost stoichiometric CZTS film. From the EDAX spectrum of the stoichiometric CZTS film (figure 3.8) peaks indicating the presence of copper, zinc, tin and sulfur could be clearly seen. Peaks due to silicon and oxygen could also be seen which were from the SLG substrate.

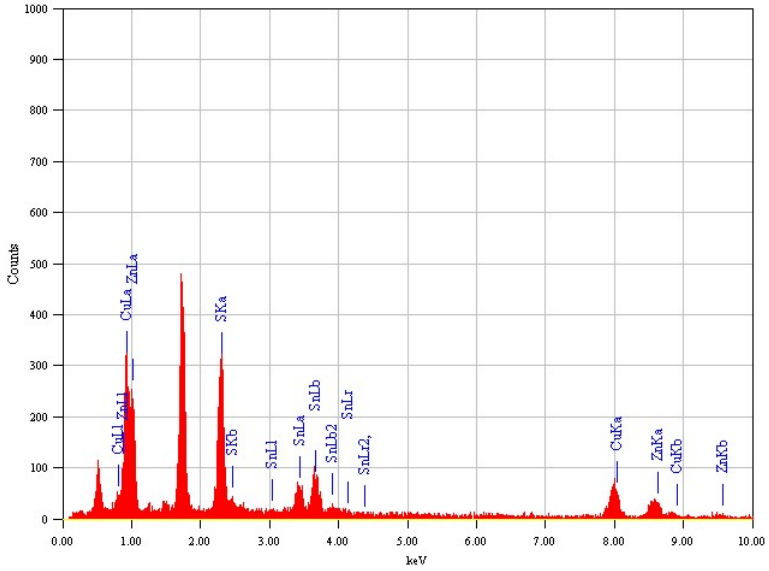

Figure 3.8 EDAX spectrum of stoichiometric CZTS film.

3.3.3.2 Structural Analysis using XRD

Since the study was on effect of copper concentration, there is a chance of formation of secondary phases. In order to confirm this, X-ray diffraction studies were done. Figure 3.9 shows X-ray diffraction pattern of CZTS films deposited with different copper concentrations. Films are polycrystalline in nature with kesterite structure. Peaks corresponding to the planes (112), (200), (220) and (312) could be clearly seen in all films. Preferential orientation was along (112) plane. As the concentration of copper increases, secondary phase corresponding to Cu_xS phase becomes visible in the pattern and intensity of the corresponding peaks increased with the concentration.

From compositional analysis it was found that copper concentration in the film is high for samples C-0.025 and C-0.03. As evident from XRD pattern, secondary Cu_xS phase is also prominent in these samples. Grain size of the samples was calculated using Scherrer formula and this was found to be maximum for the nearly stoichiometric film C- 0.015 (~30 nm).

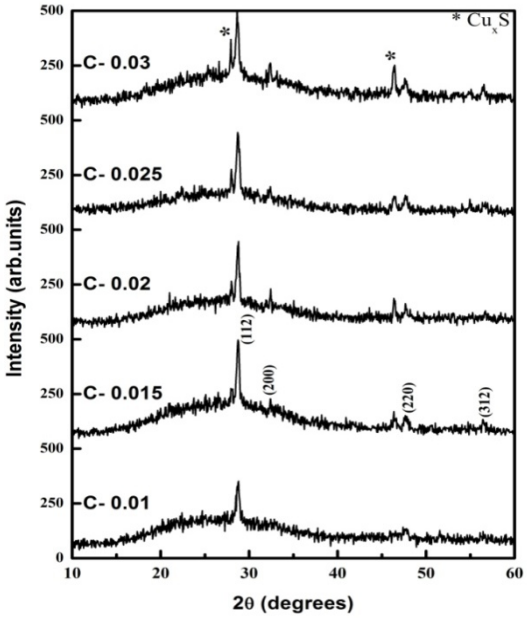

Figure. 3.9. X-ray diffractograms of CZTS samples prepared with different copper concentrations

3.3.3.3 Structural analysis using Raman spectra

To clarify the presence of secondary phases in these films, Raman microprobe measurements were performed. Raman spectroscopy is a technique that can detect both organic and inorganic species, and measure crystallinity of solids [35]. Raman spectroscopy is based on the Raman effect, first reported by Raman in 1928 [48].

If the incident photon imparts part of its energy to the lattice in the form of phonon, it emerges as a lower energy photon. This 'down converted frequency

shift' is known as Stokes shifted scattering. Anti-Stokes shifted scattering results when the photon absorbs a phonon and emerges with higher energy. Anti-Stokes mode is much weaker than the Stokes mode and hence Stokes-mode scattering is usually monitored. In Raman spectroscopy a laser beam, referred to as the pump, is incident on the sample. The weak scattered light or the Raman signal is passed through double monochromator to reject the Rayleigh scattered light and the Raman shifted wavelengths are detected by a photo detector.

Various properties of the semiconductors, mainly composition and crystal structure, can be determined using this technique. Information about structure, phase, grain size, phonon confinement etc. can be obtained from Raman spectroscopy. The lines become very broad for amorphous semiconductors, allowing distinction to be made between single crystal, polycrystalline, and amorphous materials.

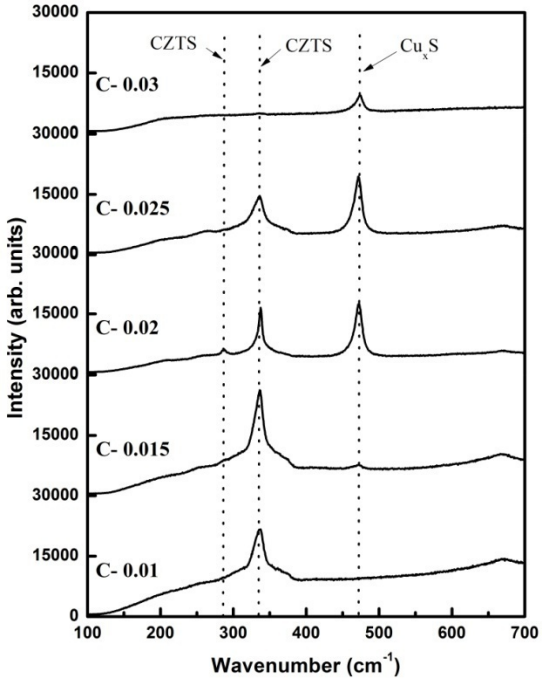

Figure. 3.10. Raman scattering spectra of CZTS samples prepared with different copper concentrations

In the present work, Raman studies were carried out, in the back scattering mode, at room temperature using micro Raman system (JobinYvon Horiba LABRAM-HR) in the visible range (400-1100 nm) with spectral resolution of 1 cm^{-1}. Argon ion laser of wavelength 488 nm was used as the excitation source.

According to the literature main peaks of the possible secondary phases are found at 352 cm^{-1} for ZnS, 475 cm^{-1} for $Cu_{2-x}S$, 314 cm^{-1} for SnS_2 and 318 cm^{-1} for copper tin sulfide (CTS) [49]. Raman spectra of CZTS films are characterized by the presence of two main peaks at about 286-289 cm^{-1} and 337-339 cm^{-1} [50-52]. According to Himmirch and Haeuseler [50] the strongest peak at 337-339 cm^{-1} is attributed to the 'A1 symmetry' and it is related with the vibration of the 'S' atoms.

Figure 3.10 Shows the Raman spectra for CZTS films deposited for various copper concentrations. It is clear that strong peak appears at 338 cm^{-1} which indicates formation of CZTS. Also there is a shoulder for the main peak at 351 cm^{-1} which is reported by some other groups also [51, 52]. As copper concentration increases beyond 0.015 M, a peak at 475 cm^{-1} due to the $Cu_{2-x}S$ phase appears and its intensity increases as the concentration increases. This peak at 475cm^{-1} is reported earlier in case of CZTS films prepared through spray pyrolysis [53] and other methods also [1, 52, 54-55]. For C-0.03 sample the prominent peak is due to the $Cu_{2-x}S$ phase.

3.3.3.4 Morphological studies

Figure 3.11 shows the SEM image of CZTS thin films prepared for various copper concentrations.

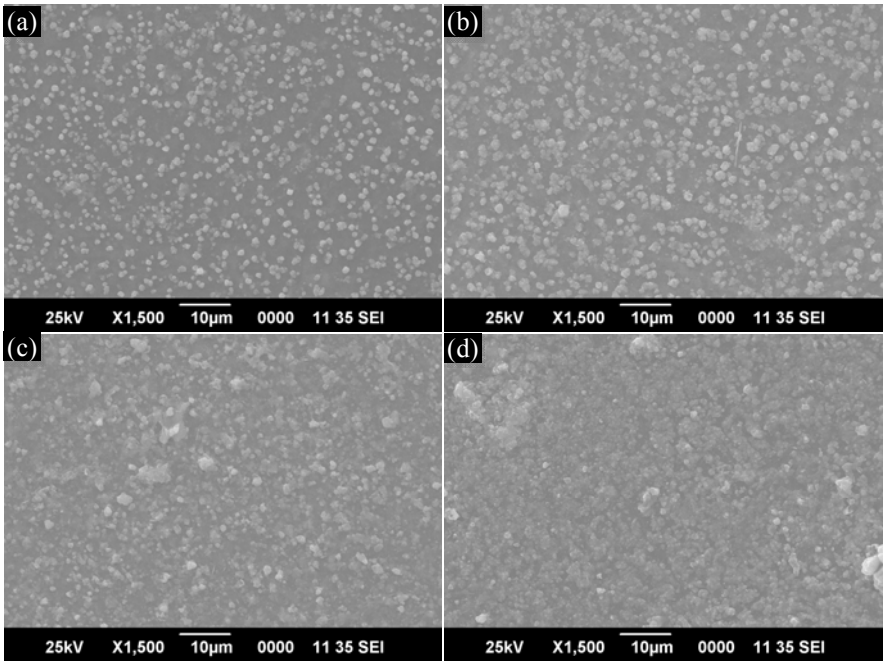

Figure.3.11. SEM micrographs of CZTS samples prepared with different copper concentrations. (a) C-0.01 (b) C-0.015 (c) C-0.02 (d) C-0.03

It is well known that efficiency of polycrystalline thin film solar cell increases with increasing grain size of the absorber layer and therefore, larger grains are required for the fabrication of high efficiency solar cells [56]. In the present work, it is obvious from the SEM images that, as the copper concentration increases there is improvement in grain morphology and size. Increase in grain size could be clearly seen when copper concentration increases from 0.01 M to 0.015 M. Beyond that, agglomeration of grains occurs. Similar observation was reported earlier for copper variation in spray deposited CZTS films [57].

3.3.3.5 Optical studies

Optical band gap was deduced from $(\alpha h\upsilon)^2$ versus $h\upsilon$ plot (figure 3.12) and it was found that it reduced from 1.55 eV to 1.21 eV as the copper concentration increased from 0.01 M to 0.03 M. Similar range of values of band gap was reported earlier by Tanaka et al. [58] for CZTS thin films.

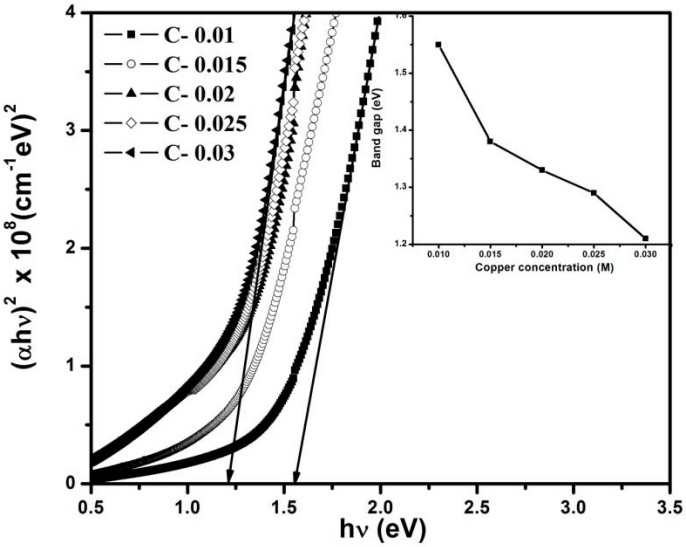

Figure 3.12 $(\alpha h\upsilon)^2$ vs. $h\upsilon$ graph of CZTS samples prepared with different copper concentrations.

Decrease in band gap with increase in copper concentration is also observed by Kumar et al. [57] for sprayed CZTS thin films and by Tuttle et al. [59] in the case of $CuInSe_2$ thin films. Absorption coefficient of the samples was greater than 10^4 cm^{-1}. Thus it was inferred that the films had good absorbance in the visible region of the electromagnetic spectrum. Any information about secondary phases was not available from absorption spectra.

3.3.3.6 Electrical studies

Sheet resistance of the samples measured using two probe technique decreased with increase in copper concentration. Thickness and roughness of the samples also increased with copper concentration. By multiplying sheet resistance with thickness, resistivity of the films was calculated and is tabulated in table 3.7. All the samples show p-type conductivity.

Table. 3.7. Thickness, roughness and resistivity of the samples prepared with different copper concentrations.

Sample name	Thickness (nm)	Roughness (nm)	Resistivity (Ω.cm)
C-0.01	875	216	8.1×10^{-1}
C-0.015	1010	238	3.8×10^{-2}
C-0.02	1165	277	1.8×10^{-2}
C-0.025	1320	331	1.2×10^{-2}
C-0.03	1530	373	6.6×10^{-3}

3.3.4 Effect of spray rate

Spray rate is another important parameter in the deposition of thin films through spray pyrolysis method. Tina et al. [60] reported that properties like crystallinity, surface morphology, resistivity and even thickness are affected by changes in spray rate. This section reports the results on the effect of spray rate on the growth of CZTS films. Precursors for copper, zinc, tin and sulfur were same as for earlier studies. Substrate temperature is kept at 350 ^{o}C and Cu:Zn:Sn:S ratio in the precursor solution is taken as 1.5:1:1:12. Spray rate was varied as 2 ml/min, 4 ml/min, 6 ml/min, 8 ml/min and 10 ml/min. These samples were named as C2, C4, C6, C8 and C10 respectively. To find out the optimum spray rate, structural, optical and electrical characterizations were done.

3.3.4.1 Structural characterization

X-ray diffraction pattern of the CZTS films deposited at different spray rates are shown in figure 3.13. For Sample C2, in addition to peaks corresponding to CZTS phase, there are peaks corresponding to secondary phases such as $Cu_{1.8}S$ (JCPDS card no. 47-1748) and Cu_xS (JCPDS card no. 42-0564). Also for high spray rate (C10) there is Cu_xS phase as indicated by the peak at 46.2 ^{o}. However sample C6 is devoid of any secondary phases. Grain size of the films decreased as the spray rate increased up to 8 ml/min and then slightly increased. Similar decrease in grain size with increase in spray rate is observed in the case of sprayed $CuInS_2$ films also [60].

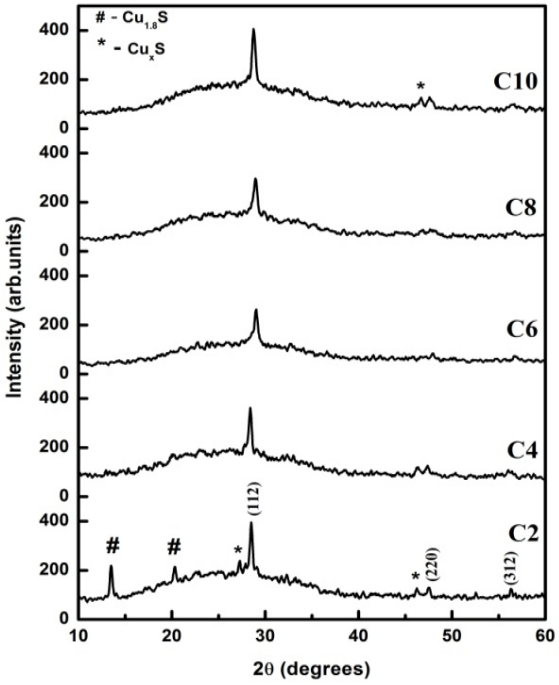

Figure. 3.13. X-ray diffractograms of CZTS samples prepared at different spray rates

3.3.4.2 Optical studies

$(\alpha h\upsilon)^2$ versus $h\upsilon$ plot of CZTS films deposited at different spray rates is shown in figure 3.14. For C2 the band gap obtained is 1.6 eV and we can see that the absorption of the tail region was extremely elevated. This elevation means that there is absorption in the lower energy region than the band gap energy. This might be due to the presence of binary compounds of 'Cu' and 'S' which were confirmed from XRD analysis. Similar observations of elevated absorption tail were made earlier for E-B evaporated CZTS thin films when the Cu/(Zn+Sn) ratio increased beyond 0.94 [61].

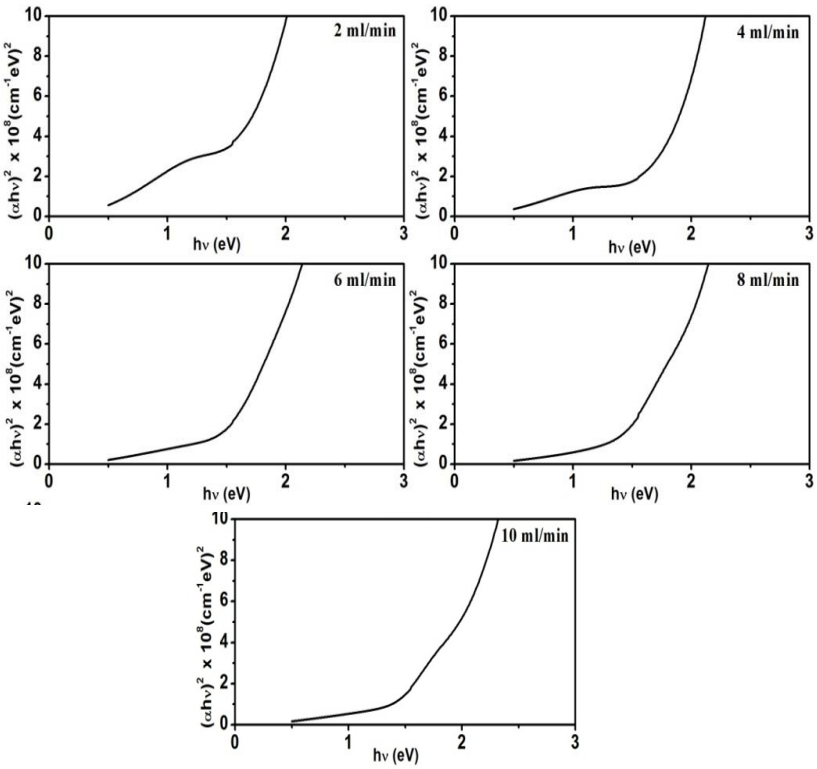

Figure.3.14. Absorption spectra of CZTS samples prepared at different spray rates

As the spray rate increased, band gap decreased and elevation of absorption tail decreased. At a spray rate of 6 ml/min (C6), the band gap was 1.5 eV, suitable for photovoltaic energy conversion. Beyond 6 ml/min there were two linear portions in the $(\alpha h\upsilon)^2$ versus hυ plot, which indicates two band gaps; one is due to the CZTS phase (at ~1.4 eV) other one is due to Cu_xS phase (~ 1.8 eV). Direct optical band gap of Cu_xS reported earlier in literature is in the range 1.7-2.16 eV based on the value of 'x'[62].

3.3.4.3 Electrical studies

Resistivity of the films was calculated from the values of sheet resistance and thickness. Thickness of the samples increased from 650 nm to 880 nm when the spray rate increased from 2 ml/min to 10 ml/min. Resistivity values increased

steadily up to 6 ml/min and then slightly decreased. This increase in resistance might be due to the decrease in crystallinity with spray rate. Roughness of the films also increased with spray rate, which is a common observation in spray deposited films [60].

Table. 3.8. Thickness, Roughness and Resistivity of the CZTS samples prepared at different spray rates.

Sample name	Thickness (nm)	Roughness (nm)	Resistivity (Ω.cm)
C2	650	152	4.6×10^{-3}
C4	690	164	4.4×10^{-3}
C6	775	171	1.8×10^{-2}
C8	820	186	2.2×10^{-2}
C10	880	195	4.6×10^{-2}

3.4 Conclusions

In this chapter we have studied the effect of choice of precursors on the properties of sprayed CZTS absorber layer and also on the performance of CZTS/In_2S_3 heterojunction. Effects of substrate temperature, copper concentration and spray rate on the properties of CZTS thin films were also investigated. From the precursor variation studies, it was found that stannic chloride and zinc acetate are better choices for tin and zinc precursors compared to stannous chloride and zinc chloride. To prove this result, rather than sticking on to just material characterization, heterojunctions were fabricated using CZTS as absorber and In_2S_3 as buffer layer. For junction fabricated using CZTS prepared from stannic chloride precursor, we got open circuit voltage of 340 mV and short circuit current density of 2.4 mA/cm^2.

It was found that, as substrate temperature increased, crystallinity increased up to 350 ^oC and then decreased. Resistivity data also supported the results from XRD, by showing a decrease up to 350 ^oC followed by an increase.

All the samples were p-type. Band gap of the samples also showed the same trend. From the variation of copper concentration we found that stoichiometric CZTS film could be deposited if we take the molarity of copper, zinc, tin and sulfur in the precursor solution as 0.015, 0.01, 0.01, 0.12 M respectively. Deposition at lower spray rates resulted in films with secondary phases. 6 ml/min was optimized as the spray rate for obtaining good quality CZTS films. Thus in the present work, we optimized substrate temperature, spray rate, choice and ratio of precursors for obtaining device quality CZTS thin film for using as an absorber layer in thin film solar cells.

References

[1]. **P. A. Fernandes, P. M. P. Salome and A. F. da Cunha.** 2009, Semicond. Sci. Technol., Vol. 24, p. 105013.

[2]. **H. Katagiri, K. Saitoh, T. Washio, H. Shinohara, T. Kurumadani and S. Miyajima.** 2001, Sol. Energy Mater. Sol. Cells, Vol. 65, p. 141.

[3]. **L. Sun, J. He, H. Kong, F. Yue, P. Yang and J. Chu.** 2011, Sol. Energy Mater. Sol. Cells, Vol. 95, p. 2907.

[4]. **G. Rajesh, N. Muthukumarasami, E. P. Subramaniam, S. Agilan and D. Velauthapillai.** 2013, J. Sol-Gel Sci. Technol., Vol. 66, p. 288.

[5]. **E. M. Mkawi, K. Ibrahim, M. K. M. Ali and A. S. Mohamed.** 2013, Int. J. Electrochem. Sci., Vol. 8, p. 359.

[6]. **X. Fontane, L. C. Barrio, V. I. Roca, E. Saucedo, A. P. Rodriguez, J. R. Morante, D. M. Berg, P. J. Dale and S. Siebentritt.** 2011, Appl. Phys. Lett. , Vol. 98, p. 181905 .

[7]. **Z. Zhou, Y. Wang, D. Xu and Y. Zhang.** 2010, Sol. Energy Mater. Sol. Cells, Vol. 94, p. 2042.

[8]. **S. S. Mali, P. S. Shinde, C. A. Betty, P. N. Bhosale, Y. W. Oh and P. S. Patil.** 2012, J. Phys. Chem. Solids, Vol. 73, p. 735.

[9]. **K. Maeda, K. Tanaka, Y. Fukui and H. Uchiki.** 2011, Sol. Energy Mater. Sol. Cells, Vol. 95, p. 2855.

[10]. **S. K. Swami, A. Kumar and V. Dutta.** 2013 , Energy Procedia, Vol. 33, p. 198.

[11]. **Y. B. Kishore Kumar, G. Suresh Babu, P. Uday Bhaskar and V. Sundara Raja.** 2009, Sol. Energy Mater. Sol. Cells, Vol. 93, p. 1230.

[12]. **B. Shin, O. Gunawan, Y. Zhu, N. A. Bojarczuk, S. J. Chey and S. Guha.** 2013, Prog. Photovolt: Res. Appl. , Vol. 21, p. 72.

[13]. **T. Prabhakar and J. Nagaraju.** 2011. 37th IEEE Photovoltaic Specialists Conference (PVSC).

[14]. **Y.B. Kishore Kumar, G. Suresh Babu, P. Uday Bhaskar and V. Sundara Raja.** 2009, Phys. Status Solidi (a), Vol. 206, p. 1525.

[15]. **Y.B. Kishore Kumar, P. Uday Bhaskar, G. Suresh Babu and V. Sundara Raja.** 2010, Phys. Status Solidi (a), Vol. 207, p. 149.

[16]. **Y. Arba, M. Rafi, B. Hartiti, A. Ridah and P. Thevenin.** 2011, M. J. Condensed Matter, Vol. 13, p. 100.

[17]. **B. Uma Maheswari and V. Senthil Kumar.** 2012, American Journal of Advanced Scientific Research, Vol. 1, p. 257.

[18]. **M. Patel, I. Mukhopadhyay and A. Ray.** 2012, J. Phys. D: Appl. Phys. , Vol. 45, p. 445103.

[19]. **S. Huang, W. Luo and Z. Zou.** 2013, J. Phys. D: Appl. Phys. , Vol. 46, p. 235108.

[20]. **Z. Seboui, Y. Cuminal and N. K. Turki.** 2013, J. Renewable Sustainable Energy, Vol. 5, p. 023113 .

[21]. **N. M. Shinde, R. J. Deokate and C. D. Lokhande.** 2013, Journal of Analytical and Applied Pyrolysis , Vol. 100, p. 12.

[22]. **G. Gurieva, M. Guc, L. I. Bruk, V. Izquierdo-Roca, A. P. Rodriguez, S. Schorr and E. Arushanov.** 2013, Phys. Status Solidi (c), p. 1.

[23]. **A. K. Sharma and P. Rajaram.** 2010, Material Science and Engineering B, Vol. 172, p. 37.

[24]. **D. Y. Lee and J. Kim.** 2010, Thin Solid Films, Vol. 518, p. 6537.

[25]. **A. Goossens and J. Hofhuis.** 2008, Nanotechnology, Vol. 19, p. 424018.

[26]. **N. Kamoun, H. Bouzouita and B. Rezig.** 2007, Thin Solid Films, Vol. 515, p. 5949.

[27]. **M. Aono, K. Yoshitake and H. Miyazaki.** 2013, Phys. Status Solidi (c), p. 1.

[28]. **C. Kittel.***Introduction to solid state Physics*. s.l. : Wiley Eastern Limtd, 1996.

[29]. **T.T. John, C. Sudha Kartha, K. P. Vijayakumar, T. Abe and Y. Kashiwaba.** 2005, Appl. Surf. Sci., Vol. 252, p. 1360.

[30]. **N. Lehraki, M. S. Aida, S. Abed, N. Attaf, A. Attaf and M. Poulain.** 2012, Current Appl. Phys., p. 1.

[31]. **Xin Zeng, Stevin S. Pramana, Sudip K. Batabyal, Subodh G. Mhaisalkar, Xiaodong Chen and K. B. Jinesh.** 2013, Phys. Chem. Chem. Phys, Vol. 15, p. 6763.

[32]. **Anjaly Jose, V. G. Rajeshmon, N. Poornima, C. Sudha Kartha and K. P. Vijayakumar.** 2011, AIP Conf. Proc., Vol. 1349, p. 707.

[33]. **V.G. Rajeshmon, C. Sudha Kartha, K. P. Vijayakumar, C. Sanjeeviraja, T. Abe and Y. Kazhiwaba.** 2011, Solar Energy, Vol. 85, p. 249.

[34]. **N. Nakayama and K. Ito.** 1996, Appl. Surf. Sci, Vol. 92, p. 171.

[35]. **D. K. Schroder.***Semiconductor materials and device characterization.* Newyork : John Wiley and Sons, 1998.

[36]. **I. V. Pankov.***Optical Processes in Semiconductors.* New York : Dover Inc., 1975. p. 34.

[37]. **K. Tanaka, N. Moritake, M. Oonuki and H. Uchiki.** 2008, Jpn. J. Appl. Phys., Vol. 47, p. 598.

[38]. **K. Moriya, K. Tanaka and H. Uchiki.** 2007, Jpn. J. Appl. Phys., Vol. 46, p. 5780.

[39]. **K. Tanaka, N. Moritake and H. Uchiki.** 2007, Sol. Energy Mater. Sol. Cells, Vol. 91, p. 1199.

[40]. **Z. Jun, S. Lexi, F. Yujun and X. Erqing.** 2006, Rare Metals, Vol. 25, p. 315.

[41]. **T. Tanaka, T. Nagatomo, D. Kawazaki, M. Nishio, Q. Guo, A. Wakahara, A. Yoshida and H. Ogawa.** 2005, J. Phys. chem. Solids, Vol. 66, p. 1978.

[42]. **C. D. Wagner, W. M. Riggs, L. E. Davis, J. F. Moulder and G. E. Muilenberg.***Handbook of x-ray photoelectron spectroscopy.* s.l. : Perkin-Elmer corporation, 1978.

[43]. **X. Zhang, X. Shi, W. Ye, C. Ma and C. Wang.** 2008, Appl. Phys. A, Vol. 94, p. 381.

[44]. **K. Djessas, S. Yapi, G. Masse, M. Ibannain and J. l. Gauffier.** 2004, J. Appl. Phys., Vol. 95, p. 4111.

[45]. **N. Kamoun, H. Bouzouita and B. Rezig.** 2007, Thin Solid Films, Vol. 515, p. 5949.

[46]. **L. I. Maissel and R. Glang.***Handbook of thin film technology.* India : McGraw-Hill, 1970.

[47]. **K. L. Chopra and S. R. Das.***Thin film solar cells.* New York and London : Plenum Press, 1983.

[48]. **C. V. Raman and K. S. Krishna.** 1928, Nature, Vol. 121, p. 501.

[49]. **P. A. Fernandes, P. M. P. Salome and A. F. da Cunha.** 2011, J. Alloys Compd., Vol. 509, p. 7600.

[50]. **M. Himmrich and H. Haeuseler.** 1991, Spectrochimica Acta Part A: Molecular Spectroscopy, Vol. 47, p. 933.

[51]. **M. Altosaar, J. Raudoja, K. Timmo, M. Danilson, M. Grossberg, J. Krustok and E. Mellikov.** 2008, Phys. Status Solidi (a), Vol. 205, p. 167.

[52]. **P. A. Fernandes, P. M. P. Salome and A. F. da Cunha.** 2009, Thin Solid Films, Vol. 517, p. 2519.

[53]. **H. Yoo and J. Kim.** 2011, Sol. Energy Mater. Sol. Cells, Vol. 95, p. 239.

[54]. **P. A. Fernandes, P. M. P. Salome and A. F. da Cunha.** 2010, Phys. Status Solidi (c), Vol. 7, p. 901.

[55]. **H. Yoo and J. Kim.** 2010, Thin Solid Films, Vol. 518, p. 6567.

[56]. **K. Tanaka, N. Moritake and H. Uchiki.** 2007, Solar Energy Materials and Solar Cells, Vol. 91, p. 1199.

[57]. **Y.B. Kishore Kumar, P. Uday Bhaskar, G. Suresh Babu and V. Sundara Raja.** 2010, Phys. Status Solidi A, Vol. 207, p. 149.

[58]. **K. Tanaka, N. Moritake, M. Oonuki and H. Uchiki.** 2008, Jpn. J. Appl. Phys., Vol. 47, p. 598.

[59]. **J. Tuttle, D. Albin, J. Goral, C. Kennedy and R. Noufi.** 1988, Sol. Cells, Vol. 24, p. 67.

[60]. **T. Sebastian, R. Jayakrishnan, C. Sudha Kartha and K. P. Vijayakumar.** 2009, The Open Surface Science Journal, Vol. 1, p. 1.

[61]. **T. Kobayashi, K. Jimbo, K. Tsuchida, S. Shinoda, T. Oyanagi and H. Katagiri.** 2005, Jpn. J. Appl. Phys, Vol. 44, p. 783.

[62]. **A. C. Rastogi and S. Salkalachen.** 1982, Thin Solid Films, Vol. 97, p. 191.

.....ꕥ.....

Chapter 4

FABRICATION OF CZTS/ In_2S_3 SOLAR CELL AND ITS IMPROVEMENT THROUGH MODIFICATION OF In_2S_3 LAYER

4.1. Introduction
4.2. Review of devices employing In_2S_3 buffer layer
4.3. CZTS/In_2S_3heterojunction using chemical spray pyrolysis technique.
4.4. Improvements of CZTS/In_2S_3 cell parameters
4.5. Role of buffer layer thickness
4.6. Large area heterojunction
4.7. Conclusions

4.1 Introduction

In most of the reports of CZTS based solar cells, CdS was used as the buffer layer. However, CdS, having band gap of 2.45 eV, limits short-wavelength response of the device and therefore the short circuit current (J_{sc}). Much more than that, replacement of hazardous CdS buffer is also motivated by concern on environmental safety [1]. Development of wide band gap materials for buffer layer application and optimization of electronic band structure at buffer/CZTS interface are key issues that are being addressed now to improve the device properties. The current chapter is focused on indium sulfide compound as the promising material for Cd-free buffer layer and describes fabrication of heterojunction solar cell using CZTS as absorber layer and indium sulfide (In_2S_3) as buffer layer followed by the steps for improvement of performance parameters of the cell.

Indium (III) sulfide is an inorganic compound with the formula In_2S_3. It is a promising III-VI semiconductor material for optoelectronic, photovoltaic and

photo-electrochemical solar cell applications due to its stability, wider band gap and photo conducting behavior. More over this is a nontoxic n-type semiconductor material with energy band gap of 2.0- 2.8 eV [2-3]. It exists in three different crystallographic structures α, β and γ in which α-In_2S_3 has defect cubic structure, β-In_2S_3 has defect spinel, tetragonal structure and γ-In_2S_3 has layered structure. Among these, β-In_2S_3 is considered to be the most stable form at room temperature.

4.2 Review of devices employing In_2S_3 buffer layer

In most of the works on CIGS and CZTS based solar cells, chemical bath deposited CdS is used as buffer layer. In the last decade, serious efforts to substitute CdS using non toxic alternative have been made. Development of Cd-free devices started in 1992 and recently reached efficiency up to 19 % [4]. Investigations suggest that the most relevant Cd-free materials are In_2S_3, ZnS, $Zn_{1-x}Mg_xO$, and their derivatives prepared using techniques such as atomic layer deposition, chemical bath deposition, evaporation, spray pyrolysis etc. All these materials are n-type and are thus suitable partners for p-type absorber layers. Among these, we focused on spray pyrolysed In_2S_3 due to its favorable properties and simplicity of the preparation technique. Moreover, we can deposit films at lower substrate temperature compared to ZnS. Also we have already reported that sprayed In_2S_3 buffer layer is quite efficient in yielding good results for ITO/$CuInS_2$/In_2S_3/Ag thin film solar cell [5]. Various techniques used to deposit In_2S_3 buffer layer and their implications in device performance is detailed below.

4.2.1 Spray pyrolysis

Spray pyrolysed In_2S_3 was first used as buffer layer in thin film solar cell by Teny Theresa John et al. [6]. Both absorber and window layers were prepared using spray pyrolysis. They reported an efficiency of 5.7 % on a cell with

configuration ITO/$CuInS_2$/In_2S_3/Ag. Also they reported that the usual superstrate structure, having buffer layer just above ITO, was not functioning mainly due to diffusion of 'Cu' into In_2S_3 layer. They later enhanced the efficiency up to 9.5 % by adjusting deposition conditions and thickness of absorber and buffer layers [5].

Ernits et al. [7] prepared In_xS_y thin film buffer layers employing ultrasonic spray pyrolysis at various substrate temperatures. By depositing indium sulfide layer as buffer layer in the CIGS solar cell configuration, maximum solar cell efficiency of 8.9 % was achieved, whilst the reference cell with CdS/CIGS on a similar absorber exhibited 12.7 % efficiency. In 2009, Buecheler et al. [8] reported an efficiency of 12.4 % with $Cu(In,Ga)(S,Se)_2$ absorber and ultrasonic spray pyrolysed-In_2S_3 buffer layer sprayed with sulfur excess. Allsop et al. [9] prepared thin film indium sulfide buffer layers using the Spray-ILGAR technique. Buffers deposited on commercially grown $Cu(In,Ga)(S,Se)_2$ absorbers produced cells reaching certified efficiency of 14·7 % and average efficiencies matching the reference solar cells prepared with a conventional cadmium sulfide buffer layer.

4.2.2 Chemical Bath deposition (CBD)

In 1996, Braunger et al. [10] reported efficiency of 11.4 % on a $CuInS_2$ solar cell with chemical bath deposited $In_x(OH,S)_y$ buffer layer. They compared the device parameters and performance to the heterojunctions with standard CdS buffer layer. Later same group reported efficiency of 15.7 % on a solar cell based on $Cu(In,Ga)Se_2$ absorber and $In_x(OH,S)_y$ buffer [11]. Asenjo et al. [12] reported the highest efficiency values of 8.8 % on $CuInS_2$ absorbers with CBD-In_2S_3 buffers deposited at relatively high temperature of 70 ^oC. Using the CBD In_2S_3-based buffer, 30×30 cm^2 modules were fabricated with efficiencies up to 9.7 % [13].

However, these cells and modules exhibited "light soaking" effect. The highest efficiency was reached after annealing and illumination. Origin for this behaviour is related to the presence of acceptor defects at the CBD In_2S_3/ZnO interface. All cells with non-CdS buffer materials which are sensitive to light-soaking also exhibit the reverse bias effect [14]. In 2003, Tokita et al. [15] proposed a novel $In(OH)_3$:Zn^{2+} buffer layer for fabricating high efficiency CIGS solar cells. An efficiency of 14 % was achieved without light soaking effect.

4.2.3 Atomic layer deposition (ALD)

In 2000, Yousfi et al. [16] investigated atomic layer epitaxy (ALE) buffer layers of zinc oxysulfide, indium sulfide and aluminum oxide deposited at low temperature (160 ^oC). The most promising results were obtained using indium sulfide buffer layers, with record efficiency of 13.5 % (without AR coating) achieved on a standard CIGS absorber. In another report they analyzed the same cell with special focus on indium sulfide properties and on doping mechanism of zinc oxide with aluminum [17]. Naghavi et al. [18] reported a record efficiency of 16.4 % for a laboratory cell with CIGS absorber and In_2S_3 buffer. This efficiency was achieved using 30 nm thick buffer layer, deposited at 220 ^oC.

In 2003, Spiering et al. [19] reported fabrication of CIGS modules with indium sulfide as buffer layer deposited using ALCVD technique. A module efficiency of 10.8 % was achieved over an area of 30×30 cm^2. In the very next year they improved module efficiency close to 13 % (η=12.9 %, aperture area: 714 cm^2 and 42 cells) [20]. Optimum deposition temperature was found to be in the range of 200–220 ^oC with optimum layer thickness of ~30–50 nm. In 2005 same group performed indoor damp heat and thermal cycling tests to investigate the long term stability of encapsulated Cd-free CIGS modules with ALD In_2S_3 buffer compared to references with a CBD CdS buffer [21].

4.2.4 Physical vapour deposition (PVD)

Barreau et al. [22] showed that β-In_2S_3 containing Na (BINS) thin films can be grown at 200 ^oC using PVD. Conversion efficiency of 8.2 %, was achieved on Mo/CIGS/BINS cell with 100 nm thick BINS thin film. Gall et al. [23] grown indium sulphide layers using PVD in which indium and sulfur are evaporated on the substrates at 130 ^oC. These 'as-deposited' thin films are then heated at 200 ^oC for 1 min. 12.4 % efficiency cell has been achieved using this process. In 2005, Strohm et al. [24] reported efficiency of 14.8 % in polycrystalline ZnO-window/PVD In_2S_3 buffer/Cu(In,Ga)Se_2-absorber thin film solar cells without antireflective coating. Jacob et al. [25] found that parameters of the cells buffered with PVD-In_2S_3 are degraded when the band gap of absorber is widened.

Gall et al. [26] showed that V_{oc} of the CIGS/In_2S_3 cells can be improved by partial substitution of sulfur by oxygen within the evaporated In_2S_3 buffer layer. By adapting this deposition process, 13.3 % efficiency devices with co-evaporated indium sulfide were realized, having performance close to that of devices with (CBD) CdS. Pistor et al. [27] deposited In_2S_3 layers through thermal evaporation from In_2S_3 powder.They analyzed J-V curves and quantum efficiencies of the cells prepared with different Cu(In,Ga)Se_2 absorbers. After post annealing step in air, best cells reached certified efficiency of 15.2 %.

4.3 CZTS/In_2S_3heterojunction using chemical spray pyrolysis technique.

In this section,we discuss fabrication and characterization of sprayed CZTS/In_2S_3heterojunction in our lab. Glass plates coated with ITO (thickness 200 nm, optical transmission 82 % and electrical resistivity 2.25×10^{-4} Ω.cm; Geomatec, Japan) were used as the substrate for junction fabrication. For depositing CZTS films, aqueous solution (containing copper chloride (0.015 M),

zinc acetate (0.01 M), stannic chloride (0.01 M) and thiourea (0.12 M)) is sprayed at the rate of 6 ml/min onto the substrate kept at 623 K using compressed air (pressure~1.5 bar) as the carrier gas. Concentration of thiourea was 3 times the stoichiometric requirement (0.04 M) to compensate for loss of sulphur during pyrolysis. Thickness of CZTS layer was ~550 nm. In_2S_3 layer of thickness 500 nm was deposited on top of CZTS layer. For depositing In_2S_3, aqueous solution containing Indium chloride (0.03 M) and thiourea (0.3 M) is sprayed, at the rate of 6 ml/min on to the CZTS layer.

Dark and illuminated J-V characteristics of the junction are shown in figure 4.1. It is clear from the dark J-V characteristics that a good junction is formed between the CZTS absorber and In_2S_3 buffer. On illumination the J-V characteristics shows shift towards fourth quadrant indicating photo response. The device shows open circuit voltage (V_{oc}) of 465 mV, short circuit current density (J_{sc}) of 2.54 mA/cm^2, fill factor (*FF*) of 26 % and efficiency of 0.3 %. Series resistance (R_s) and shunt resistance (R_{sh}) of the device were 176 Ω.cm and 209 Ω.cm respectively.

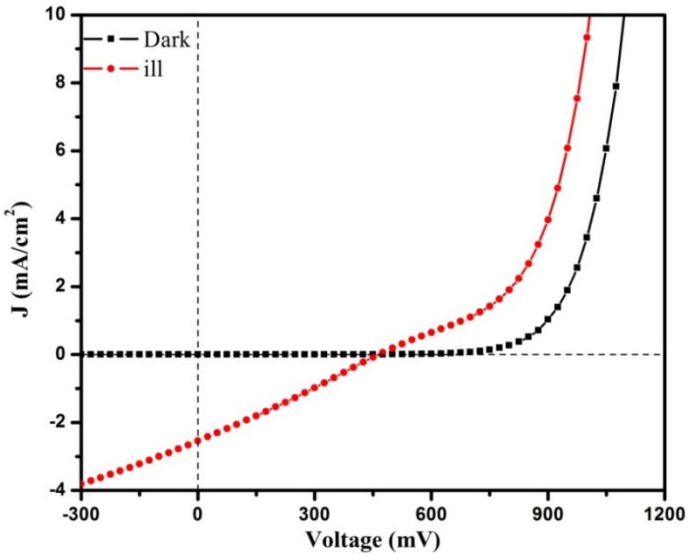

Figure 4.1.Dark and illuminated J-V characteristics of the CZTS/In_2S_3 hetero-junction

Only the open circuit voltage is comparable to that of CZTS devices reported so far. All other parameters were very low. The low values of J_{sc} and *FF* are due to high series resistance of the device, which is contributed mainly by the high resistance of In_2S_3 buffer layer. Our next aim is to improve the performance parameters by the modification of In_2S_3 buffer layer.

4.4 Improvements of CZTS/In_2S_3 cell parameters

Sprayed In_2S_3 is highly resistive material in its pristine form [28]. Referring to the results of previous section we could see that series resistance of the solar cell, prepared using CZTS as absorber and pristine In_2S_3 as buffer, was very high. Main contribution to this high series resistance is from the pristine In_2S_3 layer. Hence in order to improve the performance of the cell one should lower the resistance of In_2S_3 layer near to the contact electrodes so as to reduce the series resistance. Also as we mentioned in the introduction, In_2S_3 contains large number of cationic vacancies inherently. Hence for reducing resistance of In_2S_3 layer, we tried diffusion of metallic indium in to the In_2S_3 thin film. In order to study the effect of 'In' diffusion on the optoelectronic properties of the In_2S_3 films we deposited films on soda lime glass (SLG) substrates and structural, optical, electrical characterizations were carried out.

4.4.1 Experimental details

In_2S_3 thin films were deposited on SLG substrates using CSP technique. Aqueous solution, containing Indium chloride (0.03 M) and thiourea (0.3 M), is sprayed at the rate of 6 ml/min onto the substrate kept at 603 K using compressed air (pressure-1.5 bar) as the carrier gas. At the substrate surface, the spray droplets vaporize leaving dry precipitate which instantly decomposes to form thin layer of In_2S_3. On completing the deposition process, films were annealed for 30 minutes at the substrate temperature. Here also, concentration of

thiourea was larger than the stoichiometric requirement to compensate for the loss of sulfur during pyrolysis.

Five samples of pristine films were prepared in a single process, out of which (each having a thickness of 500 nm) four were taken and four different quantities of indium was evaporated. Thicknesses of the evaporated layers were 4 nm, 6 nm, 8 nm, 10 nm (monitored using quartz-crystal thickness monitor attached to the vacuum evaporation unit) respectively. These films were then annealed at 100 ^{o}C for 1 hour. The samples were named accordingly as P:4In, P:6In, P:8In and P:10In. The pristine In_2S_3 film was named as P.

4.4.2 Structural analysis

Figure 4.2 depicts XRD patterns of pristine as well as indium diffused In_2S_3 thin films, which shows well defined peaks corresponding to the (103), (109), (220) and (309) planes of β-In_2S_3 could be clearly observed. The 'd' values coincided with that of β-In_2S_3 in standard JCPDS data card (25-390). Intensity of peak corresponding to (220) plane was observed to be much greater than that of the other peaks present, indicating strong preferential orientation in the (220) plane. Crystallite size was calculated (table 4.1) from Scherrer equation. Also no metallic phase was observed in the film in the detection limits of XRD analysis even for 10 nm 'In' diffused sample (P:10In).

Table. 4.1. XRD data for pristine as well as 'In' diffused In_2S_3 thin films

Sample	d (Å)	Preferential orientation	FWHM (degrees)	Crystallite size (nm)
P	2.67	[220]	0.36	23.0
P:4In	2.67	[220]	0.35	23.7
P:6In	2.69	[220]	0.25	33.2
P:8In	2.70	[220]	0.24	34.5
P:10In	2.70	[220]	0.38	21.8
Std. JCPDS (25-390)	2.69	[220]	…	…

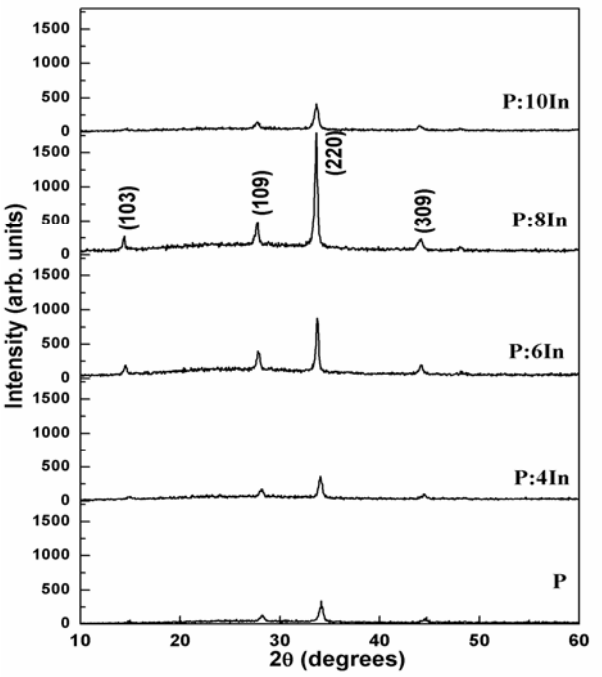

Figure. 4.2. X-Ray diffraction patterns of pristine as well as 'In' diffused In_2S_3 thin films prepared on SLG substrates.

With increase in indium content, Bragg peaks in the XRD pattern become more intense and the full width at half maximum (FWHM) of the diffraction peak narrows, indicating clear improvement in crystallinity. However, there exists an optimum for the quantity of indium to be diffused, up to which the crystallinity increases and beyond this, retracing phenomenon is observed. For the 500 nm thick In_2S_3 film studied here, the optimum thickness of indium to be diffused was 8 nm.

4.4.3 XPS Studies

In order to confirm the formation of In_2S_3 and to understand the variation of In/S ratio from surface to depth of the film on indium diffusion, XPS measurements were done. Figure 4.3 shows the XPS depth profile of samples P and P:8In which indicates that indium and sulfur were uniformly distributed

throughout the depth of the samples. Binding energies of indium and sulfur indicated formation of In_2S_3 (162.5 eV for S 2p, 444.9 eV and 452.9 eV for In $3d_{5/2}$ and In $3d_{3/2}$ respectively) and were in agreement with the reported values [29].

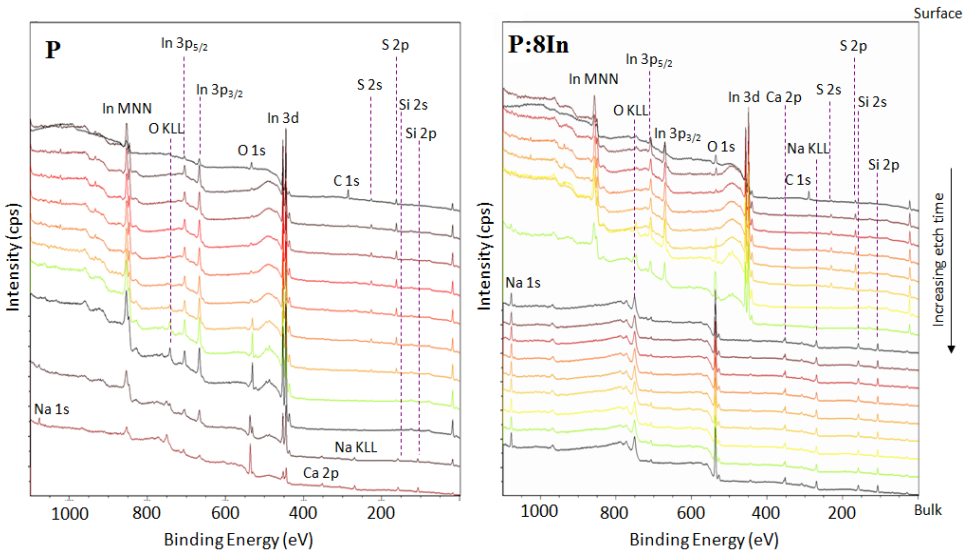

Figure 4.3.XPS depth profile of samples: P (pristine In_2S_3 sample) and P:8In (In_2S_3 sample in which 8 nm thick layer of 'In' is diffused).

Carbon was present as surface contaminant (285 eV). Oxygen at the surface, (which is found for all spray deposited samples), is due to surface contamination in the form of sulfite or sulfate [29]. Oxygen content in the bulk of the sample is very low, but as we approach the substrate, it can be observed that oxygen concentration is higher in the film, probably due to diffusion of oxygen from glass to the film. The atomic concentration versus sputter time graph is shown in figure 4.4. Sputter time zero indicates sample surface and as sputter time increases we get information from the depth.

It can be seen clearly that in sample P:8In, 'In' concentration is high in a few surface layers when compared to sample P. 'In' concentration in the bulk is almost the same for both samples. The In/S ratio in the surface was calculated

(from the area under the peak) for both samples and it was found that In/S ratio is 2.3 times higher in P:8In when compared to sample P.

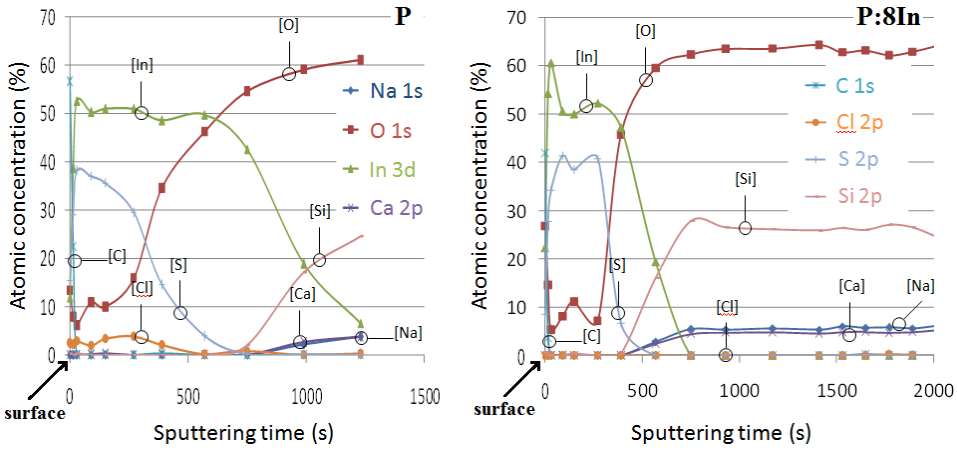

Figure 4.4. Atomic concentration versus sputter time graph of elements obtained from X-ray photo electron spectroscopy for P (pristine In_2S_3 sample) and P:8In (In_2S_3 sample in which 8 nm thick layer of 'In' is diffused)

4.4.4 Optical Studies

4.4.4.1 Optical absorption studies

Optical absorption spectra were recorded in the wavelength region 190–2500 nm. In order to determine optical band gap, $(\alpha h\nu)^2$ vs. hν graph was plotted (figure 4.5).

Optical band gap was determined from this plot for all films by applying "linear fit" to the straight line portion of the graph. Band gap of sample P was 2.64 eV which progressively decreased with increase in quantity of 'In' diffused and became 2.57 eV for P:8In. This shift in band gap can be justified by the improved crystallinity of the samples with 'In' diffusion.

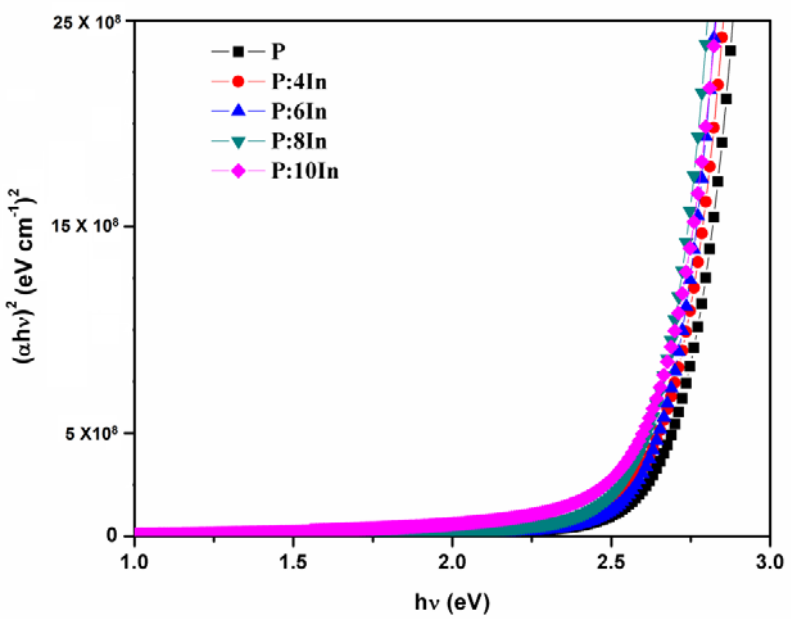

Figure 4.5. $(\alpha h\nu)^2$ vs. hν plot for pristine and 'In' diffused In_2S_3 films.

4.4.4.2 Photoluminescence studies

PL spectra of In_2S_3 consist of two emission bands- a green emission centered at 540 nm and the red emission at 680 nm [30]. The green emission is due to transition between donors created by vacancies of sulfur (V_s) and acceptors due to vacancies of indium (V_{In}). The red emission arises due to transition from indium interstitial (In_i) donors to oxygen in vacancy of sulfur (O_{Vs}) acceptors [30]. In_2S_3 is a material where two thirds of the lattice sites are vacant inherently [31]. When indium is diffused into In_2S_3, it occupies the vacant cationic sites. Focusing mainly on the green emission in the PL spectrum (figure 4.6) of pristine as well as 'In' diffused In_2S_3 sample, it can be observed that the intensity of green emission decreases as the quantity of 'In' diffused increases. The reduction in intensity of green emission might be due to the decrease in concentration of defect centers V_{In} on indium diffusion.

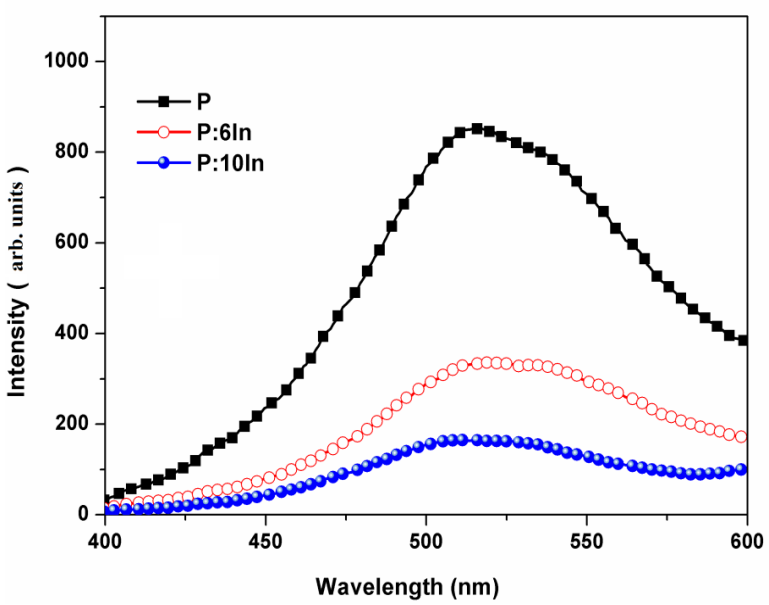

Figure 4.6.Photoluminescence spectra of pristine as well as 'In' diffused In_2S_3 films.

4.4.5 Electrical studies

Resistivity of samples was obtained using 'two probe' measurements. For pristine sample, resistivity was found to be 2.3×10^5 Ω.cm. It reduced by five orders on indium diffusion and the variation in resistivity with the quantity of 'In' diffused is shown in figure 4.7.

Reduction in acceptor concentration (as observed from PL studies) will naturally enhance the donor concentration and this might be the reason for the reduction in resistivity of In_2S_3 with indium diffusion. Resistivity of the samples increased slightly beyond the optimum diffusion, which may be because of the excess 'In' getting incorporated in interstitial positions, thereby increasing resistance to the flow of carriers. 'In' diffusion was done with an aim to reduce resistivity and improve the crystallinity so as to ensure better carrier collection. Above studies clearly indicate that we could successfully accomplish our aim and to confirm the results we fabricated devices with indium diffused In_2S_3 as buffer layer.

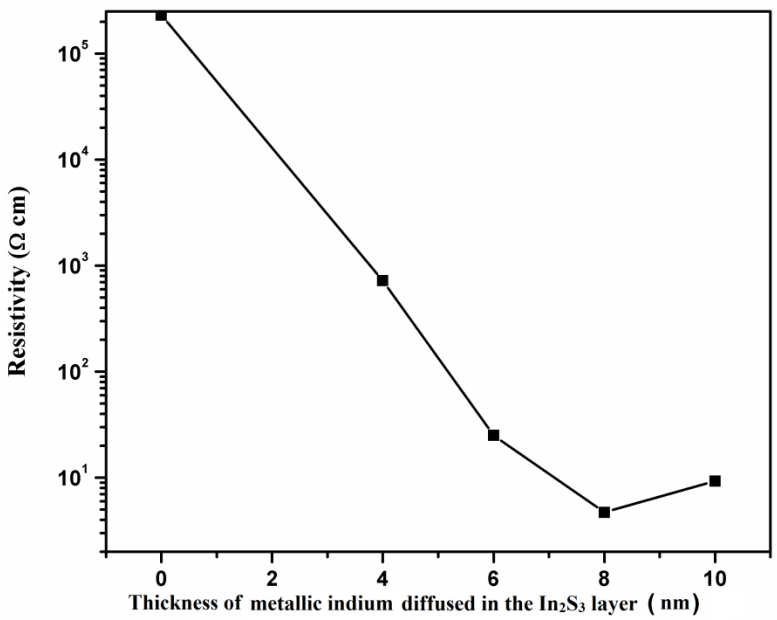

Figure 4.7. Plot showing the variation of resistivity with 'In' diffusion.

4.4.6 Junction Trials using pristine as well as 'In' diffused buffer layer

Five CZTS/In_2S_3heterojunctions were prepared in a single process using pristine In_2S_3 layer as explained in section 4.3. Out of the 5 devices four were taken and four different thickness of metallic 'In' (4 nm, 6 nm, 8 nm and 10 nm) were diffused before deposition of silver electrode. In the remaining device, silver electrode was directly deposited over the pristine In_2S_3 buffer layer. Junctions fabricated using pristine and 'In' diffused In_2S_3 layers were named as D-P, D-P:4In, D-P:6In, D-P:8In and D-P:10In respectively.

4.4.7 J-V characteristics of the CZTS/In_2S_3heterojunction with 'In' diffused buffer layer

Dark J-V characteristics of the CZTS/In_2S_3heterojunction prepared using 'In' diffused In_2S_3 buffer layer is shown in figure 4.8. It could be observed that the 'knee voltage' (which is a measure of the junction voltage) decreases with 'In' diffusion. As quantity of 'In' incorporated increases, it diffuses deeper,

causing reduction in thickness of high resistance region near the junction which leads to reduction in accumulation of charge and hence the 'knee voltage'.

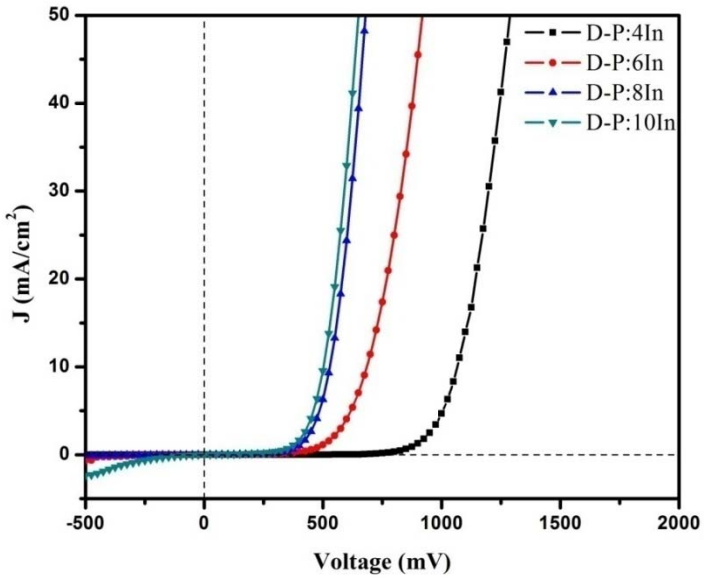

Figure 4.8. Dark J-V characteristics of the CZTS/In_2S_3heterojunctions fabricated with different thickness of 'In' diffused into the buffer layer.

Short circuit current density of 3.0 mA/cm^2 and fill factor of 27 % for the device prepared with pristine In_2S_3 film is very low compared with devices fabricated with indium diffused buffer layer which is clearly evident from the illuminated J-V characteristics of the devices (figure 4.9). This low value of J_{sc} is due to the high series resistance caused by the resistive In_2S_3 buffer layer.

There is not much variation in the open-circuit voltage between devices except for D-P:10In. More or less constant open circuit voltage for the other four devices may be because the diffused 'In' does not enter the junction region. In the case of D-P:10In, quantity of diffused 'In' being higher, it enters the junction and reduces the resistance. This, in turn, leads to larger leakage current (which is quite evident from the third quadrant of figure 4.8) and lower open circuit voltage.

The short-circuit current density on the other hand increases steadily with increase in 'In' thickness up to the optimum value of 8 nm (i.e. up to D-P:8In) and then decreases. As the quantity of 'In' diffused is increased, the vacancies of indium (which are native defects) are filled thereby reducing the resistivity of In_2S_3 considerably and increasing short circuit current density.

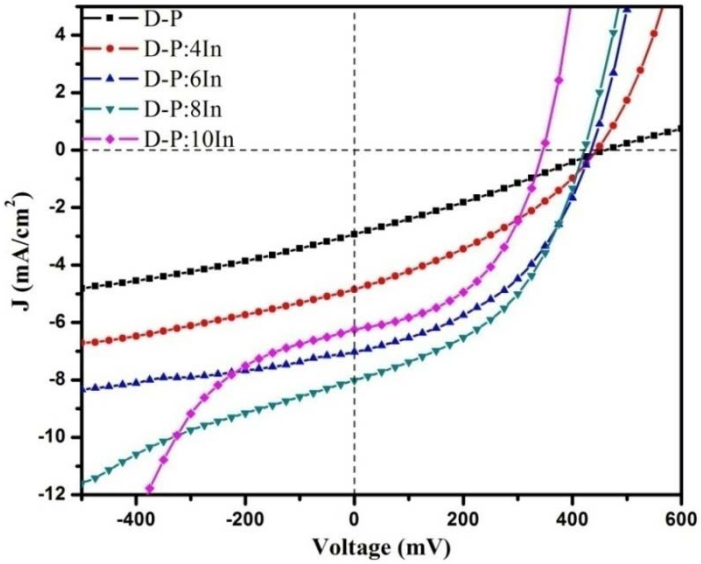

Figure 4.9. Illuminated J-V characteristics of the CZTS/In_2S_3heterojunctions fabricated with pristine and 'In' diffused buffer layer.

Table 4.2. A comparison of the photovoltaic parameters of the CZTS solar cells prepared using pristine as well as 'In' diffused 500 nm thick buffer layer.

Sample name	V_{oc} (mV)	J_{sc} (mA/cm^2)	*FF* (%)	η (%)	R_s (Ω.cm^2)	R_{sh} (Ω.cm^2)
P	462	3.0	27	0.37	166	194
P:4In	444	4.8	35	0.74	38	178
P:6In	434	7.1	43	1.33	17	270
P:8In	430	8.0	44	1.51	15	178
P:10In	345	6.3	47	1.02	14	223

The device fabricated using optimum 'In' diffused In_2S_3 layer showed fill factor of 44 % and efficiency of 1.51 %. The performance parameters of all the devices fabricated have been tabulated in table 4.2.

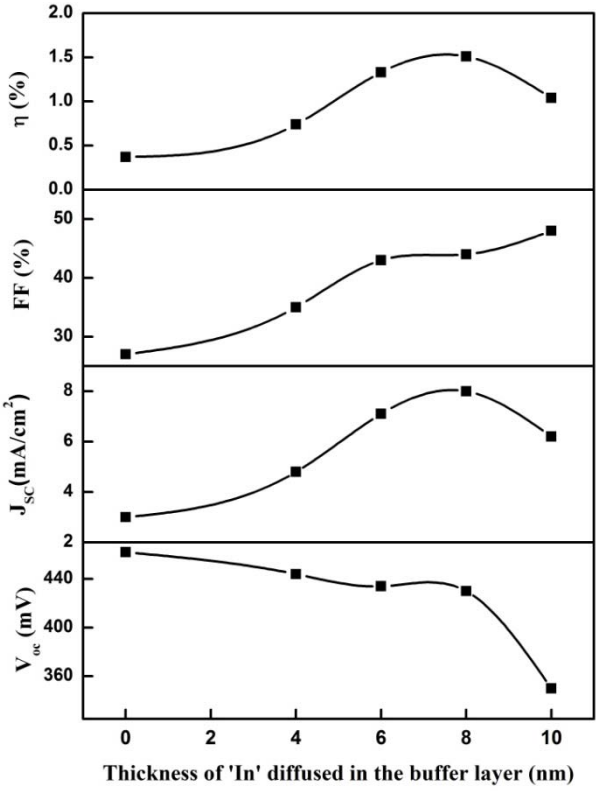

Figure 4.10. Variation of V_{oc}, J_{sc}, FF and η for CZTS/In_2S_3heterojunctions prepared with different thicknesses of indium diffused into the buffer layer.

Variation of V_{oc}, J_{sc}, FF and η with different thickness of indium diffused in the buffer layer is depicted in figure 4.10. Buffer layer is modified in such a way that we achieved 'high resistance region' near the junction (Intrinsic layer) which helps to produce a positive conduction band offset (CBO) and 'low resistance region' towards the contacts to enhance carrier collection. Using this we propose a possible band diagram for CZTS/In_2S_3 junction as shown in figure 4.11. For calculating the exact position of Fermi level and for finding the value of

CBO further studies using photo electron spectroscopy (PES) and inverse photoelectron spectroscopy (IPES) should be done.

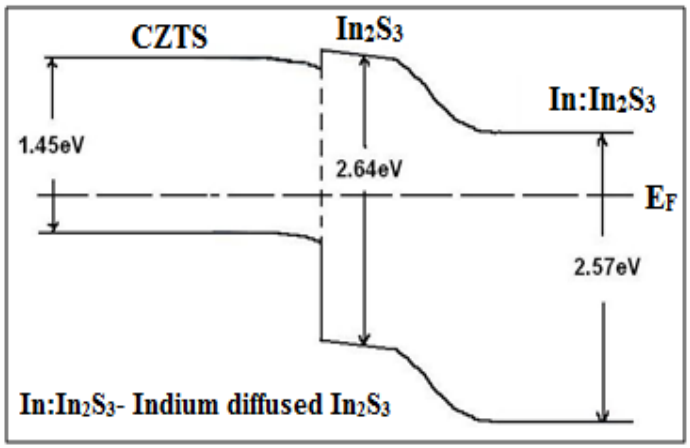

Figure 4.11. Possible schematic of the band alignment between In_2S_3 and CZTS

From the present study it is clear that the performance parameters of the CZTS/In_2S_3heterojunction could be significantly improved using 'In' diffused In_2S_3 buffer layer. The device D-P:8In (fabricated using buffer layer with optimum quantity of 'In' diffused), showed a short circuit current density of 8.0 mA/cm^2, open circuit voltage of 430 mV, fill factor of 45 % and an efficiency of 1.51 %.

4.5 Role of buffer layer thickness

The quantity of metallic indium to be diffused in order to get optimum performance for a CZTS/In_2S_3 device might depend on the thickness of In_2S_3 buffer layer. In order to have a clear idea about this, we prepared devices having slightly higher and also lower buffer layer thickness compared to the previous case. Two sets of devices were fabricated with buffer layer thickness 400 nm and 600 nm respectively (earlier it was 500 nm). All the other experimental conditions were same as earlier; thickness was varied by changing the volume of spray solution.

In the first set, five samples were prepared having thickness 400 nm and four of them were deposited with 4 different thickness of 'In' (2 nm, 4 nm, 6 nm and 8 nm) diffused. The pristine as well as 'In' diffused devices samples were named as 4D-P, 4D-P:2In, 4D-P:4In, 4D-P:6In and 4D-P:8In respectively. J-V characteristics of the device with 400 nm thick In_2S_3 layer were shown in figure 4.12.

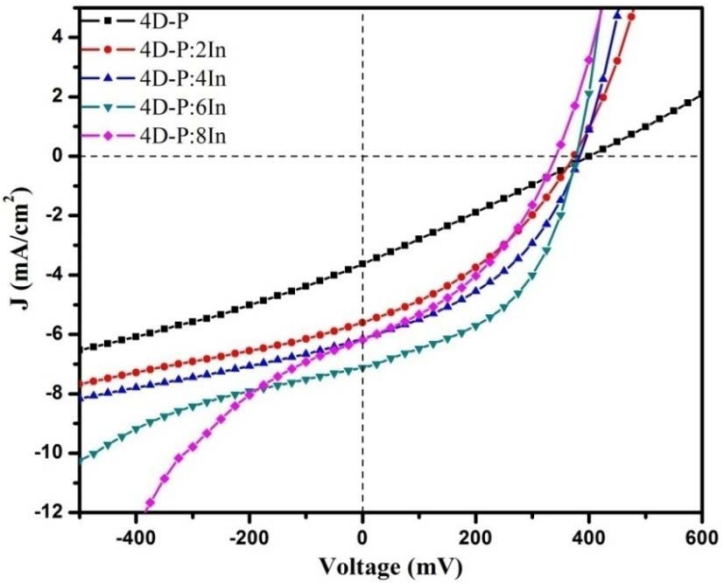

Figure 4.12.Illuminated J-V characteristics of the CZTS/In_2S_3heterojunctions fabricated with pristine and 'In' diffused 400 nm thick buffer layer.

Table 4.3. A comparison of the photovoltaic parameters of the CZTS solar cells prepared using pristine as well as 'In' diffused 400 nm thick buffer layer.

Sample name	V_{oc} (mV)	J_{sc} (mA/cm^2)	*FF* (%)	η (%)	R_s (Ω.cm^2)	R_{sh} (Ω.cm^2)
4D-P	401	3.6	26	0.38	103	126
4D-P:2In	373	5.6	36	0.75	30	160
4D-P:4In	385	6.2	40	0.95	19	174
4D-P:6In	388	7.3	47	1.33	11	232
4D-P:8In	340	6.2	39	0.83	21	134

Performance parameters of the device are given in table 4.3. As in the earlier case, it was found that, J_{sc} and *FF* improved with 'In' diffusion. Open circuit voltage is comparatively low for both pristine as well as 'In' diffused samples due to the low thickness of buffer layer. Further there is not much variation in V_{oc} up to indium diffusion of 6 nm and beyond that voltage decreased considerably. Also we can see that, due to the enhancement in J_{sc} and *FF*, efficiency improved significantly for devices fabricated using 'In' diffused buffer. It is also evident that as the thickness of In_2S_3 layer decreases the optimum quantity of 'In' to be diffused decreases. In the present case, for the device having 400 nm thick In_2S_3, the optimum thickness of 'In' to be diffused is 6 nm compared to 8 nm for 500 nm In_2S_3.

In the second case devices were prepared with In_2S_3 thickness of 600 nm. Out of six samples prepared, five were taken and 5 different thickness of 'In' (4 nm, 6 nm, 8 nm, 10 nm and 12 nm) were diffused. The pristine as well as 'In' diffused devices samples were named as 6D-P, 6D-P:4In, 6D-P:6In, 6D-P:8In, 6D-P:10In and 6D-P:12In respectively. The J-V characteristics of the device with 600 nm thick In_2S_3 layer were shown in figure 4.13.

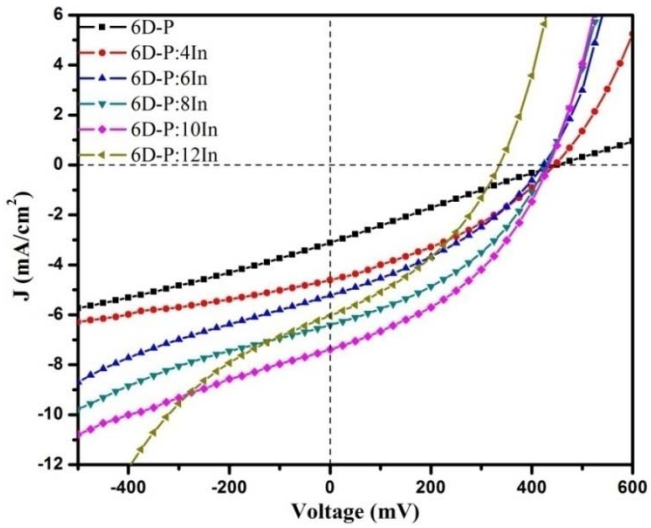

Figure 4.13. Illuminated J-V characteristics of the CZTS/In_2S_3heterojunctions fabricated with pristine and 'In' diffused 600 nm thick buffer layer.

Similar to the previous results, in this case also there was an optimum quantity of 'In' for better performance. However, here the optimum thickness of metallic indium increased to 10 nm. For the optimum 'In' diffused device we got an efficiency of 1.28 %. Here the J_{sc} is low compared to device with 500 nm thick buffer layer, due to the increased thickness of the layer. The performance parameters of the devices having 600 nm thick In_2S_3 buffer layer are given in table 4.4.

Table 4.4. A comparison of the photovoltaic parameters of the CZTS solar cells prepared using pristine as well as 'In' diffused 600 nm thick buffer layer.

Sample name	V_{oc} (mV)	J_{sc} (mA/cm^2)	*FF* (%)	η (%)	R_s (Ω.cm^2)	R_{sh} (Ω.cm^2)
6D-P	460	3.1	25	0.35	156	152
6D-P:4In	452	4.6	35	0.72	45	219
6D-P:6In	425	5.1	36	0.78	35	165
6D-P:8In	430	6.4	39	1.08	24	175
6D-P:10In	435	7.4	40	1.28	22	161
6D-P:12In	337	6.1	36	0.74	26	124

4.6 Large area heterojunction

In order to explore the potential of chemical spray pyrolysis, a large area (active area 4 cm×4 cm) cell was fabricated using the optimized CZTS layer as absorber and optimum 'In' diffused, 500 nm thick, In_2S_3 as buffer layer. ITO coated glass plates having area 25 cm^2 (5 cm×5 cm) was used as the substrate. CZTS is deposited employing the optimized conditions and then In_2S_3 buffer layer is deposited above that. Finally 'In' was diffused over an area 16 cm^2 (4 cm×4 cm) and silver electrodes were evaporated over the same area. Current and voltage of the device were measured under sunlight (~1000 W/cm^2), which is shown in figure 4.14. We got an open circuit voltage of 315 mV and short circuit current of 20.8 mA.

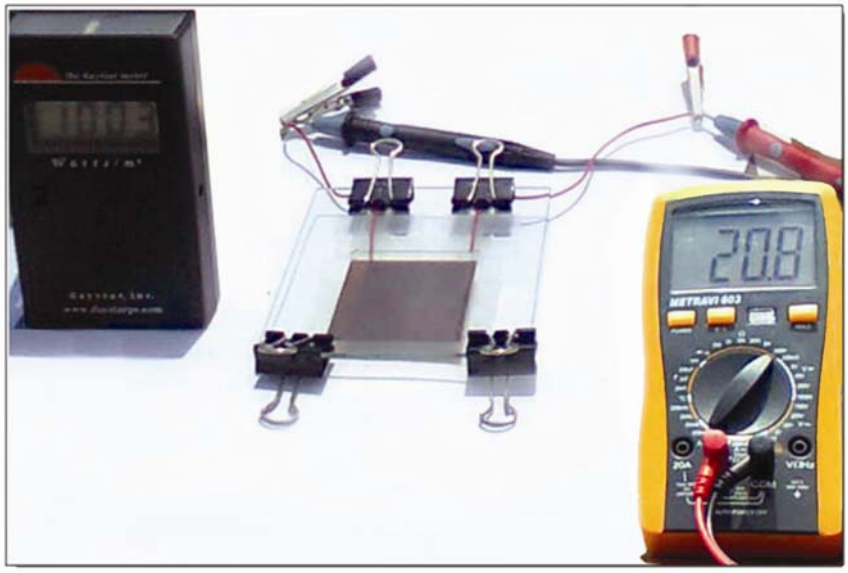

Figure 4.14 (a). Current measurement of large area (16 cm^2) cell in direct sunlight

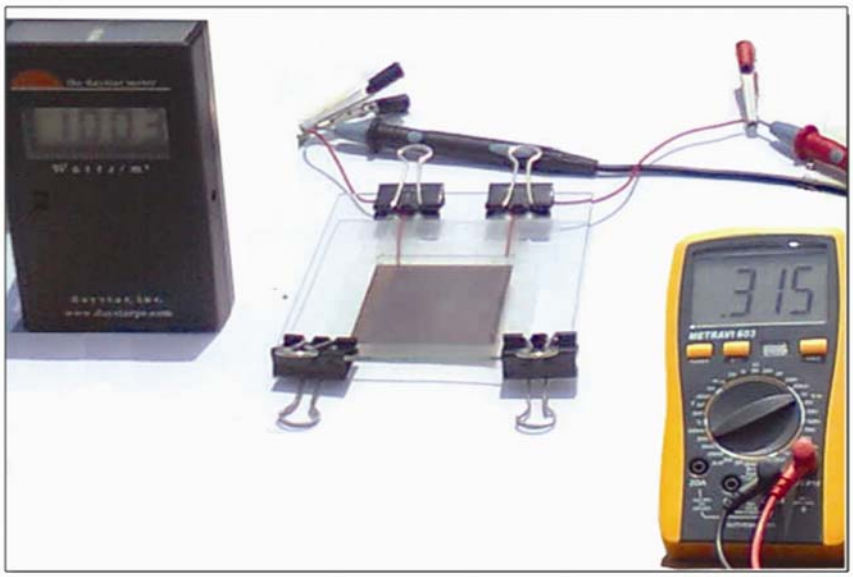

Figure 4.14 (b). Voltage measurement of large area (16 cm^2) cell in direct sunlight

4.7 Conclusions

The aim of this work was to develop CZTS/In_2S_3heterojunction on ITO-coated glass substrates using CZTS absorber described in chapter 3. The major conclusions from this work are given below.

1) Diffusion of Indium improves cell parameters through reduction in series resistance.

2) There is dependence of quantity of Indium diffused on thickness of In_2S_3 layer.

Table 4.5. Performance parameters obtained for different thickness of In_2S_3 buffer layer

Thickness of In_2S_3 layer (nm)	Thickness of 'In' evaporated (nm)	V_{oc} (mV)	J_{sc} (mA/cm^2)	*FF* (%)	η (%)
400	6	388	7.3	47	1.33
500	8	430	8	45	1.51
600	10	435	7.4	40	1.28

A cell having active electrode area 16 cm^2 could be fabricated with conversion efficiency 1.25 %.

References

[1]. **K. Kim, L. Larina, J. H. Yun, K. H. Yoon, H. Kwon and B. T. Ahn.** 2013, Phys.Chem. Chem. Phys., Vol. 15, p. 9239.

[2]. **N. Barreau, S. Marsillac, J. C. Bernede, T. B. Nasrallah and S. Belgacem.** 2001, Physica status solidi (a), Vol. 184, p. 179.

[3]. **N. Barreau, S. Marsillac, D. Albertini and J. C. Bernede.** 2002, Thin Solid Films, Vols. 403-404, p. 331.

[4]. **N. Naghavi, D. Abou-Ras, N. Allsop, N. Barreau, S. Bucheler, A. Ennaoui, C. H. Fischer, C. Guillen, D. Hariskos, J. Herrero, R. Klenk, K. Kushiya, D. Lincot, R. Menner, T. Nakada, C. P. Bjorkman, S. Spiering, A. N. Tiwari and T. Torndahl.** 2010, Prog. Photovolt: Res. Appl., Vol. 18, p. 411.

[5]. **T. T. John, M. Mathew, C. Sudha Kartha, K. P. Vijayakumar, T. Abe and Y. Kashiwaba.** 2005, Sol. Energy Mater. Sol. Cells, Vol. 89, p. 27.

[6]. **T. T. John, C. S. Kartha, K. P. Vijayakumar, T. Abe and Y. Kashiwaba.** 2006, Appl. Phys. A, Vol. 82, p. 703.

[7]. **K. Ernits, D. Bremaud, S. Buecheler, C. J. Hibberd, M. Kaelin, G. Khrypunov, U. Muller, E. Mellikov and A. N. Tiwari.** 2007, Thin Solid Films, Vol. 515, p. 6051.

[8]. **S. Buecheler, D. Corica, D. Guettler, A. Chirila, R. verma, U. Muller, T. P. Niesen, J. Palm and A. N. Tiwari.** 2009, Thin Solid Films, Vol. 517, p. 2312.

[9]. **N. A. Allsop, A. Schönmann, H.-J. Muffler, M. Bär, M. C. Lux-Steiner, Ch.-H. Fischer.** 2005, Prog. Photovolt: Res. Appl. , Vol. 13, p. 607.

[10]. **D. Braunger, D. Hariskos, T. Walter and H. W. Schock.** 1996, Sol. Energy Mater. Sol. Cells, Vol. 40, p. 97.

[11]. **D. Hariskos, M. Ruckh, U. Ruhle, T. Walter, H. W. Schock, J. Hedstrom and L. Stolt.** 1996, Sol. Energy Mater. Sol. Cells, Vol. 41/42, p. 345.

[12]. **B. Asenjo, A. M. Chaparro, M. T. Gutierrez, J. Herrero and J. Klaer.** 2005, Sol. Energy Mater. Sol. Cells, Vol. 87, p. 647.

[13]. **B. Dimmler, E. Gross, D. Hariskos, F. Kessler, E. Lotter, M. Powalla,J. Springer, U. Stein, G. Voorwinden, M. Gaeng and S. Schleicher.** Vienna, Austria : s.n., 1998. Proceedings 2nd World Conference of Photovoltaic Energy Conversion. p. 419.

[14]. **U. Rau, K. Weinert, Q. Nguyen, M. Mamor, G. Hanna, A. Jasenek and H.W. Schock.** 2001, Mater. Res. Soc. Proc., Vol. 668 , p. H9.1.1.

[15]. **Y. Tokita, S. Chaisitsak, A. Yamada and M. Konagai.** 2003, Sol. Energy Mater. Sol. Cells, Vol. 75, p. 9.

[16]. **E. B. Yousfi, T. Asikainen, V. Pietu, P. Cowache, M. Powalla and D. Lincot.** 2000, Thin Solid Films , Vols. 361-362, p. 183.

[17]. **E.B. Yousfi, B. Weinberger, F. Donsanti, P. Cowache and D. Lincot.** 2001, Thin Solid Films, Vol. 387, p. 29.

[18]. **N. Naghavi, S. Spiering, M. Powalla, B. Cavana and D. Lincot.** 2003, Prog. Photovolt: Res. Appl., Vol. 11, p. 437.

[19]. **S. Spiering, D. Hariskos, M. Powalla, N. Naghavi and D. Lincot.** 2003, Thin Solid Films, Vols. 431-432, p. 359.

[20]. **S. Spiering, A. Eicke, D. Hariskos, M. Powalla, N. Naghawi and D. Lincot.** 2004, Thin Solid Films , Vols. 451–452, p. 562.

[21]. **S. Spiering, D. Hariskos, S. Schroder and M. Powalla.** 2005, Thin Solid Films, Vols. 480-481, p. 195.

[22]. **N. Barreau, J. C. Bernede, S. Marsillac, C. Amory and W. N. Shafarman.** 2003, Thin Solid Films, Vols. 431-432, p. 326.

[23]. **S. Gall, N. Barreau, S. Harel, J. C. Bernede and J. Kessler.** 2005, Thin Solid Films, Vols. 480-481, p. 138.

[24]. **A. Strohm, L. Eisenmann, R. K. Gebhardt, A. Harding, T. Schlotzer, D. Abou-Ras and H. W. Schock.** 2005, Thin Solid Films, Vols. 480-481, p. 162.

[25]. **F. Jacob, N. Barreau, S. Gall and J. Kessler.** 2007, Thin Solid Films, Vol. 515, p. 6028.

[26]. **S. Gall, N. Barreau, F. Jacob, S. Harel and J. Kessler.** 2007, Thin Solid Films, Vol. 515, p. 6076.

[27]. **P. Pistor, R. Caballero, D. Hariskos, V. Izquierdo-Roca, R. Wachter, S. Schorr and R. Klenk.** 2009, Sol. Energy Mater. Sol. Cells, Vol. 93, p. 148.

[28]. **M. Mathew, M. Gopinath, C. Sudha Kartha, K. P. Vijayakumar, Y. Kashiwaba and T. Abe.** 2010, Sol. Energy, Vol. 84, p. 888.

[29]. **T. T. John, C. Sudha Kartha, K. P. Vijayakumar, Y. Kashiwaba and T. Abe.** 2005, Appl. Surf. Sci., Vol. 252, p. 1360.

[30]. **R. Jayakrishnan, T. Sebastian, C. Sudha Kartha and K. P. Vijayakumar.** 2012, J. Appl. Phys., Vol. 111, p. 093714.

[31]. **K. Kambas, J. Spyridelis and M. Balkanski.** 1981, Phys. Status Solidi (b), Vol. 105, p. 291.

[32]. **M. Mathew, R. Jayakrishnan, P. M. Ratheesh Kumar, C. Sudha Kartha and K. P. Vijayakumar.** 2006, J. Appl. Phys., Vol. 100, p. 033504.

.....ഇ൦ര.....

Chapter 5

ENHANCEMENT OF CELL PARAMETERS BY MODIFICATION OF CZTS ABSORBER LAYER

5.1. Introduction
5.2. Effect of starting solution pH on properties of CZTS layer.
5.3. Effect of 'Cu' concentration
5.4. Effect of 'Sn' concentration
5.5. Effect of double layer structure
5.6. All sprayed FTO/CZTS/In_2S_3 solar cell
5.7. Conclusions

5.1 Introduction

CZTS is a quaternary compound semiconductor having properties suitable for a good absorber layer in thin film solar cells. The highest efficiency reported so far for a device with CZTS absorber layer is 8.4 % [1]. The device structure was Mo/MoS_2/CZTS/CdS/i-ZnO/Al:ZnO/Ni-Al/MgF_2. But on the perspective of cost effective solar cells, the problem with this device is that vacuum based techniques have been used for deposition of various layers. Our aim is to develop CZTS based solar cell using the low cost non-vacuum technique, chemical spray pyrolysis (CSP). In third chapter we discussed preparation and characterization of CZTS absorber layer using CSP. Device fabrication and characterization were explained in chapter 4. We were able to achieve an efficiency of 1.51 % and a fill factor of 44 %.

One of the main challenges with spray deposition of CZTS thin films is the instability of precursor solution. Precipitation occurs in the solution as time progresses. In order to get rid of this issue, we varied the pH of precursor solution. The effect of pH variation on material properties and device

performance was studied. To improve device performance the concentrations of 'Cu' & 'Sn' were varied and a double layer structure was introduced in the deposition of CZTS layer. This chapter gives a detailed account of these studies.

5.2 Effect of starting solution pH on properties of CZTS layer.

In chapter 3 we selected copper chloride, zinc acetate, stannic chloride, and thiourea as the precursors for copper, zinc, tin, and sulfur respectively. Aqueous solutions of 'Cu', 'Zn', 'Sn' and 'S' were mixed together to form the precursor solution (pH of the precursor solution was 3.6). But after sometime there is an onset of precipitation in the solution. A white gel like precipitate appears, due to formation of $Sn(OH)_2$ (when 'Sn' reacts with water) and settles at the bottom of the container. Owing to this precipitation of 'Sn', precursor solution will be 'Sn' deficient. Thus a large compositional variation will occur in the CZTS formed with a possibility for the formation of secondary phases. There are reports of similar problem in the case of spray deposition of $CuInSe_2$ thin films [2], where the authors have commented on the instability of precursor solution and proposed that lowering the pH of the solution will reduce the rate of precipitation and make the solution more stable. So in order to avoid precipitation in starting solution we lowered the pH.

5.2.1 Experimental

In the present work we tried CZTS film deposition using two different pH for starting solution viz. 2.8 and 3.2 (which are less than the pH value of 3.6 at which precipitation occurred). Except for the difference in pH of the precursor solution, all the other spray parameters were the same as was optimized in the previous chapters. More details of the preparation of precursor solution are given in our patent application (No. 021/PF-PIC/2013/KSCSTE). This precursor solution with reduced pH was sprayed on to the substrate kept at a temperature of 350 ^{o}C. The prepared films were named according to the pH as CZTS:pH-2.8 and CZTS:pH-3.2

5.2.2 Structural analysis

X-ray diffractograms of the deposited CZTS thin films are shown in figure 5.1. Peaks corresponding to the (112), (200), (220) and (312) planes of CZTS could be identified. Preferential orientation was along (112) plane. The peaks become more intense and FWHM decreases with decrease in pH of spray solution. Crystallite size calculated using Scherrer formula has been tabulated in table 5.1.

Table 5.1. FWHM and crystallite size of CZTS films prepared with different pH values of spray solution.

Sample name	FWHM (degrees)	Crystallite size (nm)
CZTS:pH-3.2	0.31	26.5
CZTS:pH-2.8	0.29	28.3

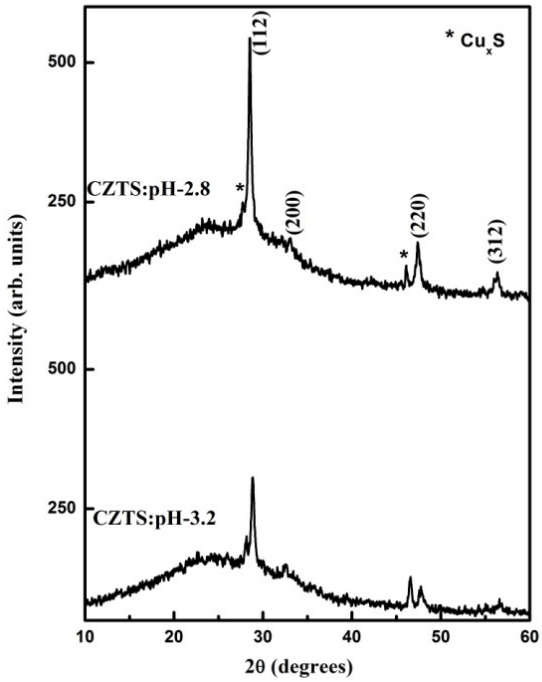

Figure 5.1. X-ray diffractograms of CZTS samples prepared with different pH values of spray solution.

Also we can see that as the pH decreases, formation of Cu_xS secondary phase is hindered. Again, stability of precursor solution increases and the rate ofprecipitation decreases. So probability of formation of secondary phase will be lowered.

5.2.3 Optical Studies

$(\alpha h\upsilon)^2$ versus $h\upsilon$ plot of the CZTS thin films deposited using precursor solutions of different pH values are shown in figure 5.2. Band gap of the samples decreases from 1.45 eV to 1.25 eV on decreasing the pH of spray solution. For CZTS:pH-3.2 band gap value corresponds well with the literature values and is near the optimum value for solar energy conversion in a single band gap device. The absorption coefficient in the visible region is in the order of 10^4 cm^{-1}. No information about Cu_xS phase was obtained from absorption spectra.

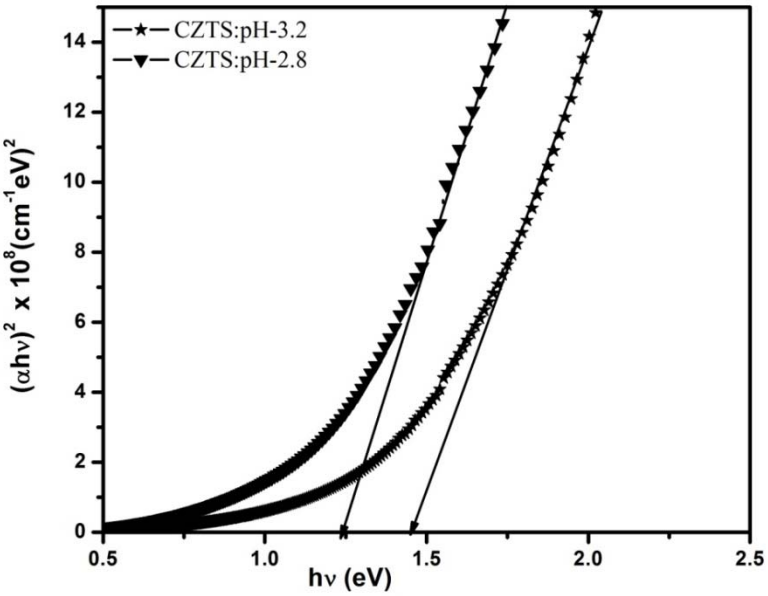

Figure5.2. $(\alpha h\upsilon)^2$ vs. $h\upsilon$ graph of CZTS films prepared with different pH values of spray solution.

5.2.4 Compositional analysis

EDAX measurements (table 5.2) were done on the samples to know the atomic concentration of various elements in the films. It was found that for CZTS:pH-3.2, Zn/Sn is high due to the unwanted precipitation of 'Sn' in the precursor solution. As pH of spray solution decreases Zn/Sn ratio decreases indicating enhanced 'Sn' content in the film. All the films were found to be slightly sulfur deficient, which is consistent with the behaviour expected for spray deposited films.

Table 5.2. Elemental composition of CZTS films prepared with different pH values of spray solution.

Sample	Cu (at.%)	Zn (at.%)	Sn (at.%)	S (at.%)	Cl (at.%)	$\frac{Cu}{Zn+Sn}$	$\frac{Zn}{Sn}$	$\frac{S}{Metal}$
CZTS:pH-3.2	21.3	16.5	13.2	45.8	3.2	0.72	1.25	0.9
CZTS:pH-2.8	20.2	14.8	15.1	46.2	3.7	0.68	0.98	0.92

5.2.5 Electrical studies

Thickness and roughness of the films increases with decrease in pH. Moreover resistivity increases by an order for films prepared with spray solution of lower pH. Thickness, roughness and resistivity are tabulated in table 5.3.

Table 5.3. Thickness, roughness and resistivity values of CZTS samples prepared with different pH values of spray solution.

Sample name	Thickness (nm)	Roughness (nm)	Resistivity (Ω.cm)
CZTS:pH-3.2	1550	305	1.6×10^{-2}
CZTS:pH-2.8	1780	384	0.8×10^{-1}

5.2.6 Junction Trials

To check the effect of CZTS films- CZTS:pH-2.8 and CZTS:pH-3.2, on the performance of CZTS/In_2S_3 heterojunction, we prepared junctions on ITO

coated glass substrates using both these layers as absorber. In_2S_3 buffer layer and electrode deposition was done using the optimized conditions as described in the previous chapter. J-V characteristics of the devices were measured using the Source Measure Unit NI-PXI-4130 (National Instruments). The devices were illuminated using Class AAA Solar Simulator (Photo Emission Tech. Inc. USA). J-V characteristics of devices prepared using absorber layers with CZTS:pH-3.2 and CZTS:pH-2.8 are shown in figure 5.3.

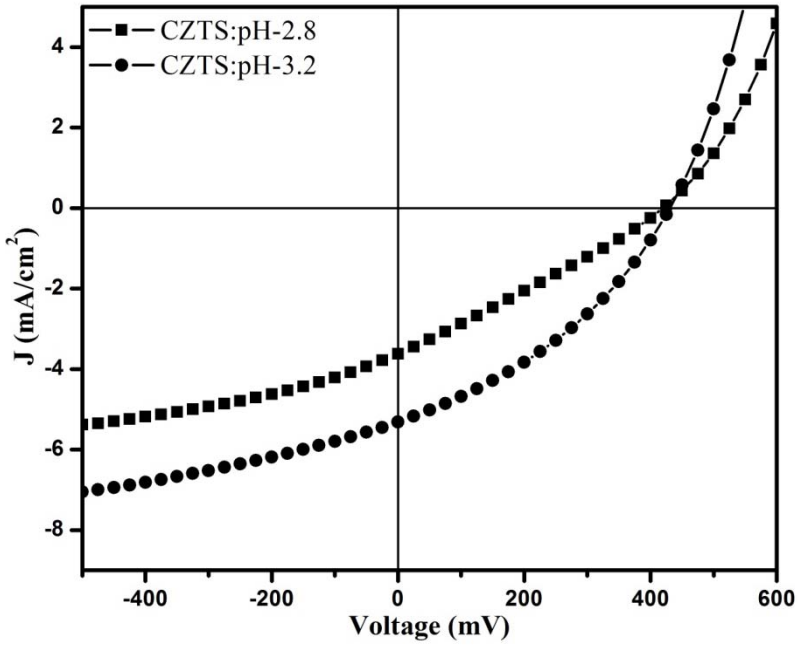

Figure 5.3. Illuminated J-V characteristics of CZTS/In_2S_3 solar cell, prepared using CZTS samples CZTS:pH-2.8 and CZTS:pH-3.2.

It could be observed that as pH decreases there is a reduction in J_{sc} (table 5.4) which might be due to the increase in resistivity of CZTS layer. V_{oc} is almost the same for both devices. Due to the enhanced J_{sc} and *FF*, efficiency of the device CZTS:pH-3.2 is nearly twice the value obtained for device CZTS:pH-2.8. So for future works we maintained the pH value of the precursor solution as 3.2.

Table 5.4. Performance parameters of CZTS/In_2S_3 solar cell, prepared CZTS samples CZTS:pH-3.2 and CZTS:pH-2.8.

Sample name	V_{oc} (mV)	J_{sc} (mA/cm^2)	FF (%)	η (%)	R_s (Ω.cm^2)	R_{sh} (Ω.cm^2)
CZTS:pH-2.8	423	3.6	28	0.42	77	148
CZTS:pH-3.2	426	5.4	36	0.82	36	179

5.3 Effect of 'Cu' concentration

We successfully reduced precipitation in spray solution by varying the pH of the solution. But from EDAX measurements it is clear that 'Cu' concentration in the sample is less than that required for stoichiometry. In the best performing CZTS based solar cells reported so far, Cu/(Zn+Sn) ratio in CZTS layer is ~ 0.9. But in CZTS:pH-3.2 thin films, Cu/(Zn+Sn) ratio is only 0.72. Performance of heterojunction fabricated using this CZTS layer is quite low compared to the values we have reported in chapter 4. Hence in order to enhance the device performance we increased copper concentration in the precursor solution. We prepared CZTS films with copper concentrations equal to 0.0175, 0.02, 0.0225 and 0.025 M, keeping the concentration of 'Zn', 'Sn' and 'S' at 0.01, 0.01 and 0.12 M respectively. All the other spray parameters were fixed, based on our initial trials. CZTS thin films hence prepared were named as CZTS:1.75C, CZTS:2C, CZTS:2.25C & CZTS:2.5C in accordance with 'Cu' concentration.

5.3.1 Structural analysis using X-ray diffraction

XRD measurements were performed in all the deposited films and the diffractograms are presented in figure 5.4. Peaks corresponding to (112), (200), (220) and (312) planes were detected indicating the polycrystalline nature of the film. But the dominant peak corresponds to the (112) diffraction line of the kesterite structure of CZTS. Crystallite size in these films was determined from the broadening of the most intense peak (112) in the XRD pattern, using

Scherrer formula. There were no notable peaks related to secondary phases from XRD; however existence of binary or ternary sulfides such as ZnS, $Cu_{2-x}S$, and Cu_2SnS_3 cannot be ruled out just because they are absent in XRD pattern because they have diffraction patterns similar to CZTS owing to their similar zinc blend-type structures. To distinguish the CZTS phase from other sulfides, Raman analysis was done.

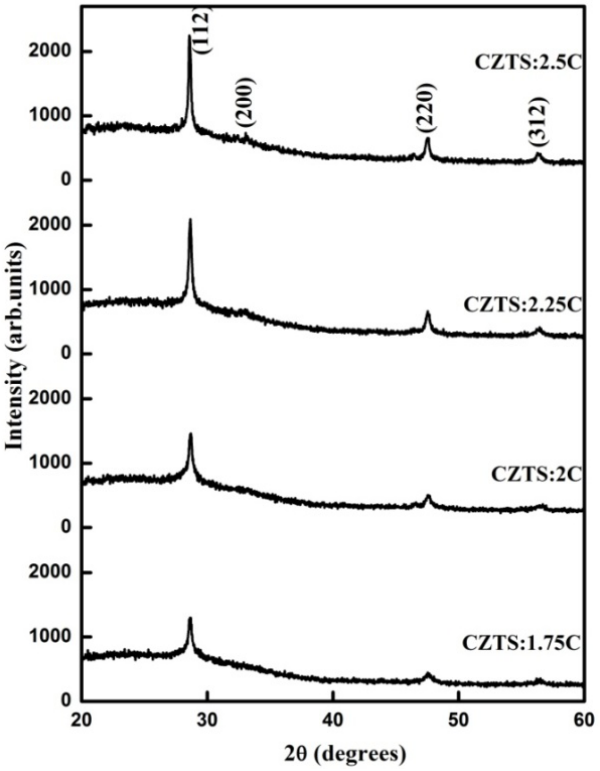

Figure 5.4. XRD spectrum of CZTS thin films prepared by varying copper concentration in the precursor solution.

5.3.2 Structural analysis using Raman spectra.

Surface Raman scattering analysis (figure 5.5) was performed since additional information on possible secondary phases can be obtained. All the deposited films showed a strong peak at 333 cm^{-1} which is attributed to the 'A1 mode' of CZTS and it is related with the vibration of 'S' atoms. There is a

small shift in peak position to lower energies with respect to the reported value 338 cm^{-1}. This shift may be due to the lattice strain [3], due to a gradient in crystal quality of the layers [4]. This peak is but related to CZTS since XRD measurements confirm the presence of CZTS. The second peak of CZTS at 287 cm^{-1} is also present in all the samples, but its intensity is very small compared to the peak at 338 cm^{-1}.

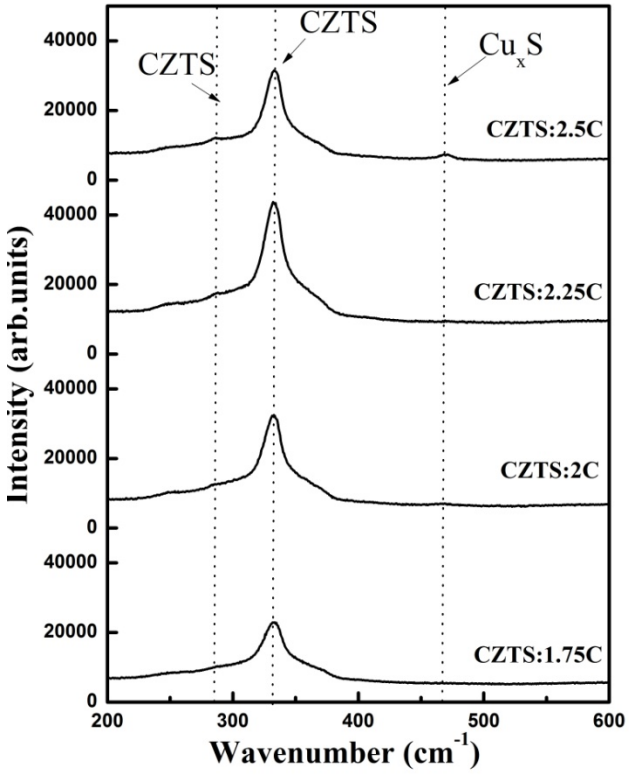

Figure 5.5. Raman spectra of CZTS thin films prepared by varying copper concentration in the precursor solution.

Advantage of Raman spectra over XRD pattern in analyzing the presence of secondary phases is that, in Raman spectra, peaks corresponding to secondary phases are not present in the vicinity of peaks corresponding to CZTS. Intensity of peaks corresponding to CZTS increases with increase in 'Cu' concentration up to 0.0225 M, beyond which intensity decreases. Formation of secondary

phases is initiated when 'Cu' concentration is raised to 0.025 M. The peak at 475 cm^{-1} indicates formation of Cu_xS phase. Even from Raman analysis, presence of ZnS and other sulfides could not be detected.

5.3.3 Compositional analysis.

Elemental composition of CZTS films deposited with different 'Cu' concentration in the precursor solution on glass substrates is shown in table 5.5. As expected, there is proportionate increase in atomic concentration of 'Cu' in the films when 'Cu' concentration is increased in the precursor solution. When concentration of 'Cu' in the solution is varied, it affects atomic concentration of not only 'Cu' but also 'Zn', 'Sn' and 'S' in the films. Even though there is slight decrease in sulfur concentration there is no systematic variation in the case of 'Zn' and 'Sn'. The $\frac{Cu}{(Zn+Sn)}$ ratio in the film increased from 0.75 to 0.92 with increase in 'Cu' concentration. Katagiri et al. [5] had reported that solar cells with high conversion efficiency are possible with CZTS films which are slightly Cu-deficient i.e. when $\left(\frac{Cu}{(Zn+Sn)} \sim 0.9\right)$.

Table 5.5:Compositional analysis of CZTS thin films prepared by varying copper concentration in the precursor solution.

Sample	Cu (at.%)	Zn (at.%)	Sn (at.%)	S (at.%)	Cl (at.%)	$\frac{Cu}{Zn+Sn}$	$\frac{Zn}{Sn}$	$\frac{S}{Metal}$
CZTS:1.75C	22.3	15.5	14.3	44.6	3.3	0.75	1.1	0.86
CZTS:2C	23.1	12.2	17	44.1	3.6	0.79	0.72	0.84
CZTS:2.25C	25.3	13.1	15.5	43.3	2.8	0.88	0.85	0.80
CZTS:2.5C	26.4	12.7	16.1	41.6	3.2	0.92	0.79	0.75

5.3.4 Junction studies

Using these four different CZTS layers, whose properties have been analyzed, CZTS/In_2S_3heterojunctions were fabricated. CZTS layers were

deposited over ITO coated glass plates by varying the concentration of 'Cu' in the precursor solution from 0.0175 M to 0.025 M in steps of 0.0025 M. In_2S_3 layer, having thickness of 500 nm, was deposited over it and then 'In' diffusion was done. Finally silver electrode was deposited using vacuum evaporation. The J-V characteristics of the devices are shown in figure 5.6.

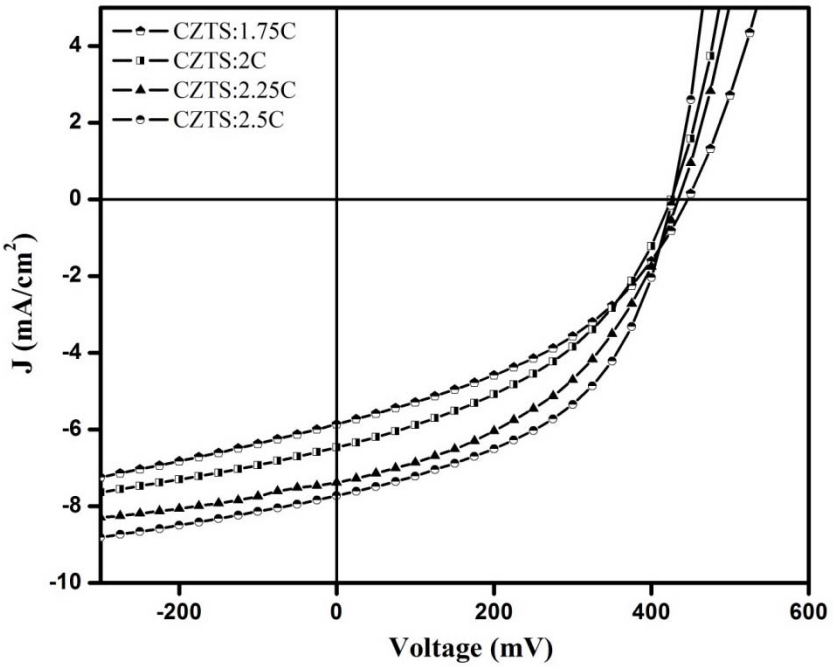

Figure 5.6. J-V characteristics of CZTS/In_2S_3heterojunction prepared using CZTS layer having different 'Cu' concentration.

V_{oc} is almost the same for all the devices whereas J_{sc} increased steadily with increase in 'Cu' concentration. As with J_{sc}, there is a significant improvement in the *FF* also. Increase in J_{sc} and *FF* may be due to the reduction in resistance of CZTS layer with increase in 'Cu' concentration. Maximum efficiency that we obtained from the set of devices was 1.6 % and it was for the device having a 'Cu' concentration of 0.025 M in the precursor solution. The cell parameters of the devices prepared using CZTS layer having different 'Cu' concentration is given in table 5.6.

Table 5.6. Performance parameters of the CZTS/In_2S_3heterojunction prepared using CZTS layer having different 'Cu' concentration.

Device name	V_{oc} (mV)	J_{sc} (mA/cm^2)	FF (%)	η (%)	R_s (Ω.cm^2)	R_{sh} (Ω.cm^2)
CZTS:1.75C	447	5.9	40	1.07	23	186
CZTS:2C	426	6.5	42	1.16	18	198
CZTS:2.25C	434	7.4	42	1.35	17	258
CZTS:2.5C	426	7.7	49	1.6	11	216

5.4. Effect of 'Sn' concentration

From the compositional analysis of the 'Cu' varied samples, we could see that Zn/Sn ratio in the film is only 0.79 for the optimum 'Cu' concentration. As per reports, slightly 'Zn' rich composition is favorable for obtaining good conversion efficiency [5]. Hence our next aim was to enhance efficiency of the CZTS/In_2S_3 device by enhancing the Zn/Sn ratio in the CZTS layer by reducing the 'Sn' concentration.

5.4.1 Experimental

Four different CZTS/In_2S_3 devices were prepared using CSP technique. In allthe devices In_2S_3 buffer layer is deposited as in earlier cases. For CZTS the concentration of 'Sn' in the precursor solution was varied from 0.009 M to 0.006 M in steps of 0.001 M, keeping the concentration of 'Cu', 'Zn' and 'S' at 0.025, 0.01 and 0.12 M respectively. All the other spray parameters were maintained the same as for previous trials. After the deposition of p-type CZTS and n-type In_2S_3 layers, the devices were completed following the same procedure as described before. These devices were named as CZTS:0.9Sn, CZTS:0.8Sn, CZTS:0.7Sn and CZTS:0.6Sn according to the 'Sn' content 0.009 M, 0.008 M etc. in the starting solution.

5.4.2 Junction analysis

J-V characteristics of the devices are shown in figure 5.7. As in the earlier case, there is not much variation in V_{oc}. But J_{sc} and FF increased up to 0.007M of 'Sn' concentration and then decreased. Efficiency also was maximum for device CZTS:0.7Sn. The maximum conversion efficiency achieved was 1.85 %. Series resistance of the devices, calculated from the inverse slope of the J-V characteristics at the open circuit voltage point, was found to be minimum for CZTS:0.7Sn and the value obtained was 10 $\Omega.cm^2$. Performance parameters of the devices are tabulated in table 5.7.

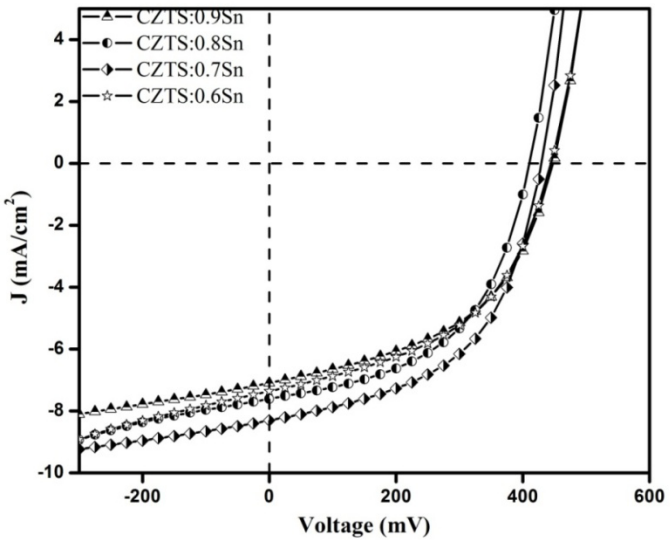

Figure 5.7. J-V characteristics of the CZTS/In_2S_3heterojunction prepared by using CZTS layer deposited by varying the 'Sn' concentration

Table 5.7. Performance parameters of the CZTS/In_2S_3heterojunctions prepared by using CZTS layer deposited by varying the 'Sn' concentration

Device name	V_{oc} (mV)	J_{sc} (mA/cm^2)	FF (%)	η (%)	R_s ($\Omega.cm^2$)	R_{sh} ($\Omega.cm^2$)
CZTS:0.9Sn	447	7.1	49	1.55	12	242
CZTS:0.8Sn	411	7.7	51	1.61	11	265
CZTS:0.7Sn	430	8.3	52	1.85	10	252
CZTS:0.6Sn	445	7.3	48	1.57	14	219

From the various studies done so far on CZTS absorber layer, we could optimize the ratio of various constituent elements in the precursor solution. For getting maximum conversion efficiency, the sprayed CZTS absorber layer should have an elemental ratio of Cu:Zn:Sn:S= 2.5:1:0.7:12 in the precursor solution. Maximum efficiency obtained was 1.85 %.

5.5 Effect of double layer structure

In our device structure, CZTS absorber is in contact with the transparent conducting electrode which may result in a barrier to the flow of holes.This may be reduced by having a conducting layer of CZTS near to this electrode. In chalcopyrite thin films, it is generally observed that, conductivity of films can be improved merely by increasing the concentration of 'Cu' [6-7]. Hence in an attempt to improve the collection of holes by the transparent electrode, a modification was introduced in the deposition of CZTS layer. Instead of depositing CZTS as a single layer over ITO, it was deposited as a 'double layer' such that a conducting 'Cu- rich' CZTS layer is adjacent to ITO and on top of this conducting layer, a second layer of CZTS ('Cu-deficient') was given. Another point we investigated is whether a resistive layer close to the junction is beneficial for the device. A conducting layer close to the junction might cause the shunt resistance to drop which in turn lowers the open-circuit voltage. Hence we tried 'Cu-deficient' resistive layer of CZTS near to the junction.

5.5.1 Experimental

Here also ITO coated glass plates were used as the substrate for junction fabrication. CZTS layer was deposited in a two-step process as a 'double layer', i.e. a conducting CZTS layer in contact with ITO and resistive CZTS layer close to the junction. As we had to optimize the right combination of conducting and resistive layers to obtain good device performance, we tried different Cu:Zn:Sn:S ratios in both conducting and resistive CZTS layers. The

Cu:Zn:Sn:S precursor ratio for depositing the conducting first layer (layer in contact with ITO) was *y*:1:0.7:12 where *y*-values were varied from 2.5 to 4 in steps of 0.5. For each y-value in first layer, Cu:Zn:Sn:S ratio in the second layer was *x*:1:0.7:12 where *x*-values were varied as 2.5, 1.5, 0.75 & 0. Thus 16 different combinations were obtained purely by varying the 'Cu' concentration in first and second layers of CZTS. Precursor ratios were adjusted by changing the concentration of the respective constituents in the precursor solution. On top of these 16 different CZTS double layers coated on ITO, In_2S_3 layer was deposited. After deposition of In_2S_3, 'In' was diffused over the In_2S_3 layer. This was followed by deposition of silver electrodes.

5.5.2 Junction Analysis

From the J-V characteristics, the performance parameters of all the 16 devices were obtained. Each parameter is plotted as function of 'Cu' concentration in first and second layers. V_{oc}, J_{sc}, FF and η are plotted as 'color maps' where different colors in each map represent different values taken by each of these parameters. The color palette shown in each color map indicates the range of values taken by each parameter. The X- and Y-axes in each color map represent concentration of 'Cu' in top and bottom layers respectively. Figure 5.8 (a),(b),(c) & (d) shows the color map of V_{oc}, J_{sc}, FF & η as a function of 'Cu' concentrations x & y in the top and bottom layers respectively. It is quite obvious from the color maps that all the parameters are maximum when top layer 'Cu' concentration x=2.5. This is contrary to our assumption that a resistive layer i.e. a 'Cu-deficient' layer near the junction will be beneficial for device performance . Even though we can specifically point out (from the colour maps) a particular 'Cu' concentration (i.e., x=2.5) in top layer for which device parameters are good, we are not able to point out a particular 'Cu' concentration (y) in bottom layer for which all device parameters are good. So in order to study

in detail, the effect of bottom layer 'Cu' concentration (y) on device parameters, we prepared 4 devices. In each of these devices, CZTS was given as double layer such that top layer 'Cu' concentration is x=2.5 and bottom layer 'Cu' concentration 'y' is 2.5, 3, 3.5 and 4.

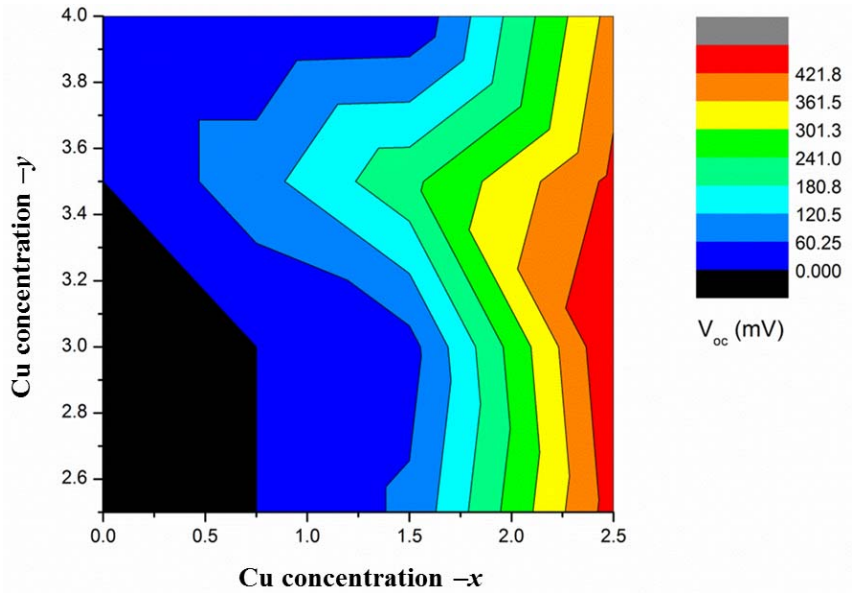

(a)

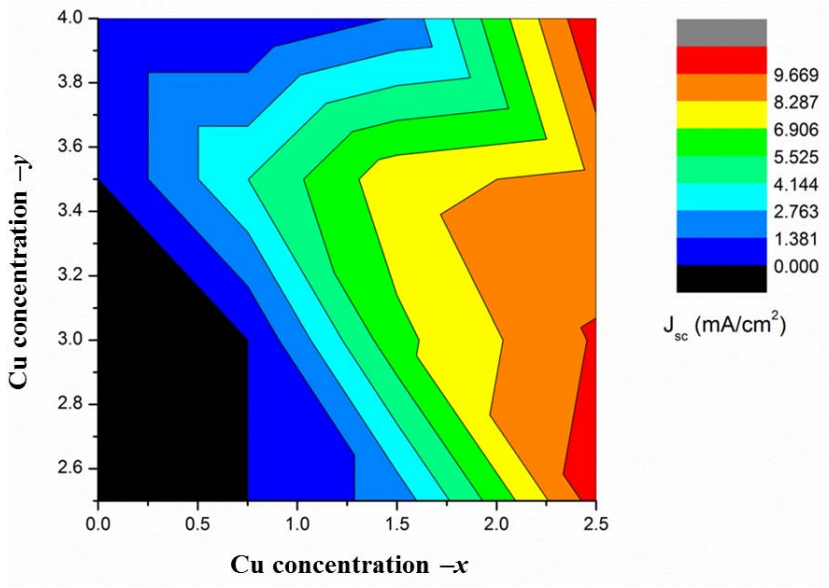

(b)

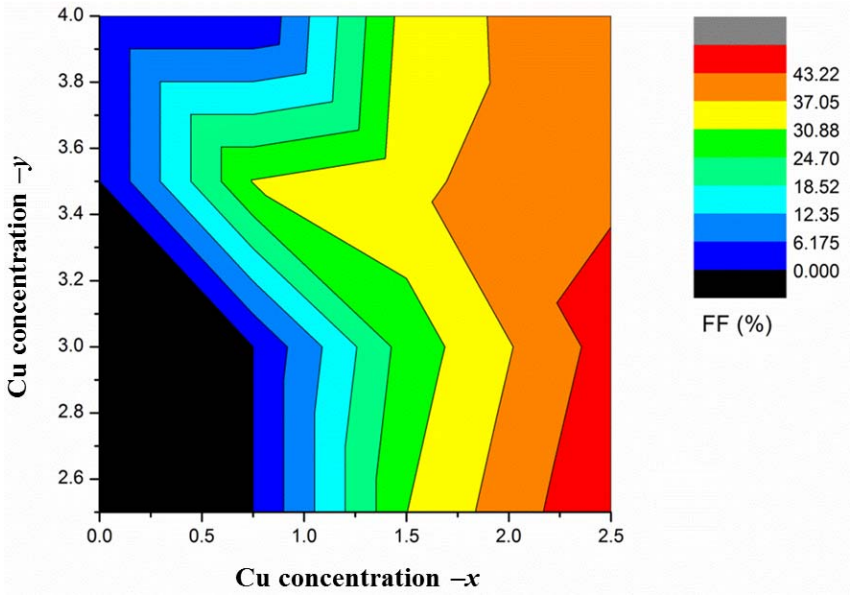

(c)

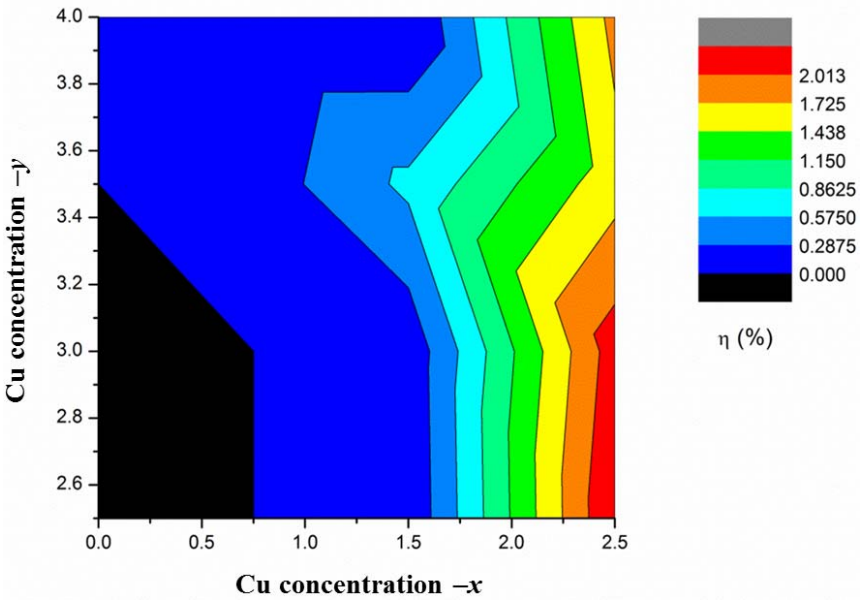

(d)

Figure 5.8. 2D-Mapping of (a) V_{oc} (b) J_{sc} (c) *FF*& (d) η of the devices with respect to '*Cu*' concentrations '*x*' and '*y*'.

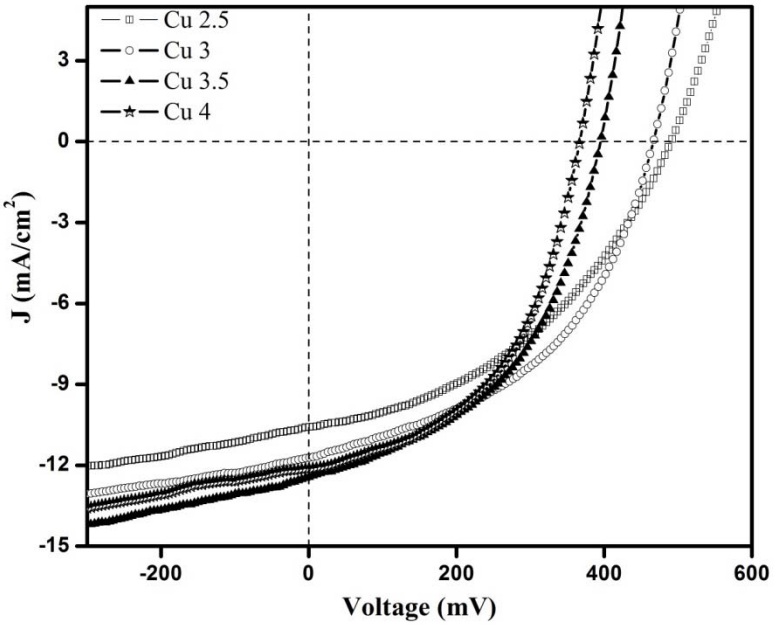

Figure 5.9. J-V characteristics of the CZTS/In_2S_3heterojunction with double layered CZTS having different 'Cu' concentration in the bottom layer

The photovoltaic parameters extracted from the J-V characteristics are tabulated in table 5.8. Both J_{sc} and *FF* of the devices increase with increase in *y*. This is an indication of the decrease in series resistance (R_s) of the device. R_s was estimated from the slope of illuminated *J-V* characteristics at the intersection of the *J-V* curve with the voltage axis. It decreases abruptly from 16.3 to 9.1 $\Omega.cm^2$ on increasing *y* from 2.5 to 3 and further, it decreases only slightly. This decrease in R_s proves our assumption that 'copper rich layer' near the transparent electrode is beneficial. However, the shunt resistance (R_{sh}) also decreases causing V_{oc} to lower and hence an optimum η = 2.52 % is observed for *y*=3. It was concluded that higher copper concentration in the bottom layer of CZTS near to the 'hole collecting electrode' is beneficial for device performance.

Table 5.8. Performance parameters of the devices prepared by varying 'Cu' concentration (*y*) in bottom layer CZTS

Device name	V_{oc} (mV)	J_{sc} (mA/cm^2)	η (%)	*FF* (%)	R_s (Ω.cm^2)	R_{sh} (Ω.cm^2)
Cu 2.5	491	10.6	2.17	41.7	16	238
Cu 3.0	468	11.7	2.52	46.0	9	182
Cu 3.5	395	12.4	2.31	47.1	8	111
Cu 4.0	369	12.2	2.19	48.7	7	180

5.6 All sprayed FTO/CZTS/In_2S_3 solar cell

In all our trials on device fabrication we made use of ITO coated glass substrates. But as we mentioned in the introduction chapter due to the scarcity of 'In', cost of ITO is very high. From the perspective of a cost effective way of fabrication of thin film solar cell, replacement of ITO is very essential. Hence our next aim was to replace ITO using sprayed fluorine doped tin oxide (FTO).

5.6.1 Experimental

Fluorine doped Tin oxide (FTO) thin films were prepared on soda lime glass substrates by automated CSP machine. The starting solutions were prepared from stannic chloride ($SnCl_4.5H_2O$) and ammonium fluoride (NH_4F). The solutions were prepared by dissolving $SnCl_4.5H_2O$ and NH_4F in 100 ml methanol. This precursor solution was sprayed on to substrates kept at a temperature of 425 ^oC. Air was used as the carrier gas. More details of the preparation of FTO are given in our patent application (No. 021/PF-PIC/2013/KSCSTE).

CZTS layers were deposited over FTO layer using CSP technique. Cu:Zn:Sn:S ratio in the precursor solution was kept at 2.5:1:0.7:12. The solution was sprayed on to FTO coated glass substrates maintained at a temperature of 300 ^oC, and during the course of spray, temperature was increased to 350 ^oC. Approximately 550 nm thick CZTS layer is deposited in a single spray followed

by In_2S_3 layer. Deposition conditions of In_2S_3 layer was retained as such. 'In' diffusion was done as before and finally silver electrodes were given by vacuum evaporation.

5.6.2 Junction Analysis

Figure 5.10 shows the illuminated J-V characteristics of the device fabricated on FTO. Performance parameters obtained from the J-V curve is tabulated in table 5.9.

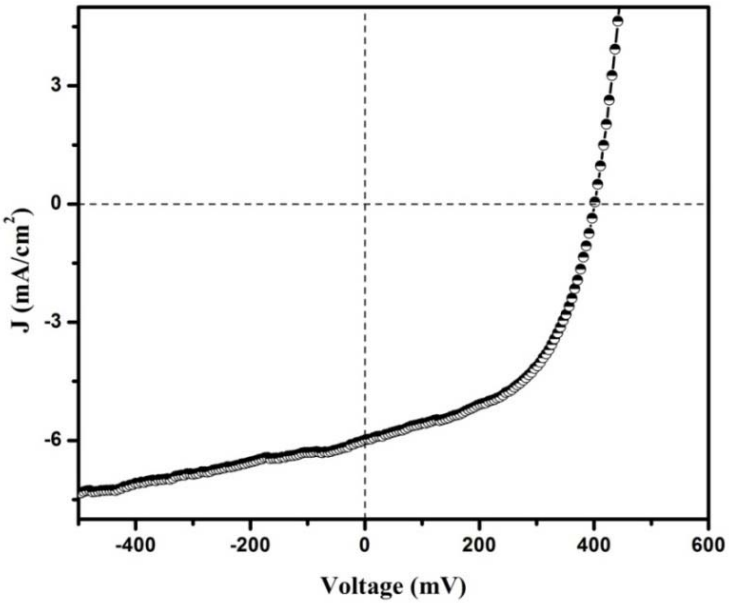

Figure 5.10. Illuminated J-V characteristics of CZTS/In_2S_3heterojunction fabricated over FTO.

Table 5.9. Performance parameters of the CZTS/In_2S_3 device fabricated over FTO.

V_{oc}	406 mV
J_{sc}	6 mA/cm^2
FF	51 %
η	1.25 %
R_s	13 Ω.cm^2
R_{sh}	250 Ω.cm^2

Short current density was 8.03 mA/cm^2 for device fabricated using single layer CZTS over ITO coated glass substrates. But J_{sc} has reduced to 6 mA/cm^2 for devices fabricated on FTO. This reduction in J_{sc} might be due to the increased sheet resistance of FTO (15 Ω/□) compared to that of ITO (10 Ω/□). There is not much variation in V_{oc} and FF. Due to the reduction in J_{sc}, efficiency of only 1.25 % was obtained which is less than the value obtained for devices fabricated on ITO (1.85 %). But if we compare the cost of ITO and FTO this result is very promising. The major highlight of this result is that all layers constituting the solar cell were deposited using spray pyrolysis. Further analysis is required in order to improve the performance of device fabricated over FTO.

5.7 Conclusions

This chapter is concerned with the effects of modification of CZTS absorber layer on the performance parameters. Variation of pH of precursor solution has been proposed as an effective method of avoiding precipitation in precursor solution for spray deposition of CZTS. Deposition of CZTS layer using Cu:Zn:Sn:S ratio of 2.5:1:0.7:12 in the precursor solution is good from device point of view. Efficiency achieved for a single layer CZTS device was 1.85 % with a short circuit current density (J_{sc}) of 8.03 mA/cm^2. Further enhancement in $J_{sc}$to 11.7mA/cm^2 could be achieved using a 'two-step' deposition process for CZTS layer. Efficiency could be improved to 2.52 %, which is the highest value reported so far for spray deposited CZTS/In_2S_3heterojunction. The major achievement was that 'all-sprayed' CZTS/In_2S_3 solar cell with efficiency 1.25 % was fabricated on sprayed FTO substrates.

References

[1]. **B. Shin, O. Gunawan, Y. Zhu, N. A. Bojarczuk, S. Jay Chey and S. Guha.** 2013, Prog. Photovolt: Res. Appl. , Vol. 21, p. 72.

[2]. **Cumberbatch, Toby John.** s.l. : European Patent Office, 1989-01-04. EP0297799 (A1).

[3]. **F.H. Pollak and M. Cardona.** 1970, Solid State Communications, Vol. 8, p. 133.

[4]. **G. Gouadec and P. Colomban.** 2007, Progress in Crystal Growth and Characterization of Materials, Vol. 53, p. 1.

[5]. **K. Jimbo, R. Kimura, T. Kamimura, S. Yamada, W. S. Maw, H. Araki, K. Oishi and H. Katagiri.** 2007, Thin Solid Films, Vol. 515, p. 5997.

[6]. **Y.B. Kishore Kumar, P. Uday Bhaskar, G. Suresh Babu and V. Sundara Raja.** 2010, Phys. Status. Solidi A, Vol. 207, p. 149.

[7]. **Tina Sebastian, R. Jayakrishnan, C.Sudha Kartha and K.P. Vijayakumar.** 2009, The Open Surface Science Journal, Vol. 1, p. 1.

Chapter 6

SUMMARY OF THE PRESENT WORK AND FUTURE PROSPECTS

$Cu(In,Ga)Se_2$ (CIGS) is the most proven and efficient material for thin film photovoltaics so far. In achieving TW-scale consumption for CIGS, the major concern lies in the availability of indium (In), which is also used in more expensive devices, such as flat panel displays. To mitigate the future effects of 'In' scarcity on TW scale consumption, it has been proposed that the 3rd group elements 'In' and 'Ga' in CIGS to be replaced with 'Zn' & 'Sn' to form CZTS.

The endeavor of the presented work was to completely characterize the material copper zinc tin sulfide (Cu_2ZnSnS_4) [commonly known as CZTS], that too prepared using an economically viable technique, to be used as an absorber layer in sprayed thin film solar cells. The idea was to first optimize the deposition conditions of CZTS using chemical spray pyrolysis (CSP) technique and the fabrication of Solar cell using sprayed CZTS as absorber layer and In_2S_3 as buffer layer. At first we characterized the deposition conditions for CZTS absorber layer and then fabricated a CZTS/In_2S_3 heterojunction. Through various modifications of absorber and buffer layers, performance of the device was enhanced and finally an all sprayed solar cell was developed.

Initially we deposited CZTS films on soda lime glass (SLG) substrates using various precursors. From material characterization as well as junction analysis, copper chloride, zinc acetate, stannic chloride and thiourea were identified as the suitable choice of precursors for deposition of CZTS. The optimum substrate temperature for CZTS deposition was found to be 350 ^oC.

Almost stoichiometric CZTS films were obtained for a 'Cu' concentration of 0.015 M (in the precursor solution). Spray rate has found to have significant effect on film properties and 6 ml/min was identified as the suitable spray rate.

The second part of the work deals with fabrication of heterojunction on ITO coated glass using CZTS absorber and In_2S_3 buffer layer with silver as the top electrode. Owing to the high resistivity of In_2S_3 layer, performance parameters of the device were very low and 'In' diffusion were identified as an effective way of reducing the resistivity of In_2S_3 layer. 'In' diffusion was achieved by depositing different thickness of metallic 'In' through vacuum evaporation followed by annealing at 100 ^oC for one hour. Optimum thickness of 'In' to be deposited depends on the In_2S_3 layer thickness. For a 500 nm thick In_2S_3 buffer layer, 8 nm 'In' was found to be the optimum thickness to be deposited and the device showed a conversion efficiency of 1.5 % and a fill factor of 44 %.

Further enhancement in conversion efficiency could be achieved by modification of CZTS absorber layer. In order to avoid precipitation of spray solution for CZTS deposition, pH of spray solution was varied. CZTS/In_2S_3 heterojunctions were prepared using CZTS layers deposited with different 'Cu' concentrations in the spray solution and for a 'Cu' concentration 0.025 M, we got an efficiency of 1.6 %. Now from device point of view, CZTS with Zn/Sn ratio ~ 1.15 is preferable and we reduced 'Sn' concentration. For a 'Sn' concentration of 0.007 M, conversion efficiency reached up to 1.85 %. The Cu:Zn:Sn:S ratio in the precursor solution for getting better conversion efficiency was identified as 2.5:1:0.7:12.

Finally we employed a "double layer" structure for CZTS, such that a layer having higher 'Cu' concentration (ie. having higher conductivity) near the electrode and a layer having low 'Cu' concentration near the junction. Using this

double layer CZTS as absorber layer, we could improve the efficiency to 2.52 %. This is the highest efficiency achieved so far for a sprayed CZTS solar cell. For reducing the cost of solar cell, we should replace ITO (our bottom electrode) with some alternatives. So we deposited fluorine doped tin oxide using chemical spray pyrolysis technique and devices were fabricated using this as bottom electrode. The devices had conversion efficiency of 1.25 %. This is a landmark achievement of our group.

Future Prospects

In the present study, we increased short circuit current and fill factor of the device through the enhancement in conductivity of In_2S_3 by ex-situ 'In' diffusion. It will be interesting if it can achieve through an in-situ process. So there will be no need of vacuum processing during the fabrication of the device. Doping with materials like 'Sn' and 'Al' can be done in order to achieve this aim. Another way of enhancing the short circuit current density of CZTS/In_2S_3 heterojunction is by depositing a highly conducting layer above the In_2S_3 buffer layer or by making the indium sulfide layer highly conducting. Also in order to reduce the diffusion of 'Cu' from CZTS to In_2S_3, a thin layer of intrinsic oxide layer can be deposited. This will reduce the leakage current and will enhance the open circuit voltage.

In the present work, only few trials is done over FTO coated glass substrate and we could get an efficiency of 1.25 %. Further studies can be done in order to improve the efficiency of all sprayed solar cell. Another aspect is the replacement of In_2S_3 buffer layer, where 'In' is a rare earth element, with some other wide band gap n-type semiconductor. ZnS is a promising candidate in this direction and the optimization of deposition condition of ZnS buffer layer and its use in CZTS based sprayed solar cell will be a remarkable effort.

.....ꕥ.....